Near-bed flow behaviour in scour holes under laterally non-uniform flow conditions

S.A.J. Paulissen

MSc Thesis
November 2020

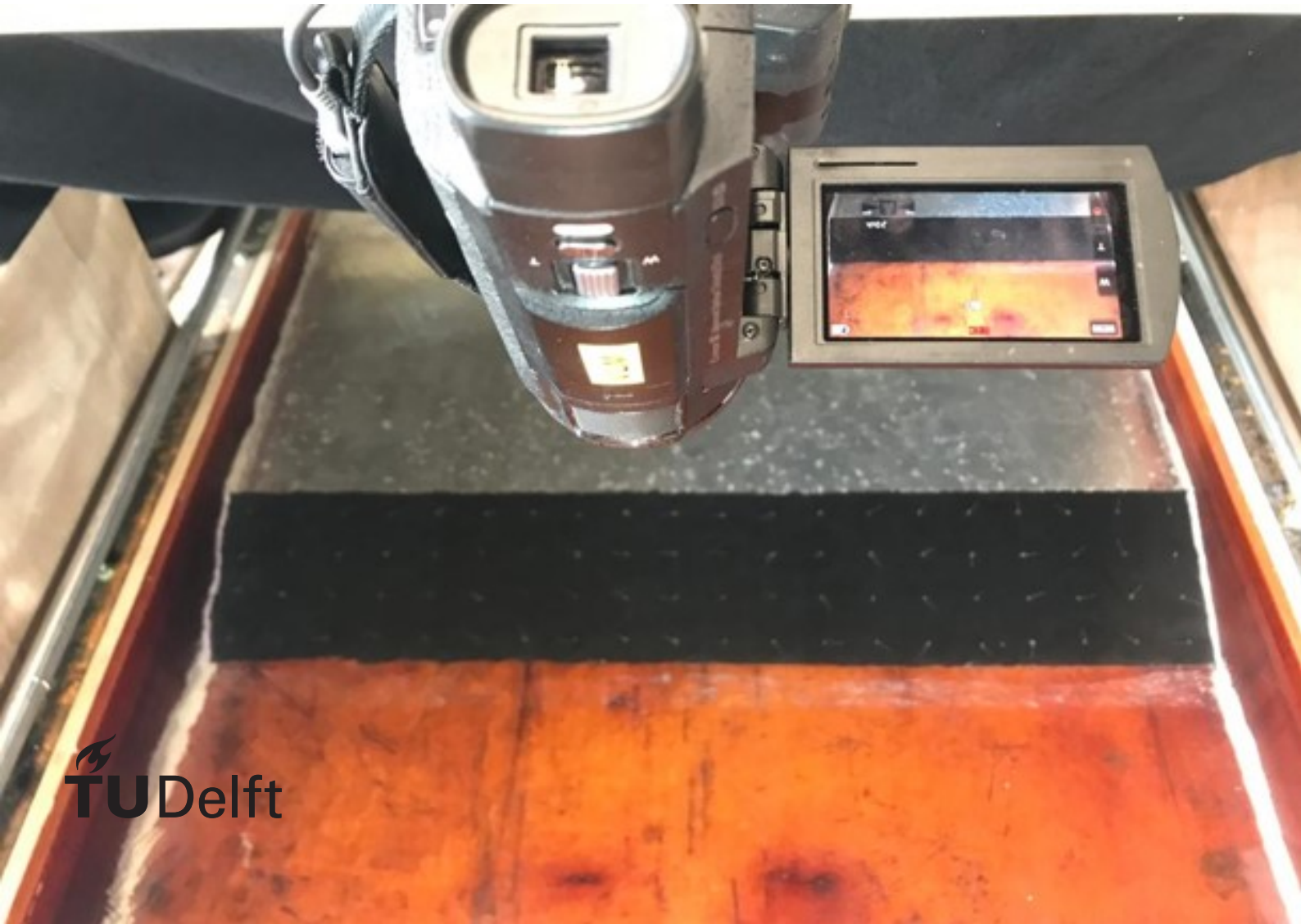

TU Delft

Near-bed flow behaviour in scour holes under laterally non-uniform flow conditions

by

S.A.J. Paulissen

to obtain the degree of Master of Science at the Delft University of Technology,

to be defended publicly on Monday November 30, 2020 at 10:00.

Student number: 4303563

Project duration: March 1, 2020 – November 30, 2020

Thesis committee:

Dr. ir. B. Hofland,	TU Delft
Dr. ing. M. Z. Voorendt,	TU Delft
Ir. G. M. Smith,	TU Delft
Ir. J. S. Reedijk,	BAM Infraconsult

TU Delft

Preface

On the screen or desk in front of you, you find the thesis 'Near-bed flow behaviour in scour holes under nonuniform flow conditions'. I wrote this thesis to obtain my Master of Science degree in Hydraulic Engineering, and I would be very pleased if this study turns out to be my first real contribution to the scientific field of Civil Engineering.

This study was carried out in cooperation with BAM Infra. I am grateful to BAM Infra for facilitating and supporting my research project. I would particularly like to thank Bas Reedijk, head of the Water Department and member of my graduation committee, since he provided me with valuable insights and helped me to make the connection between laboratory observations and practice.

Committee members Bas Hofland, Mark Voorendt and Greg Smith provided great guidance and encouraged me to push this study to a higher level, both in terms of scientific depth and methodology. I am very grateful for the time they were willing to generously spend to help me forward.

Yorick Broekema is the absolute expert on my research topic. Having had the opportunity to discuss my thoughts and findings with him greatly helped my research forward. This is an enormous luxury, which I appreciate a lot.

I conducted my experiments in the Hydraulic Engineering Laboratory of Delft University of Technology. I would not have been able to finalise this study without the help of the laboratory staff. Arno Doorn contributed hugely to the creation of my experimental setup. His skill and inventiveness when it comes to building and fine-tuning a laboratory setup are impressive. In addition, the support of Sander de Vree, Pieter van der Gaag, and Jaap van Duin should not go unmentioned.

Finally, I would like to thank my dear Emilie, Loek en Mariet, Lotte, Tommy, my roomies, Jack Poels, and my road bike to help me get my mind off when I needed it the most.

Enjoy your reading!

S.A.J. Paulissen
Rotterdam, November 2020

Summary

Scour can jeopardise a hydraulic structure if not adequately dealt with. Hence, a good understanding of scour development during the design of a hydraulic structure is required. Empirical relations can be applied to obtain an initial estimate on scour dimensions in a quick and cheap manner. Currently available empirical relations, however, lack accuracy in 3-D geometries. A better understanding of the scour-driving mechanisms in 3-D geometries is required to improve the ability to accurately predict scour.

State-of-the-art research by Broekema et al. (2018) identified a novel scour-enhancing flow mechanism related to 3-D flow situations. Under specific conditions, vertical flow separation at the upstream crest of a scour hole can be suppressed as a result of lateral nonuniformities in the main flow. The boundary layer stays attached to the deflecting bed. This so-called vertically attached flow state is associated with increased scour potential due to increased bed shear stresses.

Using laboratory experiments, Broekema et al. (2019) elegantly demonstrated the existence of the nonuniformity-induced flow attachment on a conceptual level. The understanding of nonuniformity-induced flow attachment in the field is still limited though. The depth-to-width ratios tested by Broekema et al. did not match real-life scour scenarios. Hence, the next step is to determine whether and how vertical flow attachment manifests itself in a setup with realistic depth-to-width ratios. The objective of this study was to evaluate the effects of lateral nonuniformities on scour-driving flow behaviour in a scour hole.

Laboratory experiments form the backbone of this study. To start with, a measurement technique was developed enabling efficient en reliable determination of near-bed flow directions. The technique is based on tufts: small threads fixed to the bed that follow the local flow direction. An algorithm was created to convert video footage of tuft movement to numerical data on flow directions. The measuring technique was successfully validated using Acoustic Doppler Velocimetry (ADV).

Next, flow behaviour was studied through a set of experiments conducted in a simple laboratory setup that simulates a common scour situation in the field. Lateral nonuniformities were generated in a mixing layer downstream a lateral expansion of the inflow channel. The effect of each geometry parameter on the flow state was individually addressed through a dedicated set of experiments in which only a single parameter varied, exposing its effect on the flow state. Dye injections and ADV were used in addition to the tuft measuring technique to visualise additional flow characteristics.

The experiments led to the following insights:

1. Two distinct horizontal flow states were observed: horizontal divergence and horizontal contraction.

    (a) Horizontally contracting flow was more likely to occur in geometries with a short bed protection, a large horizontal expansion and a narrow inflow channel.

    (b) The transition point between both flow states was narrow. Only a slight change in geometry could entirely turn around the flow state.

    (c) A graph was created that plots the flow state against geometry parameters. It can be used to estimate the flow state for alternative configurations.

2. Each horizontal flow state is associated with distinct near-bed flow behaviour at the upstream scour slope.

   (a) The horizontally diverging flow state is accompanied with constant vertical flow separation at the slope's crest. The corresponding return current entails a near-bed flow in upward direction.

   (b) The horizontally contracting flow state is related to an alternating vertical flow pattern in which vertical flow separation and vertical flow attachment take turns. An alternating vertical flow regime was never identified before in this context. The alternating flow state is not present in the jet's centre. Instead, vertical separation takes place here. Additionally, a consistent lateral near-bed flow from the mixing layer to the centre of the jet is present.

3. The frequencies in which vertical attachment and separation alternate match the frequencies of two-dimensional coherent turbulence structures (2DCS) in the mixing layer. This similarity indicates a relation between mixing layer instabilities and suppression of vertical flow separation, which is a valuable new insight into the process of understanding nonuniformity-induced flow attachment.

The presence of the horizontally contracting and vertically alternating flow state likely increases scour dimensions. As a scour hole develops, unidirectional lateral near-bed flow velocities stay relatively high, maintaining scour potential. Scour potential is largest in and around the mixing layer. This most likely results in a strongly 3-D scour hole with maximum scour depths in the areas directly affected by the mixing layer.

Comparing this study's findings with previous scour experiments in a similar setup by Üsenti (2019) provides additional insights into scouring behaviour under the newly identified flow state. Based on a comparison of general flow behaviour and experimental parameters, it is very plausible that the alternating flow state was present in Üsenti's experiments. The observed scour behaviour was very much in line with the previously introduced reasoning that the lateral unidirectional near-bed flow leads to additional scour in the mixing layer area. A similar comparison was made for the Afsluitdijk model tests. It is deemed likely that the newly identified flow state is also the cause of the excessive scour observed at the Afsluitdijk model tests. The premise that excessive scour is caused by an alternative flow state provides the opportunity to further improve and extend the abilities of empirical scour prediction.

Contents

1 Introduction

1.1 Motivation for this study

Excessive scour can endanger a hydraulic structure. If controlled and kept at a safe distance from the structure though, structural integrity is not at risk. Bed protections are generally applied to make sure this is the case. When designing a bed protection, the goal of the structural engineer is usually not to entirely prevent scour from happening. Instead, the engineer aims to control scour at a minimal cost. It is necessary to predict scour development in advance to facilitate an efficient final design. Two types of methods are used to estimate scour dimensions: empirical relations and physical-model studies.

Empirical prediction methods evolved based on decades of scour research. Among others Breusers (1967), Dietz (1969) and Zanke (1978) made important contributions. Empirical relations allow for quick and cheap prediction of scour dimensions. For non-standardised situations, on the other hand, empirical relations often lack the accuracy (Balachandar et al., 2000). Currently existing relations are only valid under specific conditions with standardised geometries. A scour prediction relation that is universally applicable has not been found yet.

In case available empirical relations are not valid, physical model testing is often applied (Hoffmans and Verheij, 2020b). Model testing makes use of a replica of a real-life scour situation on a smaller scale. When accurately replicated, scour development in the downscaled setup is representative for the prototype, and fairly accurate estimates on scour dimensions are generated. Model testing is expensive and time consuming on the other hand.

For small projects, engineers often solely rely on empirical relations, whereas for more complicated projects, empirical methods are mostly used to get a first impression of scour development, followed by model testing in the later stages of the design process.

Even though empirical relations are only accurate under specific conditions, they are nonetheless widely used for final designs. Hoffmans and Verheij (2020b) described a recently constructed tidal culvert that connects the Eastern Scheldt with a natural reserve in the Netherlands. Scour downstream of the culvert was estimated using the scour prediction method described by Dietz (1969). After opening the culvert, scour developed much quicker and deeper than predicted. The predicted equilibrium scour depth was reached within 8 weeks. To prevent serious damage, the culvert was closed and adjusted twice. Such errors are costly and therefore highly undesirable.

Despite potentially large consequences, the flawed application of empirical relations is still a regularly

Author	Year of publication	Percentage of overpredictions greater than 300%	Percentage of underpredictions
Aberibigbe and Rajaratnam	1998	31	14
Altinbilek and Basmaci	1973	80	4
Breusers and Raudkivi	1991	22	34
Chatterjee et al.	1994	7	51
Dey and Sarkar	2006	3	34
Hoffmans	1998	35	24
Hopfinger et al.	2004	0	88
Lim and Yu	2002	2	52
Valentin	1967	8	41

Table 1.1: Comparison of empirically predicted scour depths and scour depths measured in practice for a broad set of cases by Melville and Lim (2014).

made mistake by engineers. This might be partly attributable to the fact that it is very easy to wrongly apply empirical relations. Parameters are simply filled in the formula, and an outcome is obtained. The outcome is meaningless in case the empirical relation is not valid for the situation that is considered. Melville and Lim (2014) applied different empirical methods to estimate maximum scour depths and compares their results. As Table 1.1 shows, large differences in estimated scour depths exist. Hence, even though each method accurately predicts scour for the situation it was designed for, it is often not applicable in other situations. Great caution is therefore required in case design decisions are based on empirical relations.

The discrepancy among the predicted scour depths can be attributed to the way empirical methods are developed. Often, a set of experiments is carried out within the boundary conditions of a setup. During these experiments, the effect of a few predefined parameters is studied. The scour depth is measured for each experiment. Subsequently, the relation between the parameters is studied and the scour depth is described by a formula. The vulnerability of this approach lies with the fact that that this relation is only valid under the boundary conditions in place during the experiments. In case the configuration deviates from the experimental setup, the empirical relation is not valid. When kept in mind that practice is rarely comparable to a laboratory setup, one can easily conclude that the application of empirical relations to situations in the field is by definition a difficult story.

Figure 1.1: Animation of the renewed discharge sluices of the Afsluitdijk near Den Oever

Such discrepancies form the direct incentive for the current study. Currently, the Afsluitdijk, a 32 km long major dam in the Netherlands, is being completely renovated. Part of this renovation is the renewal of the discharge sluices, shown in Figure 1.1. Model tests were conducted by BAM Infra to obtain insights into the scouring patterns at the renewed discharge sluices. The results of these model tests differed

greatly from the empirically predicted scour depths prior to the tests.

This again indicates that model tests are necessary in case of non-standard scour situations. This does not detract from the fact that methods that reliably predict scour development without the immediate need for model tests would be of great value. Currently though, scouring phenomena in complex geometries are insufficiently understood to develop a prediction method. Underlying phenomena of scour have to be better understood first. Recent research by Broekema et al. (2018) made an important contribution to a better understanding of local scour. This state-of-the-art study points out that a phenomenon called vertical flow attachment at the upstream scour slope can potentially intensify scour development. There are reasons to believe that vertical flow attachment might explain a significant part of the discrepancy between model tests and 2-D empirical relations. Current understanding about this phenomenology is still very limited though. This study focuses on increasing the understanding of flow attachment in relation to scour.

1.2 Problem analysis

Conventional understanding of the mechanisms related to local scour is based on a detaching flow at the crest of the upstream scour slope. Instead of following the contours of the deflecting bed, the flow remains in the top part of the water column. A wake forms in the scour hole underneath. This so-called vertically attached flow state was thought to be generally present behind hydraulic structures with large scour development. Instead, Broekema et al. (2018) found that lateral velocity gradients triggered at a widening of the channel upstream can suppress vertical separation. Alternatively, the flow stays vertically attached and follows the bed slope. This flow state is called vertical flow attachment. Vertical flow attachment has more scour potential than a similar setup with vertically separating flow. Figure 1.2 provides an impression of both flow states.

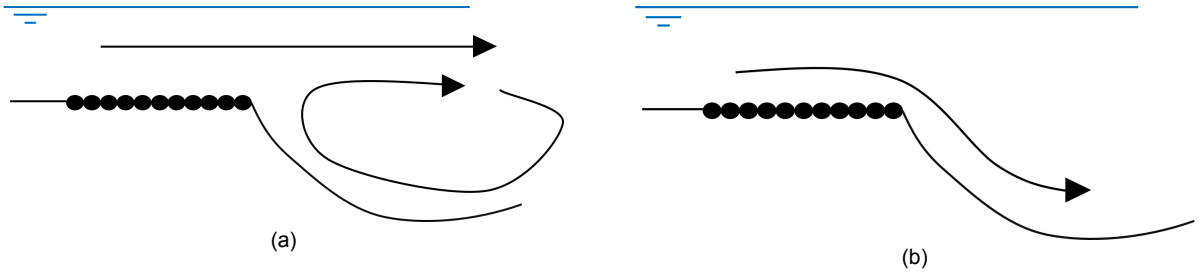

Figure 1.2: Schematisation of the main vertical flow patterns in a scour hole downstream of a bed protection: (a) vertical flow separation and (b) vertical flow attachment.

Several methods exist that reliably predict the presence of either vertical flow separation or vertical flow attachment in a 2-D situation (Gerthart and Bober, 1974). When this knowledge is applied on scour holes, one would expect vertical flow separation to occur. Scour surrounding hydraulic structures, however, almost exclusively occurs in 3-D situations. Hence, the existing methods are not valid. Understanding of flow separation in 3-D situations is still very limited.

Broekema et al. (2018) show that 3-D effects greatly influence the flow state in scour holes. Novel flow phenomena were identified around the Eastern Scheldt storm surge barrier. These phenomena point out lateral velocity gradients as a driver for vertical flow attachment at an upstream scour slope. In a follow-up study, Broekema et al. (2019) demonstrated that vertical flow attachment potentially increases scour in real-life applications. Flow attachment therefore might be an explanation for deviant scour predictions.

Despite the big knowledge leap accomplished by Broekema et al. (2018) and Broekema et al. (2019), research on flow attachment induced by lateral velocity gradients is still in its infancy. Broekema et al.

(2019) proved that lateral velocity gradients can cause vertical flow attachment in open channel flow, but used an experimental setup that does not replicate practice very well as in-the-field situations are often much shallower. Van der Zande (2018) used a shallower experimental setup to study the same phenomena, but only focused on slopes much more gentle than those present in the field. The question that thus remains is whether and how vertical flow attachment manifests itself under shallow and relatively steep conditions.

In addition to this knowledge question, a prominent practical challenge prevails. So far, it has been hard for researchers to efficiently study flow attachment. Previous studies made use of Acoustic Doppler velocimetry (ADV) to measure flow patterns. ADV uses acoustic techniques to measure flow velocities right next to the head of a submerged probe. Although ADV enables high-quality measurements, it also has two major drawbacks:

1. Visualising a full flow pattern using ADV is very laborious. ADV only allows for measurements at one single location at a time, which require about 5 minutes each. In case a single experimental configuration is tested for flow attachment, a high double-digit or even a triple-digit number of measurements might be required. Often, a researcher wants to obtain insights into the effects of a single variable on the flow state by regularly varying the experimental setup. Loads of configurations need to be tested, which is very time consuming using ADV.
2. ADV cannot measure close to a surface due to reflection of the acoustic signal. Flow attachment is by definition a near-bed phenomenon. The minimum distance from the bottom at which can be measured is in the order of 0.5-1 cm. This is quite significant as water depths in a laboratory setup are often in the order of 10 cm. The most relevant information can therefore not be measured using ADV. This issue was one of the main limitations in the study of Broekema et al. (2019).

In the context of further developing the understanding of flow attachment the upcoming decade, it is essential to have a pragmatic measurement technique that allows for quick large-scale data collection on near-bed flow patterns.

Problem statement

After this problem analysis, it becomes apparent that vertical flow attachment induced by lateral nonuniformities has the potential to cause increased scour. Understanding of this phenomenon is still very limited. Flow attachment has only been demonstrated in laboratory setups that are not representative of scour situations in the field. It is unclear if flow attachment occurs in real-life applications, and if so, what its characteristics are. The consequence is that scour for certain configurations cannot be predicted with sufficient accuracy, which can lead to the problems described in Section 1.1.

1.3 Research objective

The ultimate objective of this study is to increase the understanding of vertical flow attachment induced by lateral nonuniformities and thereby contribute to the development of better scour prediction methods. With reliable methods, costly cases like the tidal culvert described in Section 1.1 might be preventable in the future. A large knowledge gap surrounding nonuniformity-induced vertical flow attachment was revealed by Broekema et al. (2018). Following up on conceptual studies on this newly identified topic, the objective of this study is to determine whether and how this phenomenon manifests itself in configurations with depth-to-width ratios that are common in the field. This leads to the main research question:

What are the effects of lateral nonuniformities on near-bed flow behaviour in a scour hole downstream of hydraulic structures?

The main question is answered using a set of subquestions. As explained in the problem analysis, no prevailing measurement technique exists to effectively map near-bed flow patterns. The first subquestion is dedicated to finding this method. The next three focus on learning more about the flow behaviour associated with vertical flow attachment. The last subquestion considers the effects of the observed flow behaviour on scour.

1. *How can near-bed flow directions be reliably and efficiently visualised across an entire flow field?*
2. *What macro flow states can be expected downstream of a hydraulic structure in case horizontal nonuniformities are present?*
3. *How does the hydraulic structure's geometry affect the flow state?*
4. *What are the characteristics of the near-bed flow behaviour in the scour hole? And what does it say about the vertical flow state?*
5. *How does the identified near-bed flow behaviour affect scour?*

1.4 Methodology

A five-stage approach is used to answer the research questions formulated in the previous section.

1. **Literature study:** Literature related to nonuniformity-induced flow attachment is studied to develop a full understanding of the current state of knowledge. This provides a basis for a parameter analysis (stage 2), which allows for pragmatic and efficient execution of this study. Additionally, the basics of empirical scour prediction in combination with a set of interesting scour cases are examined. This ensures that even though this study is of a fundamental nature, the link with the eventual goal, application on scour, is never overlooked.
2. **Parameter analysis:** A list is composed of all parameters that are relevant to the situation studied and the laboratory setup (stage 3). The parameter list is formed based on previous research and common sense. Subsequently, using dimensional analysis, this list is transformed into a minimum number of dimensionless variables that describe the situation studied. For each dimensionless parameter is considered how it affects the studied phenomenology and which parameter ranges should be studied to 1) maximise the likelihood of novel results, and 2) replicate practice in the best possible way.
3. **Experiment design:** The laboratory setup is designed based on the insights obtained during the parameter analysis. Appropriate measurement techniques are selected and a test plan is developed. The experimental setup is then constructed. To enable effective near-bed flow direction measurements, a tuft-based measurement technique is developed.
4. **Execution of laboratory tests and analysis of the results:** The experiments are conducted according to the test plan. Gathered data are processed and interesting insights are followed up with additional experiments.
5. **Interpretation of results:** Experimental findings are interpreted and compared with findings of previous studies. Implications of the findings on scour and scour prediction are considered. Research questions are answered and openings for further research are presented.

1.5 Thesis outline

Table 1.2 presents the outline of this thesis.

Methodological step	Thesis chapter
1. Literature study	Chapter 2
2. Parameter analysis	Chapter 3
3. Experiment design & development of tuft measurement technique	Chapter 4 & 5
4. Laboratory experiments (execution + analysis)	Chapter 6
5. Interpretation of results	Chapter 7 & 8

Table 1.2: Thesis outline

2

Theoretical framework

This chapter presents the results of the literature study (methodological step 1). As this study builds on previous research on vertical attachment induced by lateral nonuniformities in scour situations, a thorough understanding of the current knowledge state is essential. A literature overview is provided in this chapter.

Firstly, the existing knowledge on flow attachment is considered, with vertical flow attachment induced by lateral nonuniformities in scour situations as the main point of focus. Additionally, the basics of empirical scour prediction are introduced as well as several scour experiments in setups with laterally nonuniform flow.

2.1 Fundamentals of flow attachment

Flow separation is a hydrodynamic phenomenon in which a flow moving parallel to a confining wall detaches and creates a turbulent wake. It is usually caused by a change in flow velocity, induced by either a sharp edge in the confining wall or a gradual widening of a passage (Schiereck and Verhagen, 2012). Flow separation downstream of a hydraulic structure often occurs at the transition from the fixed bed protection to the freely erodible bed. The flow state opposite to flow separation is flow attachment. In this case, the flow stays attached to the surface it travels next to, even if it encounters a widening of the section or a sharp edge in the confining wall.

To understand the basic principles behind flow separation and flow attachment, the concept of a boundary layer needs to be made clear first. A boundary layer is the section of the flow directly adjacent to a confining wall. The flow within this area is affected by the presence of the adjacent surface, as opposed to the part of the flow outside of the boundary layer (White, 1999). Flow velocities vary logarithmically within the boundary layer, being smallest right adjacent to the confining wall. A widening of a passage causes the boundary to layer thicken. Thickening of the boundary layer induces an adverse pressure gradient that decelerates the flow in the boundary layer (Simpson, 1996). Whenever the flow velocity in the boundary layer reaches zero, separation occurs. The boundary layer then detaches from the confining wall at the separation point. A wake behind the separation point forms. A return current behind the separation point is initiated in case the adverse pressure gradient is sufficiently large (White, 1999). This mechanism is illustrated in Figure 2.1.

Numerous studies on flow separation have resulted in several methods to predict flow separation (Gerthart and Bober, 1974). Similar to empirical scour prediction methods, flow separation prediction

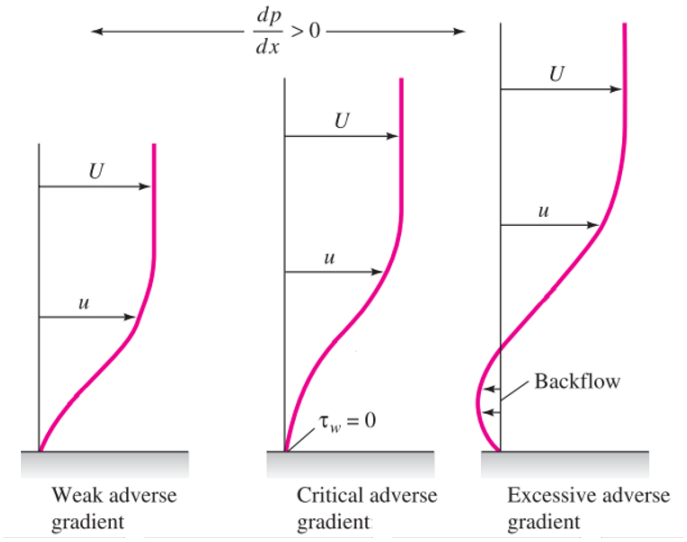

Figure 2.1: Schematic overview of the relation between pressure gradients and flow separation, adapted from White (1999).

methods are reliable for standardised situations but struggle to make accurate estimates for arbitrarily-shaped bodies (Schiereck and Verhagen, 2012). Moreover, flow separation does not occur in a stationary separation point. Instead, the separation point constantly moves within an area depending on the flow situation at that exact time (Simpson, 1996).

A flow situation can be called two dimensional whenever velocity gradients in the third dimension are negligible. In open channel flow, two types of flow separation in the 2-D plane can be distinguished: 1) separation in the 2-D vertical plane; and 2) separation in the 2-D horizontal plane. At hydraulic structures, flow separation in the vertical plane often occurs at the end of a bed protection, whereas the contours of a hydraulic structure generally trigger flow separation in the horizontal plane. Figure 2.2 illustrates both cases of flow separation.

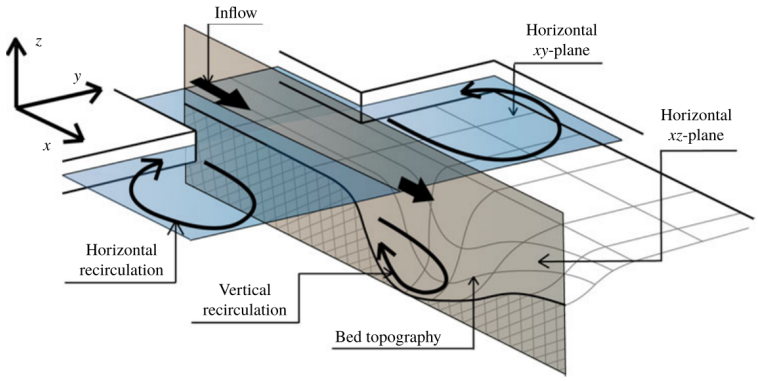

Figure 2.2: Sketch of flow separation in the 2-D vertical plane and the 2-D horizontal plane (Broekema et al., 2019).

Research has developed a thorough understanding of flow separation in the 2-D plane (Gad-el Hak and Bushnell, 1991). In practice though, exclusive 2-D flow is rather rare downstream a hydraulic structure. Hence, a 3-D situation needs to be considered. Flow separation in 3D is much less well understood (Simpson, 1996). The extra degrees of freedom introduced with the third dimension largely complicate the situation (Broekema et al., 2019). Nevertheless, extensive effort has been put into understanding 3-D flow separation for specific circumstances, for example by Yates and Chapman (1992), Cherrye et al. (2008) and Gao et al. (2015). Especially for aviation applications, knowledge on flow separation in 3-D situations is sufficient to be applied in practice. Yet this has not led to a generally applicable prediction method for 3-D flow separation Simpson (1996).

2.2 3-D effects on the flow attachment

A breakthrough in the understanding of 3-D flow separation around hydraulic structures was recently made by Broekema et al. (2018). This study demonstrated that lateral velocity gradients in a flow can trigger a mechanism that suppresses flow separation at a downward slope. Instead of vertical separation, which can be predicted based on 2-D understanding, the flow stays attached to the deflecting bed. This is an often occurring situation around hydraulic structures. The horizontal expansion, e.g. at the outflow of a culvert or at a discharge sluice, introduces lateral nonuniformities to the flow, while the scour hole behind the bed protection is represents the deflecting bed. Broekema et al. (2019) proved this concept in a simple laboratory setup. Two distinct flow states were distinguished:

- Vertically attached flow in combination with horizontal contraction; and
- Vertically separated flow in combination with horizontal divergence.

Figure 2.3 schematises both flow states. The mechanisms that drive both flow states are further explained in the next sections.

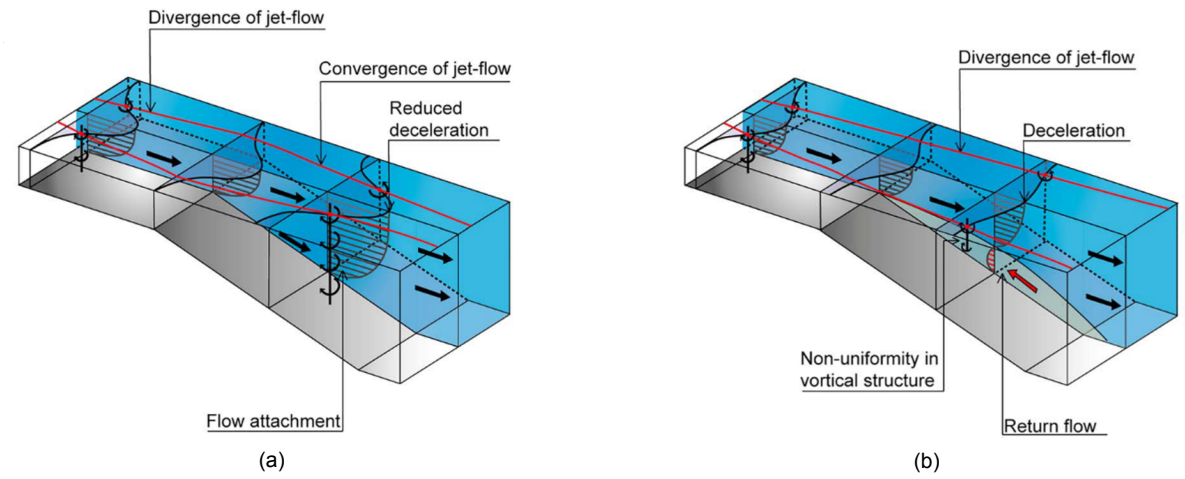

Figure 2.3: Qualitative sketch of the flow states distinguished by Broekema et al. (2018). Figure (a) shows a flow with significant lateral nonuniformities, causing the flow to stay attached to the bottom at the downward slope. Figure (b) on the other hand shows a comparable configuration with less lateral nonuniformities. In this situation the flow vertically separates.

2.2.1 Vertical attachment + horizontal convergence

The lateral nonuniformities that cause the flow to attach to the downward slope are induced upstream. After a jet-like flow leaves the confining sidewalls of a hydraulic structure, a horizontal mixing layer forms between the jet and the stationary water at its sides. The velocity difference along the mixing layer width cause lateral velocity gradients. These lateral velocity gradients trigger horizontal contraction of the flow, as is shown in 2.3. The exact mechanisms that link lateral nonuniformities to horizontal flow contraction have not yet been revealed, but Broekema et al. (2018) and Broekema et al. (2019) argue that conservation of potential vorticity most likely plays an important role. The principle of potential vorticity conservation is explained in Appendix A.

Contraction at the downward slope squeezes the streamlines in the main flow, accelerating individual flow particles. This acceleration is associated with a positive pressure gradient in the main flow. Opposite to this positive pressure gradient, the deflecting bed causes an adverse pressure gradient at the downward slope. Whenever the positive pressure gradient in the mixing layer is sufficiently large to counteract the adverse pressure gradient, flow separation is suppressed. In such a case, the boundary layer stays attached to the bed along the downwards slope.

2.2.2 Vertical separation + horizontal divergence

Whenever lateral velocity gradients are limited, the flow does not contract at the downward slope and vertical flow attachment is not triggered. Instead, the mixing layer keeps diverging across the downward slope, and vertical separation takes place at the slope's crest

Broekema et al. (2019) varied the amount of lateral nonuniformity by adapting bed protection length. The width of the mixing layer tends to develop linearly with downstream distance (Uijttewaal and Tukker, 1998). It widens and velocity differences across the mixing layer decrease, causing a reduction of the lateral velocity gradient (Van Prooijen and Uijttewaal, 2002).

In case a long bed protection is present, lateral nonuniformities have largely dampened out before reaching the downward slope. Contraction is not triggered, and subsequently, no positive pressure gradient is present to counteract the adverse pressure gradient. Hence, vertically separation occurs and the main flow continues through the top part of the water column across the downward slope. In the meanwhile, a return flow develops in the bottom part of the water column. The phenomenology of this flow state corresponds with the traditional understanding of mixing layers and flow separation in 2D.

2.3 Specifics of previous experimental studies

Two studies have demonstrated the effect of lateral nonuniformities on the vertical flow state: Broekema et al. (2019) and Van der Zande (2018). This section discusses the specifics of each study and highlights the differences between the studies.

Broekema et al. (2019) observed strong and continuous manifestation of either vertical attachment in combination with horizontal contraction or vertical separation in combination with horizontal divergence. In configurations with the first flow state present, vertical attachment manifested itself across the entire width of the flume, even though the mixing layer only covered a part of the flume width at the crest of the downward slope. In configurations with the second flow state present, separation is present across the entire flume width. Figure 2.4 shows the corresponding time-averaged flow fields.

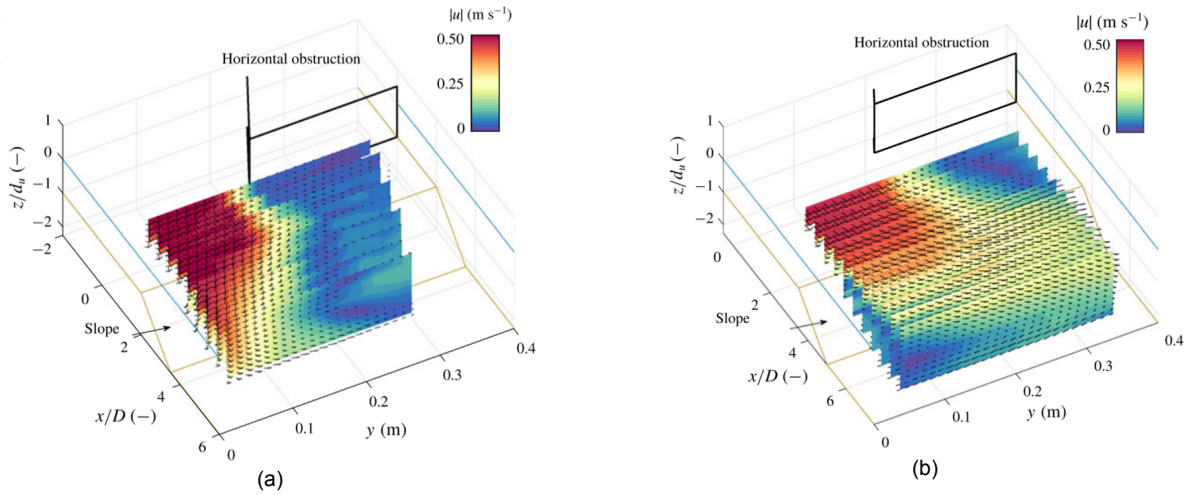

Figure 2.4: Time-averaged flow fields of (a) the horizontally contracting and vertically separated case and (b) the horizontally diverging and vertically attached case, by Broekema et al. (2019).

Figure 2.5 visualises the time-averaged flow velocities near the surface for the horizontally diverging

and vertically attached case. In line with the return current that is associated with vertical flow separation, the near-bed flow at the downward slope is expected to be directed upward. Flow directions measured at upper half of the slope are not in line with this reasoning. This can be explained by the Acoustic Doppler Velocimetry (ADV) measurement technique used. Due to the limitations ADV, the flow was measured at 0.6. The recirculation zone in the upstream half of the slope is too flat to be measured at 0.6 cm. Instead, the top part of the recirculation zone instead of the return current is measured.

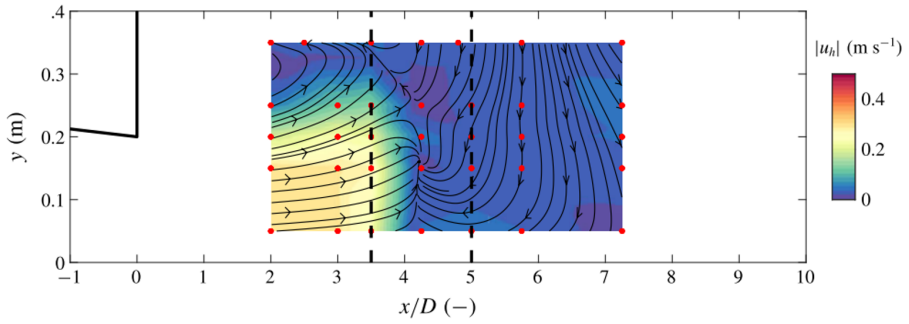

Figure 2.5: Time-averaged flow field near the bed of the horizontally diverging and vertically attached flow state (Figure 2.4 (b)). The location of the slope is marked by the dotted black line. Measurements were conducted at 0.6 cm from the bed using ADV.

In contrast to Broekema et al. (2019), Van der Zande (2018) observed horizontal contraction across the downward slope in all tested configurations. Two distinct vertical flow states could be distinguished: 1) attachment along the entire flume width and 2) attachment in and around the mixing layers in combination with separation in the centre of the jet. Figure 2.6 shows the second flow state. The second flow state was present in cases with steep slopes and long bed protections.

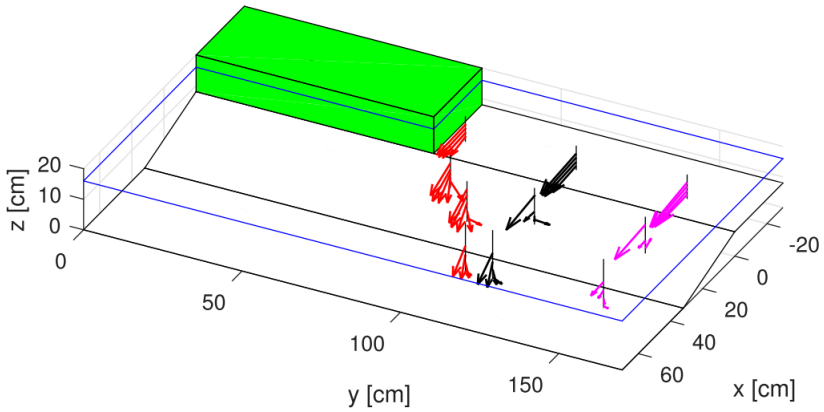

Figure 2.6: Time-averaged flow directions measured by Van der Zande (2018). The red and black arrows show vertical separation to be suppressed in and around the mixing layer, whereas the pink arrows indicate vertical flow separation.

The difference between the full-width flow attachment of Broekema et al. (2019) and the local flow attachment of Van der Zande (2018) can probably be attributed to the shallowness of the tested configuration. Depth-to-width ratios are about a factor ten smaller for the latter. In such shallow conditions, contraction can be considered a 2-D effect. Broekema (2020) experimented in shallow conditions with only a vertical step and no horizontal nonuniformities. Horizontal contraction nevertheless occurred, demonstrating the 2-D character of the mechanism in shallow cases.

2.4 Mixing layers & recirculation zones

Flow behaviour upstream the downward slope plays an important role in the generation of vertical flow attachment. Behind a horizontal expansion, a mixing layer and a recirculation zone forms. This section explains important aspects related to these phenomena.

2.4.1 Mixing layers

A mixing layer forms between two bodies of fluid that move along each other with different velocities. The low-velocity fluid accelerates due to momentum transfer from the high-velocity body. The mixing layer forms the transition between the low-velocity body and the high-velocity body. As it travels downstream, the mixing layer widens and velocity gradients decrease.

Shear stresses in a mixing layer induce severe turbulence. In shallow mixing layers, coherent large-scale 2-D turbulence structures form (Talstra, 2011). 2-D coherent structures (2DCS) are structured vortices that follow the mixing layer while it propagates downstream. A characteristic of 2DCS is that vortices all have the same sign of rotation. Figure 2.7 visualises typical 2DCS.

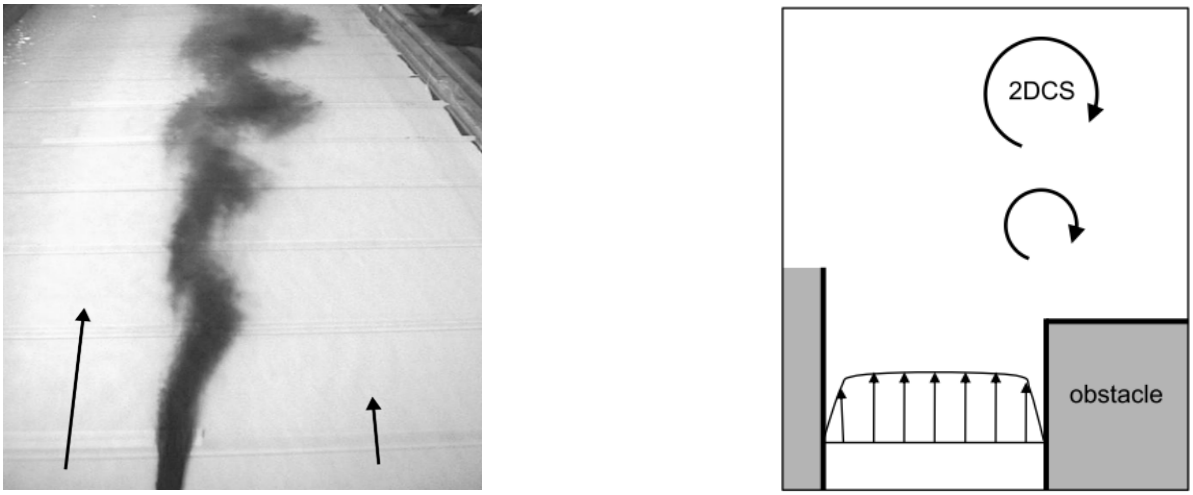

(a) (b)

Figure 2.7: Visualisation of large-scale coherent 2-D turbulence structures by means of (a) dye injection (Van Prooijen, 2004) and (b) a schematisation (Talstra, 2011).

The dominant frequency (f) of 2DCS in a shallow mixing layer ($\mathcal{L} >> H$) is given by the following relation (Talstra, 2011):

$$f = St * \mathcal{U}/\mathcal{L} \tag{2.1}$$

In which:	St	= geometry-dependent dimensionless Strouhal number	[-]
	$\mathcal{L}$	= turbulence length scale	[m]
	$\mathcal{U}$	= velocity scale	[m/s]
	H	= water depth	[m]

One should notice the linear relation between the turbulence length scale and the dominant frequency. The frequency increases proportionally as vortices travel downstream and as the mixing layer widens.

2.4.2 Recirculation zones

Zones of steady recirculating flow, also known as gyres, form behind a horizontal expansion. Recirculation zones develop when the jet-like main flow leaves the confined inflow channel and a mixing layer forms between the horizontally separated flow and the stagnant area. Streamwise momentum is laterally transferred in the mixing layer. A return current provides conservation of mass behind the horizontal expansion, forming the recirculation zone.

Much research is conducted on recirculation zones across flat beds, e.g. by Van Prooijen (2004) and Talstra (2011). Broekema et al. (2019) found strong similarities between their recirculation zones, which develop across a downward slope, and the recirculation zones for flat beds, as defined by Van Prooijen (2004) and Talstra (2011). It is therefore expected that the general characteristics of recirculation zones for flat beds are also valid for recirculation zones across a slope.

In addition to the primary recirculation zone, a secondary gyre can develop (Talstra, 2011). Secondary gyres rotate in the opposite direction of the primary gyre. Whether a secondary gyre forms depends on the local geometry. Development of a secondary gyre takes much longer to develop than a primary gyre. Figure 2.8 sketches a single and a double recirculating zone.

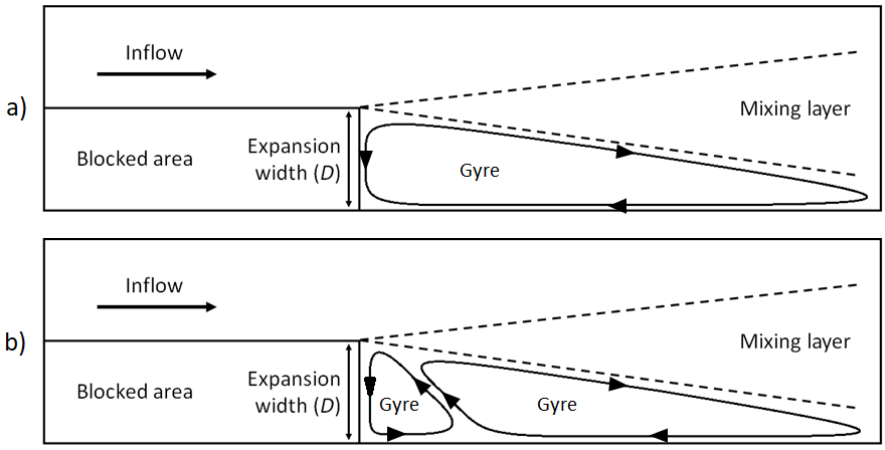

Figure 2.8: Schematisation of a single horizontal recirculation zone (a) and a double horizontal recirculation zone (b) (top view). Adapted from Talstra (2011).

2.5 Scour in nonuniform flow

Broekema et al. (2018) showed that vertically attached flow is associated with more scour than vertically separated flow. Near-bed flow velocities and bed shear stresses drop much quicker in vertically separated flow than in vertically attached flow while the scour hole develops and its depth increases (Broekema et al., 2019). Hence, vertical attachment allows erosion to continue for longer, enabling a deeper scour hole.

2.5.1 Breusers' Method

It is interesting to evaluate how the observed 3-D flow phenomena of Broekema et al. (2019) fit within existing scour prediction methods. The so-called Breusers' method is a widely used method to predict local scour development behind a bed protection. The method is based on conformity of local scour, demonstrated by Breusers (1966). Conformity means essentially that local scour processes are scalable. This enables physical model test results to be transferable to prototypes. The following relation tracks scour development in time:

$$\frac{h_{max}}{h_0} = (\frac{t}{t_1})^{\gamma} \tag{2.2}$$

In which:			
	h_{max}	= maximum scour depth of a scour hole	[m]
	h_0	= water depth at the end of the bed protection	[m]
	t	= time	[s]
	t_1	= characteristic time of the scouring process, time at which h_{max} = h_0	[s]
	γ	= constant, 0.38 for 2-D scour, 0.4-0.8 for 3-D scour (Breusers, 1967, Van der Meulen and Vinjé, 1975)	[-]

Breusers (1967) followed up on these findings and defined the following scaling relation:

$$n_t = n_{h_0}^{2.05} \cdot n_{\Delta}^{1.6} \cdot n_{(U_{max}-U_{crit})}^{-4} \tag{2.3}$$

In which:			
	n_t	= time scale	[-]
	n_{h_0}	= depth scale	[-]
	n_{Δ}	= material density scale	[-]
	$n_{(U_{max}-U_{crit})}$	= velocity scale	[-]

In the following decades Breusers' method was further developed. Van der Meulen and Vinjé (1975) and De Graauw and Pilarczyk (1981) improved its accuracy using more than 250 laboratory and prototype tests. This led to the following prediction relation for the characteristic time:

$$t_1 = \frac{K\Delta^{1,7} h_0^2}{\left(\alpha \bar{U} - U_{crit}\right)^{4.3}} \tag{2.4}$$

In which:			
	K	= dimensionless numerical coefficient, ranging from 250 to 330 (De Graauw and Pilarczyk, 1981, Van der Meulen and Vinjé, 1975)	[-]
	Δ	= relative material density, $(\rho_s - \rho)/\rho$	[-]
	ρ_s	= bed material density	[kg/m^3]
	ρ	= water density	[kg/m^3]
	α	= dimensionless flow factor dependent on turbulence intensity	[-]
	$\bar{U}$	= mean flow velocity at the end of the bed protection	[m/s]
	$\bar{U}_{crit}$	= critical velocity for initiation of motion	[m/s]

Geometry-specific effects are included through factor α. De Graauw and Pilarczyk (1981) determined α as a function of the structure's geometry. This only made the relation applicable in a very specific set of cases. Jorissen and Vrijling (1989) later formulated α as a function of the turbulence intensity at the end of the bed protection, increasing the applicability of the method:

$$\alpha = 1.5 + 5r_0 \tag{2.5}$$

In which:			
	r_0	= relative turbulence intensity, $r_0 = \sigma_{\bar{U}/\bar{U}}$	[-]
	$\sigma_{\bar{U}}$	= depth-averaged standard deviation of $\bar{U}$	[m/s]

Hoffmans and Booij (1993) further optimised Equation 2.5 and included bed roughness, finding the following relation:

$$\alpha_1 = 1.5 + 4.4 r_0 f_C \tag{2.6}$$

In which:	f_C	= friction coefficient, $f_C = C/45$	[-]
	C	= Chézy coefficient	[-]

2.5.2 Scour experiments in a nonuniform flow regime

The question that arises is is whether or not this method can accurately predict scour in a 3-D situation as studied by Broekema et al. (2019). Üsenti (2019) replicated nonuniformity-induced flow attachment in a setup with an erodible bed instead of a fixed bed. No vertical flow attachment was observed by Üsenti. This does not mean that no flow attachement was present since the measurement techniques used were not ideal to observe this flow behaviour.

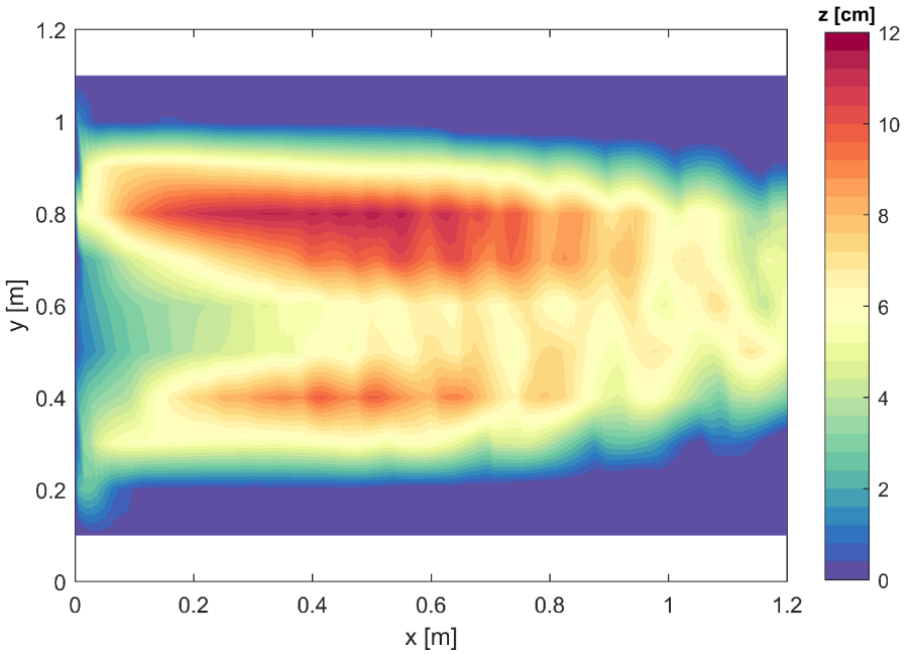

Figure 2.9: Bed profile after being exposed to lateral non-uniform flow. Mixing layers are triggered upstream at x = 0.4 m and x = 0.8 m by a jet-like flow (Üsenti, 2019).

Figure 2.9 shows the bed geometry after being exposed to lateral non-uniform flow. Üsenti (2019) also applied Breusers' method to the cross-section in the centre of the yet (at y = 0.6 m). The development rate of the maximum scour depth roughly matches the predicted scour depths based on the measured characteristic time. Conversely, predictions based on the calculated characteristic time, in which α is based on local turbulence intensities, are far off. Figure 2.10 shows scour depths predicted by Breusers' method using the measured characteristic time (in blue) and a calculated characteristic time (in red). The maximum scour depth is underestimated by almost a factor two for the calculated characteristic time. This comparison would be even more interesting for the centre of the mixing layer at y = 0.8 m, where scour depths are largest. Unfortunately, no measurements on turbulence were conducted here.

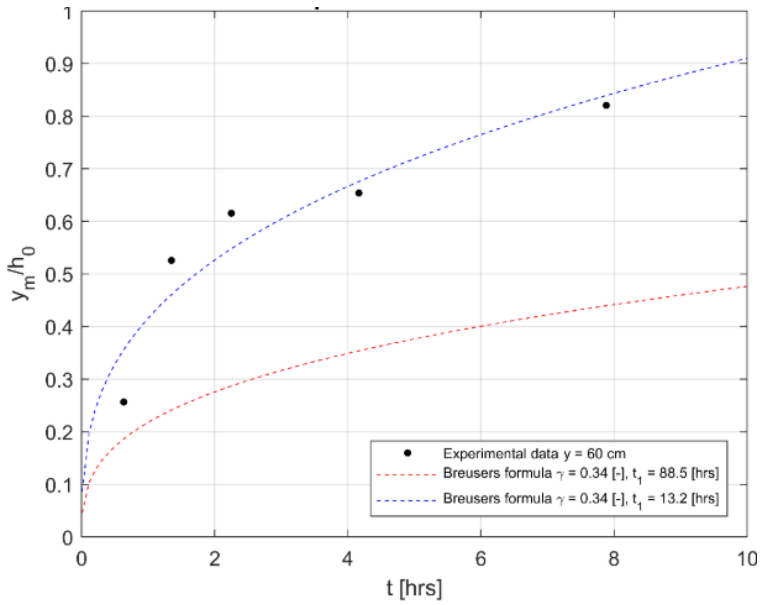

Figure 2.10: The black dots indicate the maximum scour depth in the y = 0.6 m plane by Üsenti (2019). The blue line represents scour estimates of Breusers' method for the measured characteristic time. The red line shows Breusers' scour depth estimate for a characteristic time calculated based on turbulence measurements.

2.5.3 Afsluitdijk physical model tests

BAM Infra is currently involved in the renewal of the Afsluitdijk discharge sluices. Model tests were conducted to get insights into scour development. Figure 2.11 illustrates the resulting bed topography. A strongly 3-D scour pattern was observed. The scour pattern shows strong similarities with the scour pattern observed by Üsenti (2019).

Figure 2.11: Bed topography observed by BAM Infra at the Afsluitdijk model tests (Levvel, 2018).

Figure 2.12: Sketch of the horizontal flow pattern observed by BAM Infra at the Afsluitdijk model tests (Top view), adapted from Levvel (2018).

Considerable contraction of the jet was visually observed at the physical model tests. Figure 2.12 sketches these observations. Near-bed flow velocities were not measured. Scour dimensions were empirically predicted for the sluice complex before conducting the model tests using the plunging jets method of Hoffmans (2009). A significant discrepancy between predicted and observed scour dimensions was present.

3

Parameter analysis

Maximising the likelihood of finding vertical flow attachment, while replicating practice as well as possible, forms the main driver for the design of the experimental setup used in this study. This chapter provides the reasoning process that leads to the parameters present in the experimental setup (methodological step 2).

Firstly, the situation studied is defined by a complete set of parameters relevant, which is subsequently converted into a minimal set of dimensionless parameters using dimensional analysis. Subsequently, the effects of each parameter on the flow state are discussed and arguments for choosing certain parameter ranges are provided.

3.1 Definition sketch of the situation studied

This study considers a simplified situation of reality. Instead freely erodible scour hole, a configuration with a fixed non-erodible bed is considered. A naturally eroded scour would have increased the applicability of the findings in the field, but drastically decreases the likelihood of convincingly identifying something new. A freely erodible bed comes with many uncertainties, which complicates the attribution of observations to specific parameters. Preference is given to maximising the probability of a sound knowledge contribution. Figure 3.1 sketches the simplified version of reality that is being studied.

Firstly, a list of all parameters that are relevant to the situation studied is formed. Each parameter is expressed in the quantities time [T], mass [M] en length [L]. Parameters are divided into three categories: geometric characteristics, material properties and external effects (Munson et al., 2009).

Geometric characteristics

Geometric characteristics have a large impact on the flow behaviour. The relevant geometric parameters are indicated in figure 3.1 and summed up below:

Bed protection length (L_b)	$[L]$
Slope angle (i_b)	$[-]$
Upstream depth (d_u)	$[L]$
Downstream depth (d_d)	$[L]$
Inflow channel width (B)	$[L]$
Expansion width (D)	$[L]$

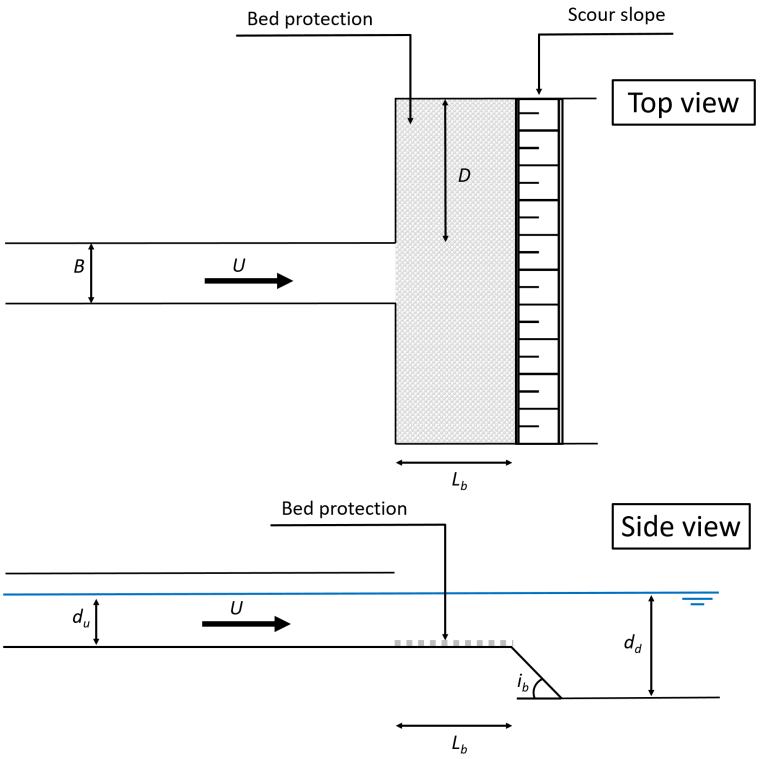

Figure 3.1: Schematisation of the situation of interest (simplified). The flow leaves the hydraulic structure across a bed protection and forms a scour hole. In this study, a fixed downward slope replicates the scour hole. The relevant geometrical parameters are indicated.

Material Properties

In addition to geometric parameters, material properties have an important effect on flow behaviour. Fluid characteristics like viscosity and fluid density are considered. Moreover, characteristics of the confining walls are included, of which only bed roughness has a relevant effect on the flow pattern.

Dynamic viscosity (μ)	$[L^{-1}T^{-1}M]$
Mass density (ρ)	$[L^{-3}M]$
Nikuradse roughness (k_r)	$[L]$

External effects

Externally imposed forces also affect flow behaviour. Considered are the incoming flow velocity and the gravitational acceleration that is imposed on the fluid present in the system.

Flow velocity (U)	$[LT^{-1}]$
Gravitational constant (g)	$[LT^{-2}]$

3.2 Dimensional analysis

The set of absolute parameters is transformed into a set of dimensionless parameters. This enables the comparison of flow states in situations with different dimensions. A useful application is a comparison between the results of experiments on flow attachment in different setups: observations in experiments or in practice can be attributed to the effect of a single dimensionless parameter.

Dimensional analysis is a tool that helps to systematically form a set of dimensionless parameters. A specific method called the Buckingham Pie theorem, which is explained by Hughes (1993), was used in this study. Table 3.1 shows the set of dimensionless parameters formed the dimensional analysis. Since time, mass and length are all three part of the problem, the number of parameters to describe it could be reduced by three Hughes (1993).

No.	Parameter name	Quantities
Π_1	Bed slope	i_b
Π_2	Bed protection length	L_b/d_u
Π_3	Inflow width	B/d_u
Π_4	Horizontal expansion	D/d_u
Π_5	Bed roughness	k_r/d_u
Π_6	Depth increase	d_d/d_u
Π_7	Froude number	$U/\sqrt{gd_u} = Fr$
Π_8	Reynolds number	$\rho UL/\mu = Re$

Table 3.1: List of dimensionless parameters that together describe the problem studied.

3.3 Parameters in relation to flow attachment

This section describes the physical meaning of each dimensionless parameter and its presumed effect on vertical flow attachment. It provides an insight into the parameters that were previously tested and the parameter ranges that are common in practice. The design for the experimental setup is based on these insights. The aim is to optimise between 1) maximising the likelihood of convincingly finding something new, and 2) replicating practice in the best possible way. Each parameter description is finished off with a decision on the preferred parameter range in the experimental setup.

Π_1: Slope gradient (i_b)

As discussed in Section 2.1, slope steepness plays plays an important role in flow attachment. Flow is also more likely to stay attached to gentle slopes. Broekema et al. (2019) and Van der Zande (2018) confirmed that this is also the case when lateral nonuniformities are involved. Broekema (2020) tested slopes varying from 1:2 to 1:5, whereas Van der Zande (2018) varied the slope gradient between 1:4 and 1:6. Vertical attachment was proved to be possible for all slopes between 1:2 and 1:6 given the other parameters were suitable.

In practice, upstream scour slopes are often in the order of 1:2. De Graauw and Pilarczyk (1981) observed a scour slope of approximately 1:2 at the 3-D scour case at the Brouwersdam. At the Rammegors culvert, a scour slope of 1:1.75 was found (Hoffmans and Verheij, 2020a). Likewise, experiments by Üsenti (2019) observed a similar slope angle. Hence, for this study, a fixed 1:2 slope is selected.

Π_2: Bed protection length (L_b/d_u)

The relative distance between the horizontal expansion and the crest of the downward slope in relation to the water depth strongly affects nonuniformity-induced flow attachment, as described in Section 2.2.2. Broekema et al. (2019) and Van der Zande (2018) conducted their experiments with relative bed protection lengths of 1.5-6 and 0-25 respectively.

In this study, the lateral velocity gradient at the top of the downward slope is controlled by the length of the bed protection. Van der Zande (2018), who in line with practice used a shallow setup, observed flow attachment at a 1:4 slope and a bed protection length (L_b/d_u) of 15. Flow attachment is less likely to occur for steeper slopes. The tipping point between flow attachment and flow separation at a 1:2 slope most likely lies somewhere between 5 and 15. Hence, bed protection lengths (L_b/d_u) of 5, 10

and 15 are selected for the experimental setup.

Π_3: Inflow channel width (B/d_u)

The effect of inflow channel width on nonuniformity-induced flow attachment has not been specifically studied before. Broekema et al. (2019) and Van der Zande (2018) conducted their experiments with very different inflow channel widths. The relative width of the inflow channel at the experiments conducted by was 3.3 and 19-38 respectively. This constitutes a difference in the order of magnitude of O(10). Scouring downstream of hydraulic structures in the field often occurs in relatively shallow flows. At the Brouwersdam for example, the relative inflow channel width is approximately 8 (De Graauw and Pilarczyk, 1981).

The inflow channel width (B/d_u) present in this study is varied between 6 and 18 to study their effects on horizontal flow expansion.

Π_4: Expansion width (D/d_u)

Neither the effect of expansion width has been studied in an isolated way. Van der Zande (2018) varied the width of the inflow channel but did not change the width of the flume. Hence, the inflow channel width and the expansion width depended on each other. These experiments demonstrated that the flow was more likely vertically attach for smaller inflow channels/larger expansion widths. This leaves the effect of expansion width on flow attachment not fully understood.

In the field, expansion width varies from very large (e.g. culvert in a wide dam) to very little (e.g. hydraulic structure in a narrow channel, or an outflow that is confined by guide walls).

BAM infra claims that it observes much more horizontal contraction–which is considered to be the driver for vertical flow attachment–at structures with much space to horizontally expand compared to structures with a confined outflow, e.g. guiding walls, BAM Infra observes less horizontal contraction.

Horizontal expansion width (D/d_u) between 3 and 9 are tested in this study to analyse its influence on vertical attachment.

Π_5: Bed roughness (k_r/d_u)

The effect of bed roughness on nonuniformity-induced flow attachment has not been studied before. In case of a smooth bed protection, a logarithmic velocity profile develops across a smooth bed. Logarithmic velocity profiles are characterised by a roughness length (k_r) that mainly depends on the flow velocity (Schiereck and Verhagen, 2012). In case of a rough bed though, the roughness length is shaped by the grain size. Previous studies were conducted with a smooth bed. In practice though, rough bed protections prevail. To ensure comparability with reference studies, a smooth bed is applied here.

Π_6: Increase in water depth (d_d/d_u)

The effect of the relative increase in water depth on the flow state has not been tested before in this context though. Broekema et al. (2019) and Van der Zande (2018) stuck with a constant water depth increase of across their experiments of respectively 2.25 and 2.0. Broekema et al. (2019) argues that the relative water depth increase likely has an effect on the flow state, but does not justify this statement with any experimental proof.

The relative increase in practice depends on the stage of the scouring process. Breusers (1966) defined the characteristic time of the scouring process, in which the relative increase in scour depth is equal to 2.

Π_7: Froude number ($U/\sqrt{gd_u}$)

The ratio between the influence of inertia versus the influence of gravity in a flow is expressed by the Froude number. In the field, critical and subcritical regimes both occur. Previous experimenters on this topic were conducted in a subcritical flow regime (Fr < 1).

In case of Froude numbers close to 1, standing surface waves tend to develop, which affects measurements (Van Prooijen and Uijttewaal, 2002). Van der Zande (2018) experimented with different Froude numbers, and found a Froude number of 0.42 to be the minimum value in which no surface disturbances are visible in his setup. This is in line with Van Prooijen and Uijttewaal (2002), who state that a maximum Froude number of 0.50 is required to prevent surface disturbances from happening.

Meanwhile, a low Froude number is neither desirable since is it implies a lower flow velocity, which leads to a less turbulent flow regime (in a setup with fixed dimensions). A Froude number of 0.42 guarantees a sufficiently turbulent flow though.

Π_8: Reynolds number ($\rho UL/\mu$)

The Reynolds number expresses the ratio between inertial and viscous forces in a flow regime. Due to scaled-down water depths and flow velocities, Reynolds numbers in the field are by definition not reproducible in a laboratory setting. This is not troublesome as long as inertia sufficiently dominates viscosity for the flow to be fully turbulent. Flow can be regarded fully turbulent in case the Reynolds number exceeds 4000 (Van Prooijen and Uijttewaal, 2002). A fully turbulent flow state was present in previous experiments on nonuniformity-induced flow attachment.

Overview of the selected parameter ranges

Table 3.2 provides an overview of the selected parameter ranges that form the basis for the design of the experimental setup in the next chapter.

No.	Dimensionless parameter	Units	Parameter values	Allowed deviation
Constant parameters				
Π_1	Bed slope	i_b	1:2	1%
Π_5	Bed roughness	k_r/d_u	$O(10^{-5})$	N/A
Π_6	Depth increase	d_d/d_u	2	1%
Π_7	Froude number	$U/\sqrt{gd_u} = Fr$	0.42	5%
Π_8	Reynolds number	$\rho UL/\mu = Re$	> 4000	N/A
Variable parameters				
Π_2	Bed protection length	L_b/d_u	5, 10, 15	1%
Π_3	Inflow width	B/d_u	6, 12, 18	1%
Π_4	Horizontal expansion	D/d_u	3, 6, 9	1%

Table 3.2: List of the dimensionless parameters and their selected paramter ranges.

4

Laboratory experiments

Laboratory experiments were conducted to answer the main research question of this study. This chapter presents the experimental design (methodological step 3). The experiments took place in the Hydraulic Engineering Laboratory at Delft University of Technology. The is presented and its specifics are discussed, a list of all tests conducted is provided, and the techniques used to measure the flow characteristics of interest are introduced.

4.1 Experimental setup

The testing setup is based on the set of requirements summarised in Table 3.2. This section presents the setup design and motivates design decisions.

Setup overview

A 7 m long, 1.2 m wide and 0.23 m deep flume formed the basis of the testing setup. The flow entered the setup through a set of flow straighteners and an inflow channel. A set of floating foam plates right behind the flow straighteners reduced surface waves. A false bed with a height of 10 cm served as the bottom of the inflow channel and a horizontal expansion zone. Here, a jet-like flow coming out of the channel developed a horizontal mixing layer behind the horizontal expansion. A fixed slope with a 1:2 gradient was installed in the setup. A flow depth of 20 cm was maintained in the flow, meaning a flow depth across the false bed of 10 cm. Figure 4.1 shows a sketch of the experimental setup.

Asymmetrical setup

Instead of having an inflow channel in the centre of the flume (symmetrical, two-sided horizontal expansion), only half the situation was considered in a setup with one-sided expansion. Two main reasons underlie this decision. First, one-sided testing allows for more efficient usage of the horizontal space in the flume. The width of the flume is limited, while the effect of the horizontal expansion width is one of the variables that is being studied. By considering only half the situation effectively twice the horizontal space is available. As a result, the width in the flow was used more efficiently. Prevent disturbances caused by the Coanda effect is another reason to choose for asymmetrical testing. In case of symmetrical expansion, the Coanda effect causes the jet to tend towards one side of the flume, causing asymmetry in the jet (Kantoush and Schleiss, 2009). This would frustrate the collection of consistent measurements and complicate their interpretation. Asymmetrical testing prevents these complications from occurring. One-sided testing can only be applied in case wall effects are negligible, which was

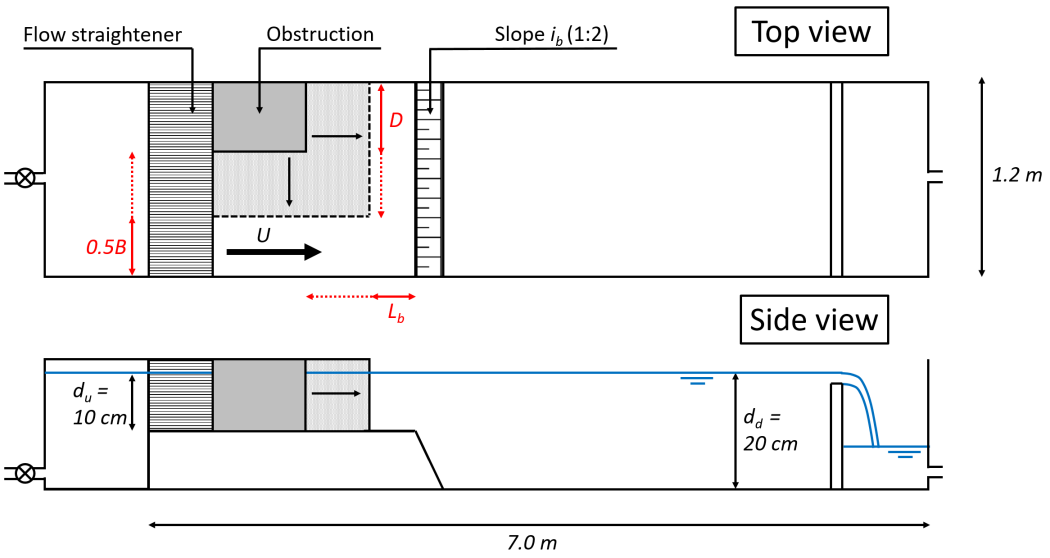

Figure 4.1: Sketch of the experimental setup (not to scale). Variable parameters are shown in red. L_b, D and 0.5B represent the distance between the horizontal expansion and the downward slope, the width of the horizontal expansion, and the width of the inflow channel respectively. d_u and d_d illustrate the upstream and downstream water depth respectively.

expected to be the case.

Inflow channel length

It is important to work with sufficiently developed flow at the horizontal expansion. It not only ensures the generalisability of the findings, but it is also required to not distort flow attachment observations: a badly developed boundary layer is expected to increase the likelihood of flow separation (Talstra, 2011). Several measures were taken to ensure reasonable flow uniformity: 1) the flow entered the channel through a set of flow straighteners, and 2) the minimum length of the inflow channel was at least ten times the flow depth (1 m). To ensure full development of the flow, it one should ideally use an even longer inflow channel. This is not viable since it would reduce the space in the remaining part of the flume. This space is important because it expected to influence the ability of horizontal recirculation zones to develop, which is one of the effects studied. Broekema (2020) found that the recirculation zone requires about eight times the expansion width (D) to fully develop. This amount of space is not available for configurations with a large horizontal expansion (e.g. D = 0.9 m). A trade-off between uniformity at the end of the inflow channel and space for recirculation zones to develop led to the current setup.

Inflow channel width

A constant inflow channel width (B/d_u) is desired in all experiments. However, since the width of the flume is fixed, adjusting the expansion width to answer the second research questions automatically also adjusts the width of the inflow channel. A longitudinal barrier across the entire length of the flume was used to modify the effective inflow channel and keep it constant.

Reynolds and Froude numbers

To obtain a Froude number of 0.42 in this setup, a flow velocity of 0.42 m/s should be maintained. With a dynamic viscosity (μ) of approximately 1 Pa·s (=kg/(m·s)) and a mass density of 10^3 kg/m^3, Reynolds numbers in the order of O(10^4) are expected. The flow can thus be considered fully turbulent (>4000).

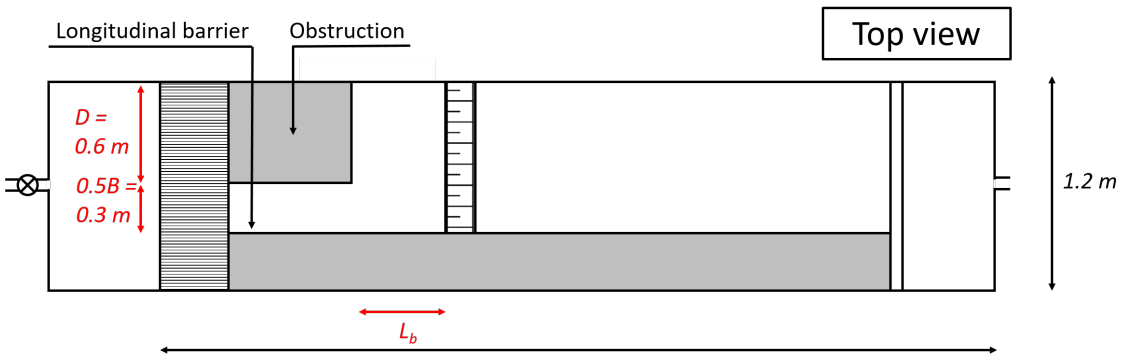

Figure 4.2: Top view sketch of one a configuration that makes uses of a longitudinal barrier (not to scale).

4.2 Experimental runs

Table 4.1 gives an overview of the configurations tested.

Test No.	L_b/d_u	L_b [m]	D/d_u	D [m]	$0.5B/d_u$	$0.5B$ [m]
0			No horizontal expansion			
1.1	5	0.5	3	0.3	9	0.9
1.2	5	0.5	6	0.6	6	0.6
1.2.B	5	0.5	6	0.6	3	0.3
1.3	5	0.5	9	0.9	3	0.3
2.1	10	1.0	3	0.3	9	0.9
2.1.B	10	1.0	3	0.3	6	0.6
2.2	10	1.0	6	0.6	6	0.6
2.2.B	10	1.0	6	0.6	3	0.3
2.3	10	1.0	9	0.9	3	0.3
3.1.B	15	1.5	3	0.3	6	0.6
3.2	15	1.5	6	0.6	6	0.6

Table 4.1: Overview of the experimental runs conducted in the context of this study. The first two numbers relate to bed protection length and horizontal expansion width respectively. The letter B is added for tests in which a longitudinal barrier limits the flume width

4.3 Coordinate system

Figure 4.3 illustrates the coordinate systems used in this study. A tilted secondary coordinate system using x' and y' is defined for the downward slope. Flow velocities in x, y, z, x' and y' direction are expressed by u, v, w, u' and w' respectively.

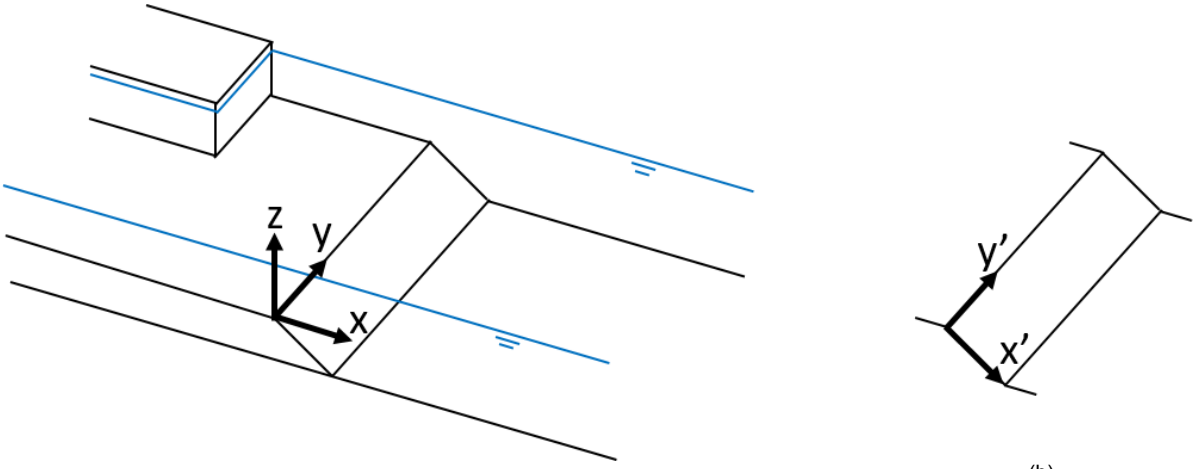

(a) (b)

Figure 4.3: Definition of the coordinate systems used: (a) shows the main coordinate systems, and (b) shows the derived coordinate system for the downward slope.

4.4 Measurement techniques

Several measurement techniques were used to visualise the flow characteristics in the experiments. Quantitative as well as qualitative methods were used. The measurement techniques used are discussed in this section.

4.4.1 Dye flow visualisation

Dye injection is a quick method to gain first insights into flow behaviour. Dye nicely follows the streamlines of the flow but disperses quickly in turbulent flow regimes. Dye was injected near the slope's bed to get a first impression of the vertical flow state. Vertical flow attachment causes the dye to disperse downstream, whereas flow separation induces upward near-bed flow. Dye was also injected in and around the mixing to get an idea about mixing layer development and horizontal recirculation zones. Observations were captured using cameras.

4.4.2 Tuft flow visualisation

Within the context of this study, a measuring technique was developed to measure near-bed flow directions across an entire flow field. The method uses little threads that follow the flow direction called tufts. A total of 80 tufts, in 4 rows of each 20 tufts, were maintained throughout the experiments. Chapter 5 describes the specifics of the measurement technique.

4.4.3 Acoustic Doppler Velocimetry (ADV)

Acoustic Doppler Velocimetry (ADV) is a measurement technique that makes use of acoustic signals reflected by submerged particles to determine local flow velocities. A side-looking fixed stem Nortek Vectrino measuring device was used. It measures flow velocity at 50 mm from the probe. Samples were taken in a frequency of 25 Hz. Submerged clay particles seeded the Vectrino. Flow velocities measured during a measuring run were averaged to remove the effect of turbulence and find average flow velocities.

ADV is used to determine the time-averaged flow velocity in and around the mixing layer. The depth-averaged velocity in a logarithmic velocity profile is present at 0.4 times the water depth (Schiereck and Verhagen, 2012). Time-averaged velocities at 0.4 times the water depth were measured at intervals of 5 or 10 cm across the width of the flume. Moreover, ADV measurements were applied at approximately 1 cm from the slope's bed. A smaller distance was not possible due to the upward the probe's arm hitting the upward slope.

Outlier filter

Raw ADV-measured data contain outliers. A Hampel filter was used to identify and replace outliers (Pearson, 1999). A Hampel filter uses a sliding window that consists of a predetermined amount of data points at each side of the evaluated data point:

$$w_k = [x_{k-K}, \dots, x_k, \dots, x_{k+K}] \tag{4.1}$$

In which: w_k = window
K = data points in a window
x_k = evaluated data point

The median and the median absolute deviation (MAD) of the selected data window are determined and lead to an estimator of the standard deviation for Gaussian data sequences S_k:

$$S_k = \lambda \operatorname{med}\left\{\left|x_{k-K} - x_k^\dagger\right|, \dots, \left|x_{k+K} - x_k^\dagger\right|\right\} \tag{4.2}$$

In which: $x_k^\dagger$ = median value of the selected window
λ = scale factor for Gaussian distribution (= 1.4826)

If a data point differs more than a predetermined threshold from the median, it is considered to be an outlier and replaced by the median.

$$y_k = \begin{cases} x_k & \left|x_k - x_k^\dagger\right| \le tS_k \\ x_k^\dagger & \left|x_k - x_k^\dagger\right| > tS_k \end{cases} \tag{4.3}$$

In which: t = threshold value

A window size of K = 10 and a threshold value of t = 2.5 were used to filter the ADV data. Figure 4.4 shows both the filtered and unfiltered data of a small window of ADV measurements.

Noise filter

Despite outliers being filtered out by the Hampel filter, the signal still carries quite some high-frequency noise. For flow velocity plots a Wiener filter was applied to remove undesired deviations. The Wiener filter is based on minimising the mean square error of a sliding window with a predefined size. A window size of 10 was iteratively determined. The in-build function of the Wiener filter in SciPy (Python) was used. Figure 4.5 presents a Wiener-filtered measurement series in contrast to the outlier-filtered data.

4.5 Frequency spectrum analysis

Frequency spectrum analysis was carried out on the near-bed ADV measurements at the downward slope. To find the power density spectra of the velocity measurements, Welch's method was applied

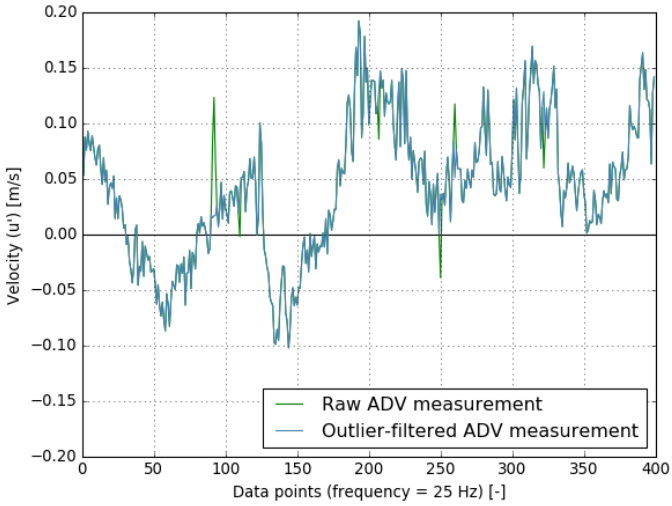

Figure 4.4: Limited window of an ADV measurement. Raw and filtered data can be distinguished (Test 2.2, x' = 0.112 m, y' = 0.625 m).

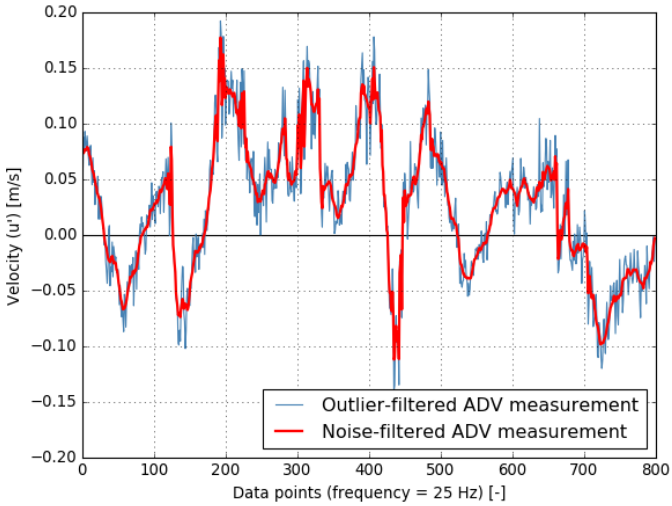

Figure 4.5: Extended window of the ADV measurement of Figure 4.4, including the velocity data after applying the Wiener filter (Test 2.2, x' = 11.2, y' = 62.5)

(Welch, 1967). In addition to a standard Fourier transform, which applies to an entire data set, Welch's method divides the data set in successive blocks and takes a Fourier transform of each data block. The resulting power spectra are averaged, resulting in a much smoother power spectrum. The analysed ADV-collected data sets consisted of 10,000 samples each, which were subdivided into blocks of 1500 samples. The analysis was carried out using the in-build function of Welch's method in SciPy (Python).

Figure 4.6 presents an u'-spectrum on a double-logarithmic scale. The descending line is typical for a turbulence spectrum. Note the -7/3 power law. This is steeper than the −5/3 power law of Kolmogorov for homogeneous turbulence (Nieuwstadt et al., 2015). As a reference, the spectrum of the lateral flow component v at the slope's crest is also provided (Figure 4.7). In contrast to the spectrum of u', the v-spectrum does contain the expected -5/3 power law. This confirms that the data are suitable for frequency analysis. Flattening of the curve for higher frequencies indicates white noise, which means that these frequencies are not suited for analysis.

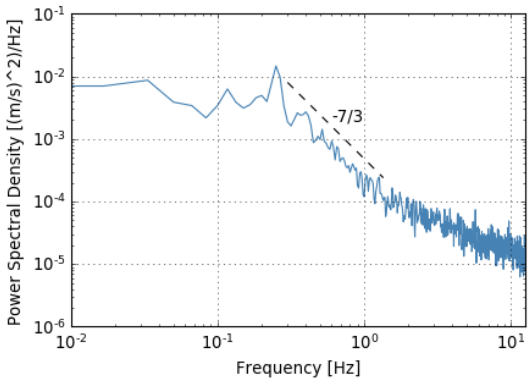

Figure 4.6: Double-logarithmic power density spectrum of u' in the centre of the mixing layer halfway the downward slope (Test 2.2)

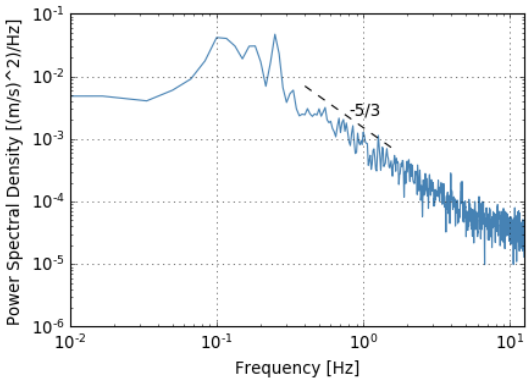

Figure 4.7: Double-logarithmic power density spectrum of v in the centre of the mixing layer at the slope's crest (Test 2.2)

The double-logarithmic scale makes it difficult to identify energy peaks. Hence, an alternative scale is used with a logarithmic horizontal axis and a linear vertical axis that is multiplied with the corresponding frequency, which is optimal for energy peak identification. Here the area under the spectrum is proportional to the amount of energy in that frequency band. Figure 4.8 shows an example.

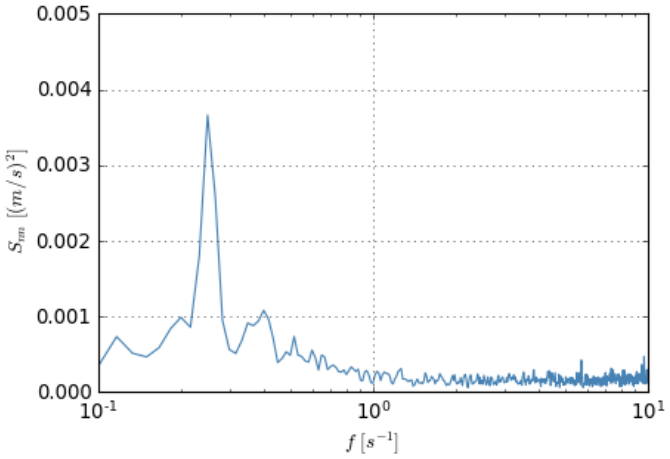

Figure 4.8: Semi-logarithmic plot of the power density spectrum multiplied by the corresponding frequency of u' in the centre of the mixing layer halfway the downward slope (Test 2.2).

5

Development of a near-bed flow visualisation technique

As indicated in the introduction of this thesis, no measurement technique was available at the Hydraulic Engineering Laboratory of Delft University of Technology that enables visualisation of near-bed flow at a slope in both efficiently and reliably. This chapter describes the development and functioning of a near-bed flow visualisation technique that meets these requirements. It is part of the experimental setup design (methodological step 3).

5.1 Basic principles of tuft measuring

The presence of either vertically attached flow or vertically separated flow at a downward slope can be easily inferred from the near-bed flow direction. In case of flow attachment, one expects a downward near-bed flow, whereas, in case of separating flow, a return current is present that corresponds with an upward near-bed flow. So far though, it has been challenging to reliably and efficiently determine the near-bed flow direction. So-called tuft flow visualisation is expected to have the potential to overcome these challenges. Tuft flow visualisation finds its origin in aerodynamics. Little strings attached to a surface visualise near-surface air flows. Figure 5.1 shows an example of tuft flow visualisation on a winglet by NASA (1979).

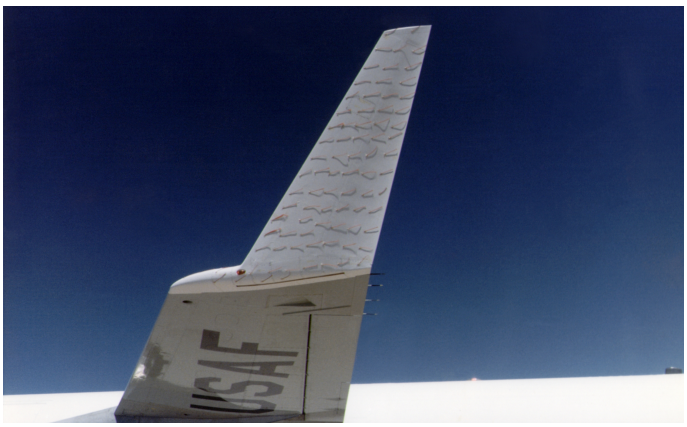

Figure 5.1: Tuft airflow visualisation on an aeroplane winglet by NASA (1979).

The same principle was applied in this study to visualise near-bed flow directions. Little strings follow and visualise the near-bed flow direction at the slope. A camera was used to capture the orientation of the strings over time. Subsequently, the video footage was converted to numerical data on string orientation using a video processing algorithm. Figure 5.2 gives an impression of the measurement setup.

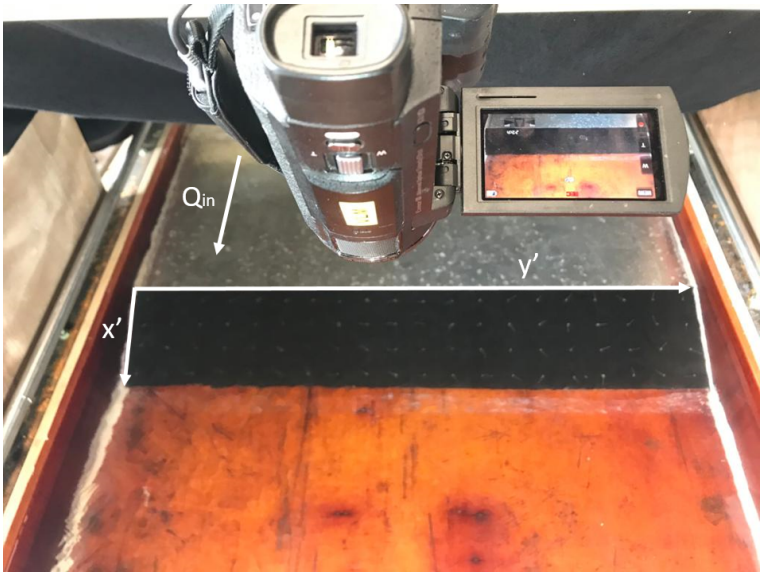

Figure 5.2: Picture of the tuft measuring setup. A secondary coordinate system (x' and y') was applied to indicate locations on the slope. Q_{in} shows the main flow direction.

5.2 Tuft design

Multiple alternative tuft designs were tested before a tuft was found that moves frictionless underwater and does not float. The selected tuft consists of 2 cm long sewing thread (0.2 mm thick) with a 2.5 mm loop at the end. The loop is attached to a nail (1 mm pole thickness, 2 mm head width) that protrudes 3 mm from the bed. Figure 5.3 shows a close-up picture of one of the tufts used.

Figure 5.3: Close-up picture of the final tuft design.

5.3 Video processing

The experiments were recorded with a Sony FDR-AX33 camera, 4k resolution at 25 frames per second. A video processing algorithm was iteratively developed to identify tuft orientations from video frames. The basic principles behind this algorithm are briefly described:

1. The OpenCV library in Python converts video footage to arrays of pixel values.
2. Within an array, the locations of the nails are located. The nail heads were painted bright green to make them easily identifiable.
3. A Region of Interest (ROI) is defined for each tuft. Each ROI contains the pixels that lie within reach of the corresponding tuft.
4. Within each ROI the locations of the pixels that exceed a certain whiteness threshold are indicated. The pixel furthest away from the nail is selected. The angle between the centre of the nail and this pixel indicates the tuft angle. Figure 5.4 shows a screenshot of a control video in which the identified tuft angle is plotted on top of the actual video footage. It was made to check the quality of the generated data.
5. The previous steps are repeated for each tuft in each frame. This yields a data set of tuft angles for each tuft for each frame.
6. Several measures are taken to minimise outside disturbances. Black sheets covered the flume to prevent reflecting light and submerged and floating particles in the water were actively removed.
7. Despite these measures, the method stays sensitive to errors. An improvised filter removes flawed measurements from the data set. Whenever the measured tuft angle increases or decreases by more than 20 degrees across two consecutive frames, the measured angle is removed from the data set.

Figure 5.5 shows the tuft angles generated by the algorithm. The method is not flawless, but sufficient test run duration ensures that the effect of flawed measurements shrinks into insignificance.

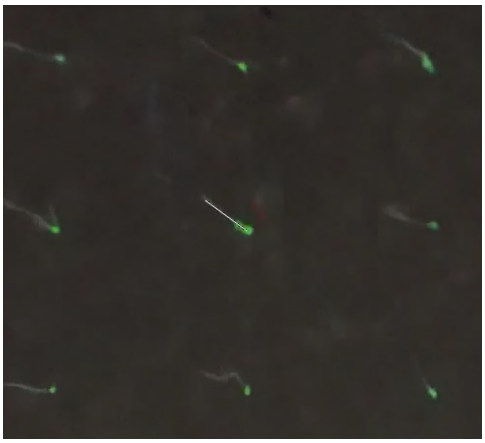

Figure 5.4: Screenshot from a video made to check whether the processed angles match the actual tuft movement. A white line representing the actual angle is projected on the video footage from the tufts.

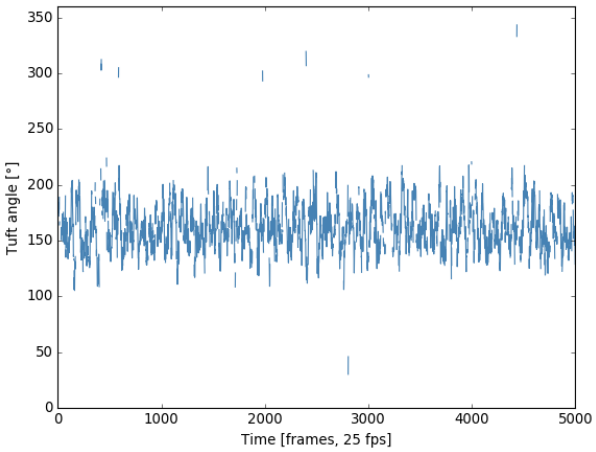

Figure 5.5: Graph of the development of a tuft angle over time after step 7 (Test 1.2, x' = 0.084 m, y' = 0.39 m). Still some slight irregularities are visible. However, since the error rate is small and the measurements are averaged before being presented (Section 5.4), the effect of the remaining irregularities is expected to be negligible.

5.4 Visualisation techniques

Three different figure types were used to present the measurements in an insightful way. Each visualisation technique uses the Cartesian convention, i.e. the direction an arrow points at corresponds to the flow direction.

1. **Time-averaged visualisation:** Arrows indicate the time-averaged flow direction at each tuft's location (Figure 5.6). This enables quick recognition of flow patterns and clear comparison between multiple tests. A major shortcoming of this visualisation technique is its lack of nuance. It does not differentiate between a highly turbulent flow and a constant flow.

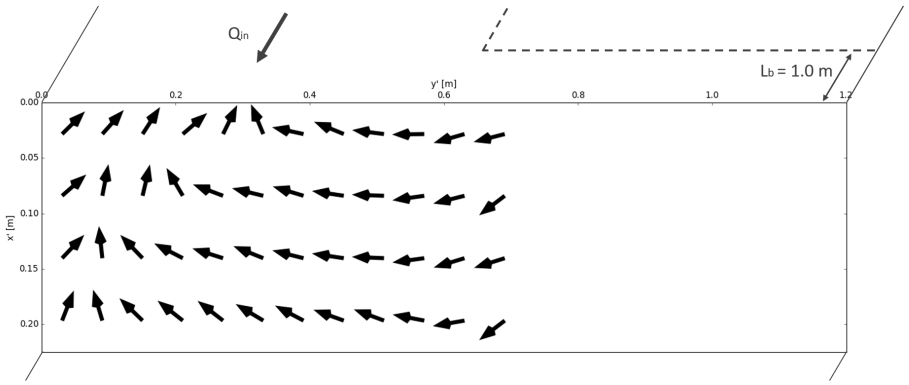

Figure 5.6: Visualisation of the time-averaged near-bed flow direction (Test 2.2)

Given its circular nature, a mean angle cannot be calculated by simply dividing the sum of the individual angles by the number of angles. Instead, each angle is converted into a vector. All vectors are summed up and the angle of the resulting vector is calculated, finding the mean angle. This method is explained in more detail by Watson (1983).

2. **Distribution visualisation:** Multiple arrows visualise common and less common flow directions (Figure 5.7). Arrow size corresponds to the prevalence of the corresponding angle. The circle is divided into sections represented by a total of 32 arrows. Each angle is located in the middle of the range it represents. The resulting image provides a comprehensive overview of flow behaviour.

   A comparison between Figure 5.6 and Figure 5.7 reveals the added value of distribution visualisation. Look for example at the flow at X' = 33.0 cm, Y' = 19.6 cm. The time-averaged flow direction is barely present.

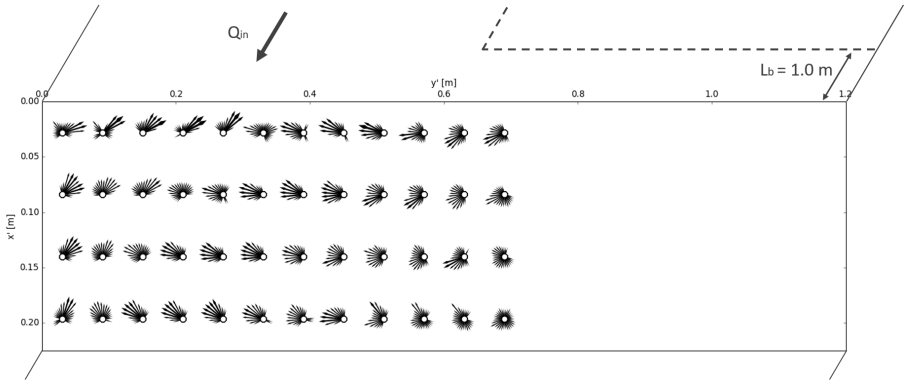

Figure 5.7: Visualisation of the distribution of near-bed flow directions (Test 2.2). Arrow size indicates the frequency of occurrence.

Additionally, consistent measurement errors are highlighted by this visualisation technique. The filter removes outliers from the data but is not able to get rid of the effects of stationary debris lying at the bed. In case debris are present for a significant amount of time during a measurement run, an inexplicable spike in the distribution visualisation shows up. This alerts the researcher that something went wrong during the experimental run.

3. **In-depth visualisation at a single location:** This technique visualises the distribution of flow directions at a single location, which allows for in-depth flow comparison at a specific location across several tests. It is comparable to the way a wind rose visualises wind directions. Figure 5.8 shows an example.

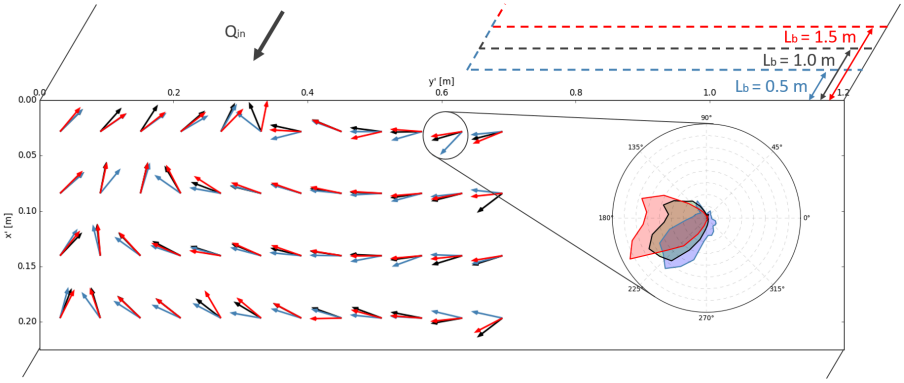

Figure 5.8: Detailed visualisation of the time-averaged flow direction in Test 1.2, 2.2 and 3.2. The flow rose provides a detailed comparison of the flow direction at x' = 0.028 m, y' = 0.6 m.

In the majority of the cases, only a part of the slope is visualised. Near-bed flow velocities leeward of the obstruction are often insufficient to sustain frictionless tuft movement, and hence do not provide reliable measurements.

5.5 Run duration

The optimal test duration of 45 minutes was iteratively determined. Such duration guarantees the flow distribution is fully mapped. As the test method in its current form lacks robustness, an additional 10-minute verification run was conducted for each test. The results of both runs were compared for significant deviations for one or more tufts. In case deviations were found, the source video was studied, and the flaw was being dealt with.

5.6 Validation

The soundness of the measurement technique was validated using ADV. The time-averaged flow directions were compared with ADV-measured flow directions (Figure 5.9). Both measurement techniques yield very similar flow patterns. A small discrepancy can be found for the upper tufts, where ADV measurements show slightly more downward flow. Note that the ADV measurements are taken at approximately 1 cm from the bed, whereas the tufts are located right at the bed.

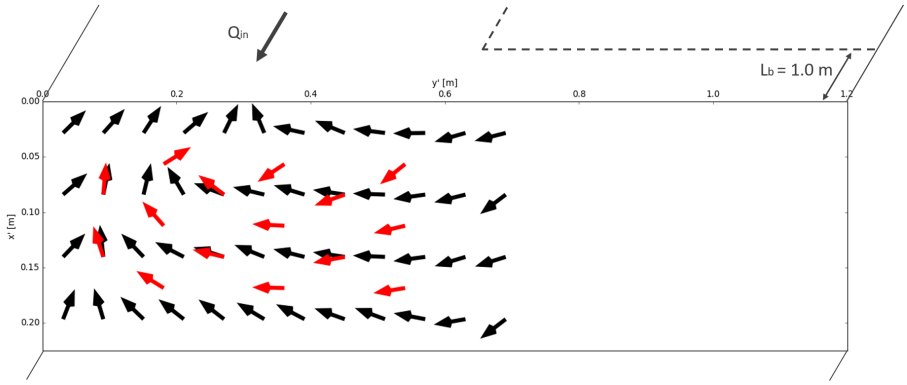

Figure 5.9: Comparison between tuft-measured near-bed flow directions in black and ADV-measured flow directions at about a centimeter from the slope's bed in red (Case 2.2)

5.7 Tufts vs ADV for near-bed flow characterisation

Especially in shallow flumes with flat recirculation zones, tuft measurements proved superior to ADV in determining near-bed flow directions. Tufts measure the flow direction at the slope's bed, whereas ADV cannot approach the bed closer than 0.5 to 1 cm. This makes a notable difference, particularly right behind the slope's crest. Recirculation currents can be very flat here. Hence, overshooting flow can severely affect measurements at 0.5 to 1 cm. Significant differences between tuft-measured and ADV-measured flow directions can arise. Broekema et al. (2019) experienced these exact disparities for a vertically separating case (Figure 2.5).

In addition to an improved determination of flow directions near a bed surface, tuft measuring also offers the possibility to quickly visualise near-bed flow directions of an entire flow field. Especially in the exploring stages of a study, this brings large benefit to a researcher. A large number of configurations can be efficiently tested and compared.

Also, a few points of attention are related to tuft measuring. The nails that hold the tufts increase bed roughness. Added roughness might increases the pressure gradient at the downward slope, introducing a suppressing effect to flow separation, causing the flow to stay attached for longer. This effect is expected to be small in most cases due to relatively small nails compared to the depth of the flume. The effect of increased roughness is expected to be more significant in very shallow setups. In addition, an obvious drawback of tuft measuring is its inability to measure flow velocities. In case these are desired, one cannot rely on tuft measuring.

6

Experimental results and analysis

This chapter describes the results of the experiments that were carried out in the context of this study (methodological step 4). Firstly, the two observed flow states are introduced, followed by an analysis of the geometry parameters required for each of the flow states to occur. Thereafter, a detailed analysis of the flow behaviour that relates to each flow state is provided, including an analysis of the near-bed flow at the downward slope.

6.1 Observed flow states

Based on ADV measurements, dye flow visualisation and tuft flow visualisation, three distinct macro-level flow states could be explicitly distinguished across the twelve experimental runs that were conducted in the context of this study.

Flow state 0: Reference case

During this reference case, no lateral nonuniformities were present. Figure 6.1 provides a qualitative sketch of the flow. Figure fig:visor0 shows the corresponding near-bed flow directions. The near-bed flow at the slope is directed upward, which corresponds to a return current that is associated with vertical flow separation.

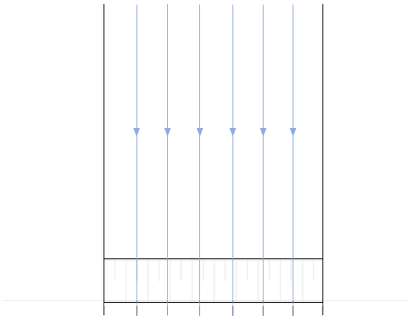

Figure 6.1: Qualitative sketch of depth-averaged and time-averaged flow in flow state 0. The sketch is based on ADV measurements and visual observations.

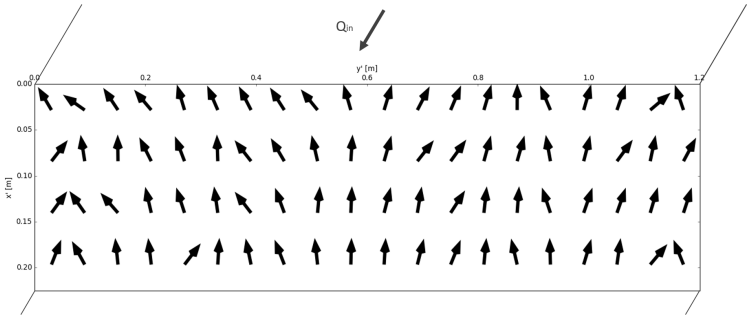

Figure 6.2: Time-averaged flow directions near the bed of the downward slope observed of flow pattern 0 (Test 0).

Flow state 1: Horizontal contraction

The qualitative sketch of the depth-averaged flow in Figure 6.3 demonstrates horizontal contraction towards the high-velocity side across the downward slope. In addition, the recirculation area extends over the slope. Figure 6.4 shows contraction is also visible near the slope's bed, except for the leftmost part of the slope, where the flow direction is upward.

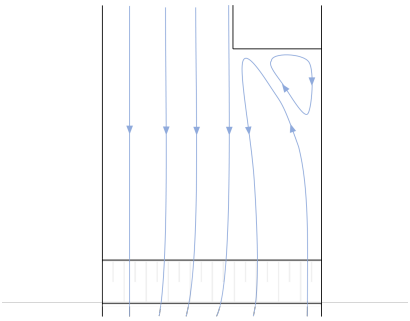

Figure 6.3: Qualitative sketch of the depth-averaged and time-averaged flow of flow state 1. The sketch is based on ADV measurements and visual observations.

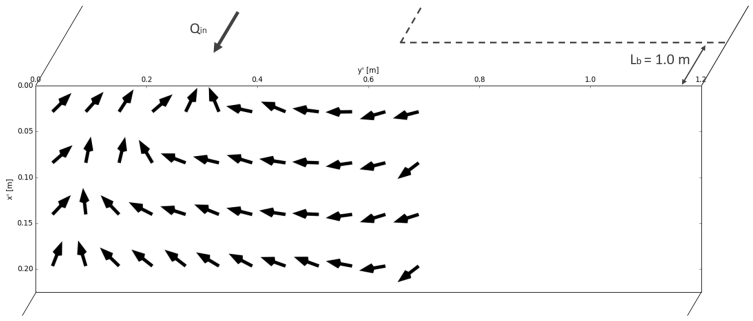

Figure 6.4: Time-averaged flow directions near the bed of the downward slope observed for flow state 1 (Test 2.2).

Flow state 2: Horizontal divergence

Figure 6.5 sketches flow behaviour that strongly differs from flow state 1. The mixing layer strongly deflects to the low-velocity side. The near-bed flow direction at the slope is predominantly directed opposite to the main flow direction (6.6).

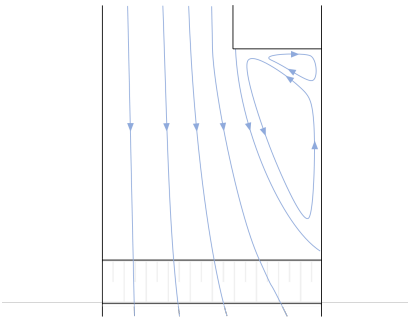

Figure 6.5: Qualitative sketch of the depth-averaged and time-averaged flow of flow state 2. The sketch is based on ADV measurements and visual observations.

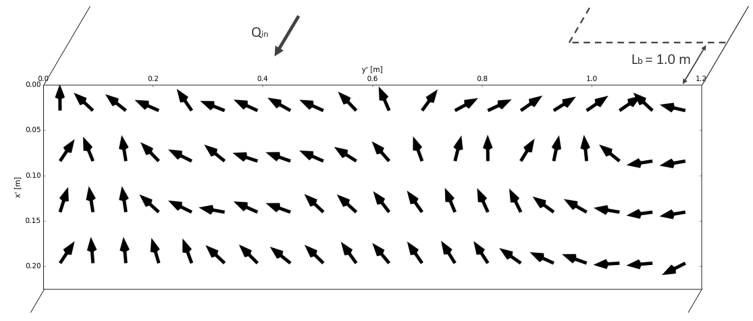

Figure 6.6: Time-averaged flow directions near the bed of the downward slope observed for flow state 2 (Test 2.1).

The characteristics of flow state 1 and flow state 2 are further reviewed later in this chapter. During all tests except the reference case, either flow state 1 or flow state 2 two was convincingly present. No transition zone between both flow states was observed. A full transition between both flow states can be induced by a minimal configuration adjustment.

6.2 The effect of geometry parameters on the flow state

The present flow state was determined based on the tuft-measured near-bed flow directions. Table 6.1 points out the flow state for each configuration that was tested. Appendix B provides the underlying

tuft-measured flow directions of all tests.

Test No.	L_b/d_u	D/d_u	$0.5B/d_u$	Flow state
0		No horizontal expansion		Flow state 0
1.1	5	3	9	Flow state 1
1.2	5	6	6	Flow state 1
1.2.B	5	6	3	Flow state 1
1.3	5	9	3	Flow state 1
2.1	10	3	9	Flow state 2
2.1.B	10	3	6	Flow state 1
2.2	10	6	6	Flow state 1
2.2.B	10	6	3	Flow state 1
2.3	10	9	3	Flow state 1
3.1.B	15	3	6	Flow state 2
3.2	15	6	6	Flow state 1

Table 6.1: Overview of tested configurations and the flow state that was observed. Identification of the flow state is based on insights presented in Appendix B and Figure 6.15, and on visual observations.

The tested configurations were selected in a way that the effect of each parameter on the flow state could be individually studied. The results of two tests with different flow states are compared for each parameter. The only differing parameter between the compared tests is the parameter that is being studied. Hence, the shift in flow state can be fully attributed to the studied parameter, and a first indication of the turning point is obtained. Geometry parameters bed protection length (L_b/d_u), expansion width (D/d_u) and inflow channel width (B/d_u) are discussed one by one.

Effect of bed protection length (L_b/d_u) on the flow state

Figure 6.7 compares two tests with different bed protection lengths. Test 2.1.B corresponds to flow state 1, whereas flow state 2 was present during Test 3.1.B. From this comparison can be inferred that bed protection length is positively related to the likelihood of the flow state 1 occurring.

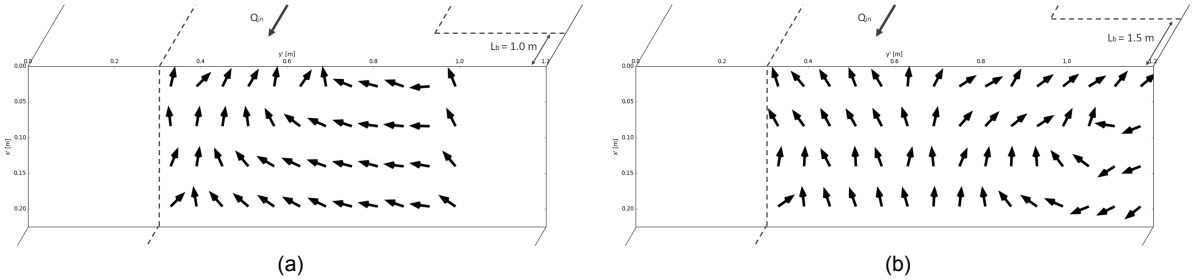

(a) (b)

Figure 6.7: Time-averaged flow directions of (a) Test 2.1.B and (b) Test 3.1.B.

In contrast, Figure 6.8 compares near-bed flow directions of three tests that all resemble the same flow state (flow state 1). L_b/d_u varied between 5, 10 and 15. The differences in flow behaviour between the three tests are notably small.

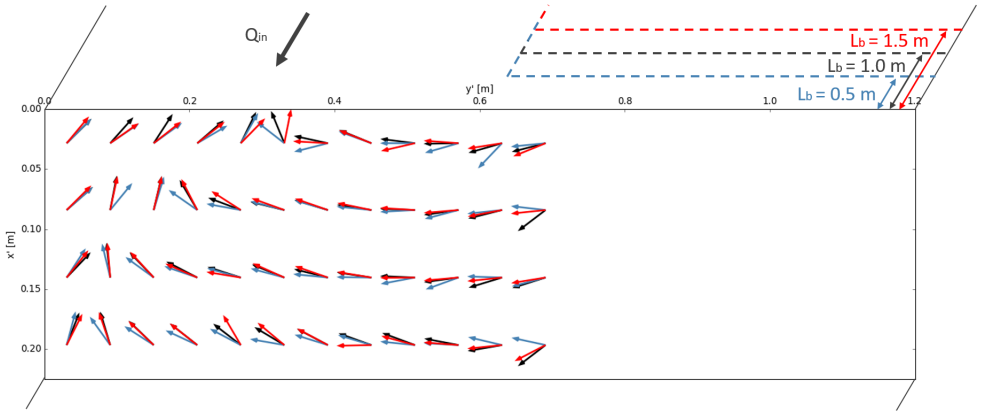

Figure 6.8: Time-averaged flow directions during Test 1.2, Test 2.2 and Test 3.2 plotted in the same figure.

Effect of width parameters on the flow state

Figure 6.9 compares Tests 2.1 and 2.2. A varying obstruction width distinguishes the two configurations. In Test 2.2, the configurations with a wide obstruction, flow state 1 was observed. Test 2.1 showed flow state 2. One can hence conclude that wide obstructions increase the likelihood of flow state 1 being present. This does not tell the entire story though. An obstruction is an artificial tool to replicate a certain expansion width and inflow channel width in the laboratory. It is not a meaningful variable in the field. In practice, expansion width and inflow channel width are independent variables. These parameters are therefore individually addressed next.

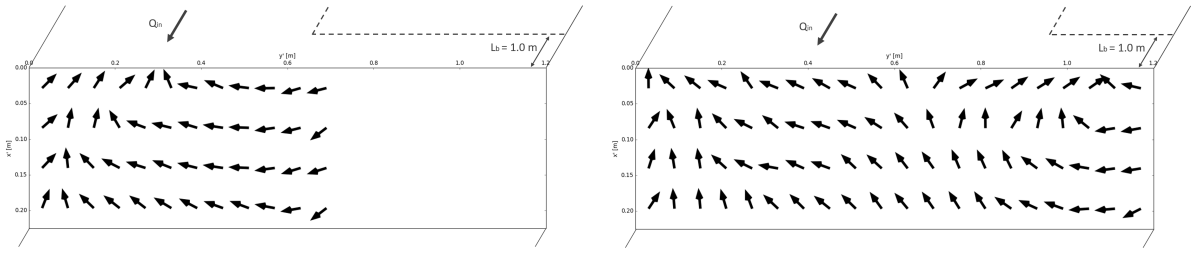

Figure 6.9: Time-averaged flow directions of (a) Test 2.2 and (b) Test 2.1.

Effect of expansion width (D/d_u) on the flow state

Figure 6.10 compares Test 3.2 and Test 3.1.B. Expansion width is the only variable that differs between both configurations. Flow state 1 is present in Test 3.2 and flow state 2 is present in Test 3.1.B. One can thus conclude that space for lateral expansion increases the likelihood of flow state 1 being present.

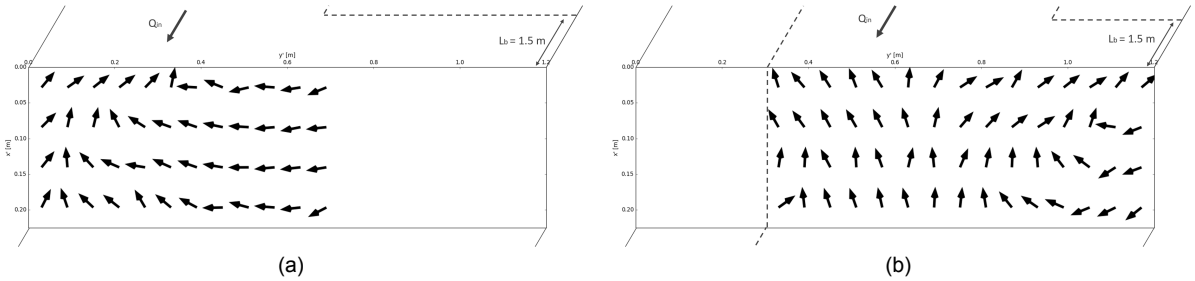

Figure 6.10: Time-averaged flow directions of (a) Test 3.2 and (b) 3.1.B.

Effect of inflow channel width (B/d_u) on the flow state

The opposite conclusion can be drawn for the inflow channel width. The comparison between Test 2.1.B and Test 2.1 in Figure 6.11 indicates that a small inflow channel width is favourable to flow state 1. Based on this binary comparison, one can conclude that inflow channel width affects the flow state.

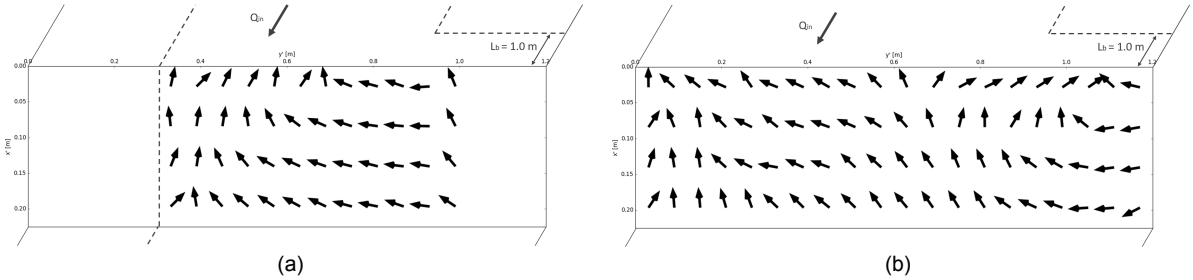

Figure 6.11: Time-averaged flow directions of (a) Test 2.1.B and (b) Test 2.1.

Flow state prediction based on geometry parameters

Figure 6.12 compares the tested configurations and their corresponding flow state. The graph can also be used to predict the flow state for configurations that deviate from the configurations tested. The flow state can be predicted with relative confidence for most possible parameter ranges. The expected flow states are indicated by coloured areas. The grey-shaded areas between both flow states show the configurations that cannot be predicted with confidence based on this study's findings. More experiments are required to further fill in these areas. Likewise, the lower limit of the inflow width to still yields flow state 1 was not considered. Obviously, when the inflow width approaches zero, the flow state will change at a certain moment. Hence, the area that corresponds to small inflow widths is also grey shaded in Figure 6.12.

Note that the coloured areas are only contoured for L_b/d_u of 5, 10 and 15. Interpolation can be applied to determine the areas for other values of L_b/d_u. When using this figure to predict the flow state, keep in mind that parameters not considered in this graph, e.g. Froude number and bed slope, also affect the flow state. These are kept constant across this study's experiments.

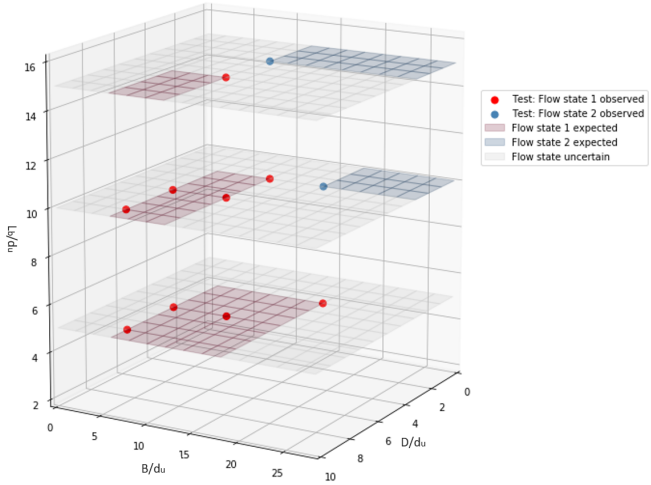

Figure 6.12: Overview of the configurations tested and the corresponding flow states. Each axis represents one of the dimensionless geometry parameters. Shaded areas indicate the expected flow state for the three bed protection lengths tested. In the grey-shaded area, the flow state cannot be predicted with certainty based on this study's findings.

6.3 Mixing layer development for both flow states

Strong differences in flow behaviour are present between flow state 1 and flow state 2. Figure 6.13 shows the streamwise development of the mixing layer in both flow states through references cases 2.2 and 2.1.

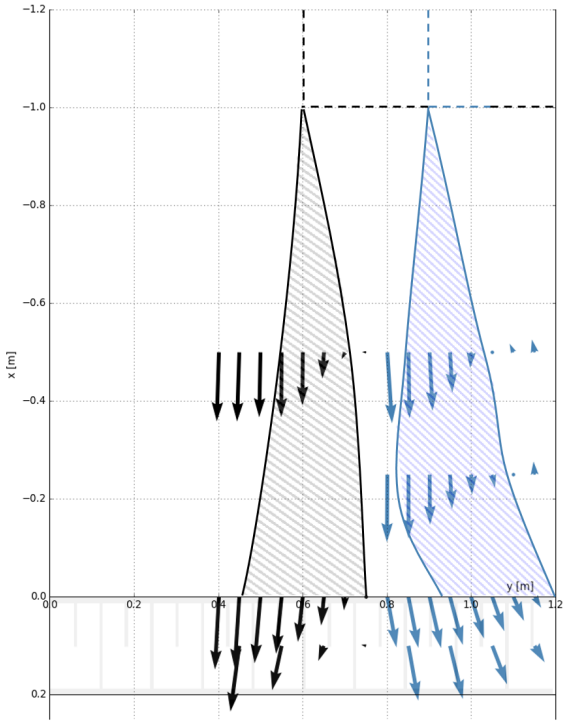

Figure 6.13: Mixing layer development related to flow state 1 (Test 2.2, in black) and flow state 2 (Test 2.1, in blue). The arrows indicate the measured depth-averaged and time-averaged flow direction and orientation in the xy-plane. Depth-averaged flow velocities were determined at 0.4 times the water depth. The shaded area highlights the mixing layer. The mixing layer is defined as the area with a local velocity between 5% and 95% of the inflow velocity.

The first flow state demonstrates a mixing layer that develops straight along across the bed protection. The y-location of the time-averaged maximum velocity gradient remains constant as the mixing layer travels downstream. When the flow reaches the downward slope, the mixing layer strongly deflects towards the centre of the jet. A primary and a secondary recirculation current forms in the wake of the lateral expansion. It stretches out till far behind the downward slope. Coherent 2-D turbulence structures (2DCS) are present in the mixing layer (Figure 6.14).

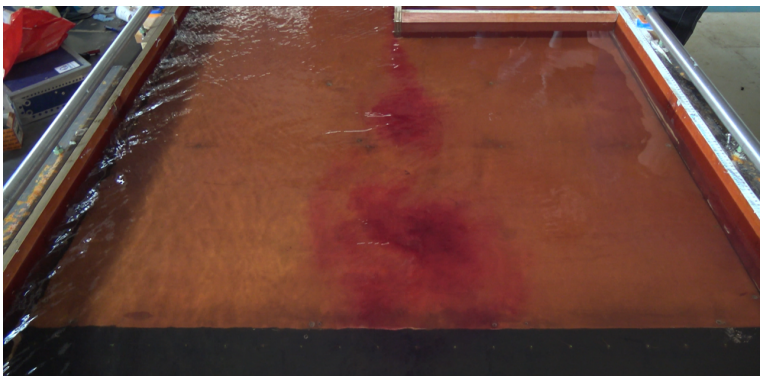

Figure 6.14: The presence of coherent turbulence structures in the mixing layer visualised by dye.

A very different horizontal flow pattern is associated with the second flow state. The mixing start deflecting leeward well before reaching the downward slope. The reattachment point is located before the slope's crest. This means that the primary gyre is cut off before it reaches the downward slope. It is just the location of the mixing layers at the crest that differs. The mixing layer widths observed for both flow states are comparable and are roughly in line with a 1:6 spreading angle.

Other tested configurations with the same flow state show very similar mixing layer behaviour. Figure 6.15 shows the streamwise flow velocity at the slope's crest. In Tests 1.1, 2.1.B, 2.1 and 3.1.B, the mixing layer is triggered at y = 0.9 m. Flow state 1 is present in Test 1.1 and Test 2.1.B, whereas flow state 2 is observed in Test 2.1 and Test 3.1.B. Deflection of the mixing layer towards the lee of the obstruction is visible in Tests 2.1 and 3.1.B as the maximum velocity gradient moved in leeward direction while propagating across the bed protection. As expected, velocity gradients are smaller for runs with longer bed protections. In Tests 1.2, 2.2 and 3.2, the mixing layer is generated at y = 0.6 m.

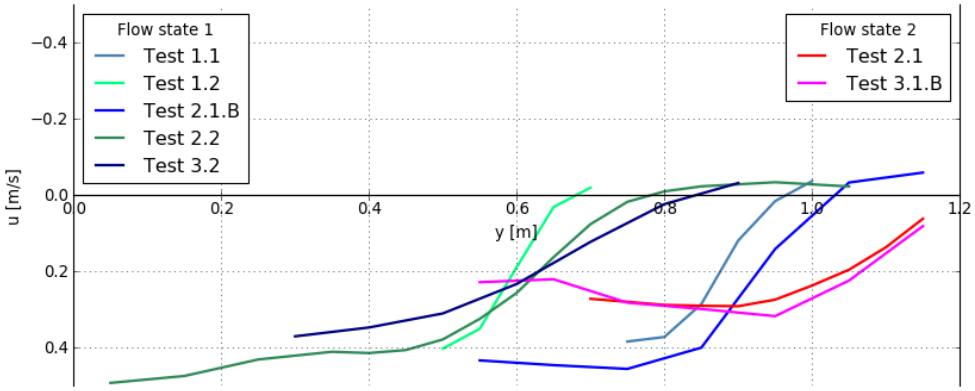

Figure 6.15: Depth-averaged and time-averaged streamwise flow velocity u at the crest of the downward slope. The blue lines depict tests with flow state 1 present. The configurations that correspond to flow state 2 are represented by the red lines. The depth-averaged velocity was based on velocity measurements at 0.4 times the water depth.

6.4 Near-bed flow behaviour for both flow states

The two observed flow states are associated with very distinct near-bed flow patterns at the downward slope. This section describes the specifics of the near-bed flow behaviour of both flow states.

Flow state 1: Horizontal contraction

Firstly, the near-bed flow related to flow state 1 is described. Broadly speaking, the near-bed flow at the slope corresponding to flow state 1 can be subdivided into three zones (Figure 6.16). In zone one, the centre of the jet, the flow direction is opposite to the main flow direction. This implies a vertical return current initiated by vertical flow separation. Zone two shows a high degree of contraction towards the high-velocity side. Zone three is located in the wake of the horizontal obstruction. Flow velocities were insufficient to sustain frictionless tuft movement, resulting in inaccurate measurements. Measurements in zone 3 are therefore disregarded.

Figure 6.17 shows the prevalence of each flow direction. Flow behaviour in and around the mixing layer (zone two) arouses particular interest. In combination with the contracting flow that is visible from the time-averaged flow direction, it shows that both upward and downward flow has a significant presence in the mixing layer. Neither vertical flow attachment nor vertical flow separation can be confidently concluded based on these observations.

Hence, additional ADV measurements are carried out in the centre of the mixing layer, halfway the

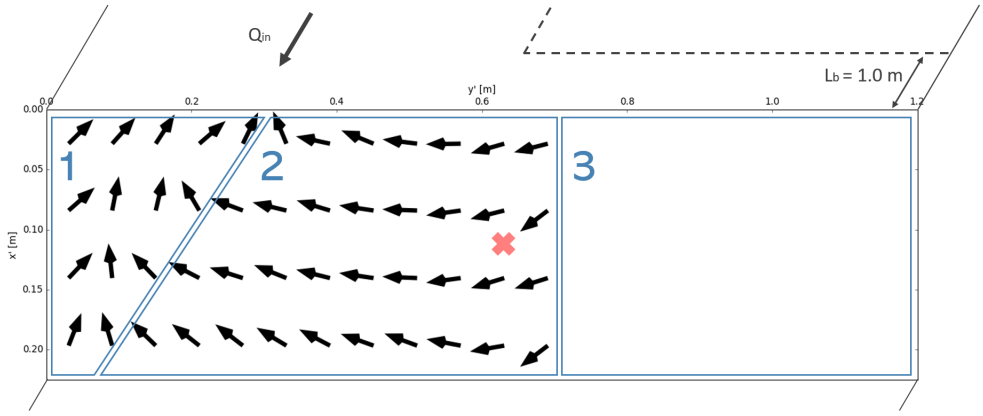

Figure 6.16: Time-averaged near-bed flow directions at Test 2.2. The slope is subdivided into three zones. The red cross at x' = 0.112 m, y' = 0.625 m (centre mixing layer) shows the location of additional ADV measurements

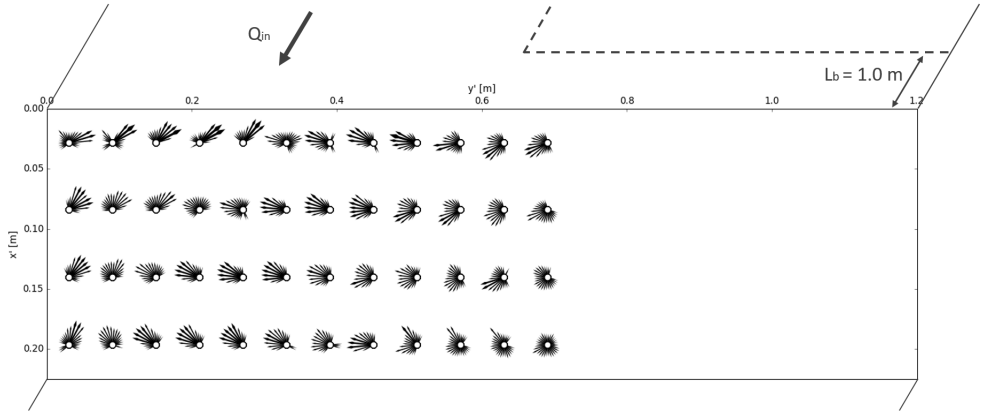

Figure 6.17: Distribution of the each near-bed flow direction during Test 2.2. Arrow size relates to the prevalence of the corresponding flow direction occurs.

downward slope (x' = 0.112 m), to learn more about the behaviour of the near-bed flow over time. The centre of the mixing layer is defined as the location with the largest velocity gradient. In Test 2.2, the centre of the mixing layer is located at y = 0.625 m. The exact location of these measurements is indicated in Figure 6.16. ADV measurements were considered to be more suitable for analysis over time than tuft measurements. Quite some data points are filtered out by the tuft video processing algorithm. This leaves the data unsuitable for analysis over time.

The histograms in Figure 6.18 show the velocity distribution in u' (a) and v' (b). Constant contraction is visible from the consistently negative value of v' in (b). In line with tuft observations, neither vertical attachment nor vertical separation can be concluded from the streamwise flow velocity u' (a). Upward and downward flow occurs just as frequent. This observation does not line up with previous experiments on this topic, that showed either convincing downward flow (vertical attachment) or convincing upward-pointing flow (vertical separation). Further analysis of the flow behaviour in x'-direction is therefore required.

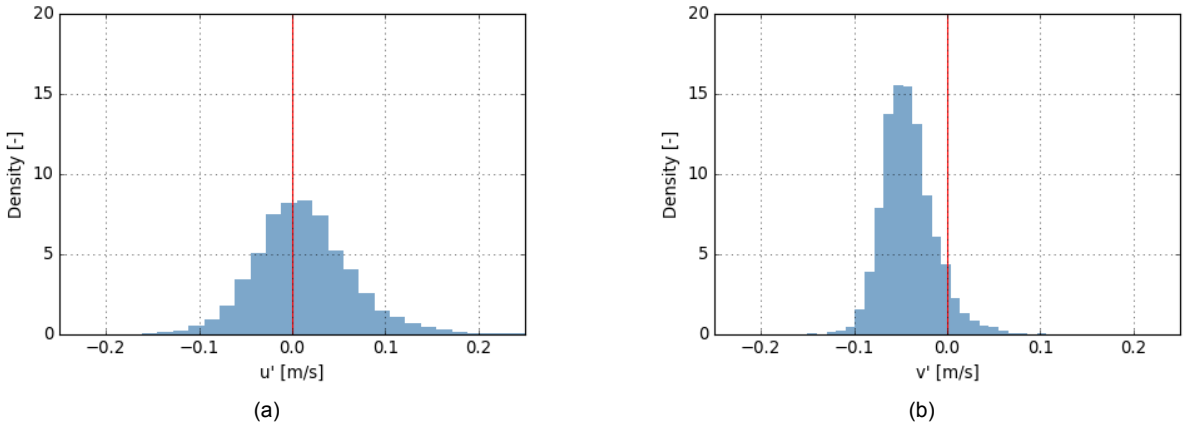

Figure 6.18: Histogram of (a) u' (velocity in x' direction) and (b) v' (velocity in y' direction) near the bed of the downward slope in zone two. The measurements were carried out using ADV at approximately 1 cm from the bed at the location highlighted in Figure 6.16

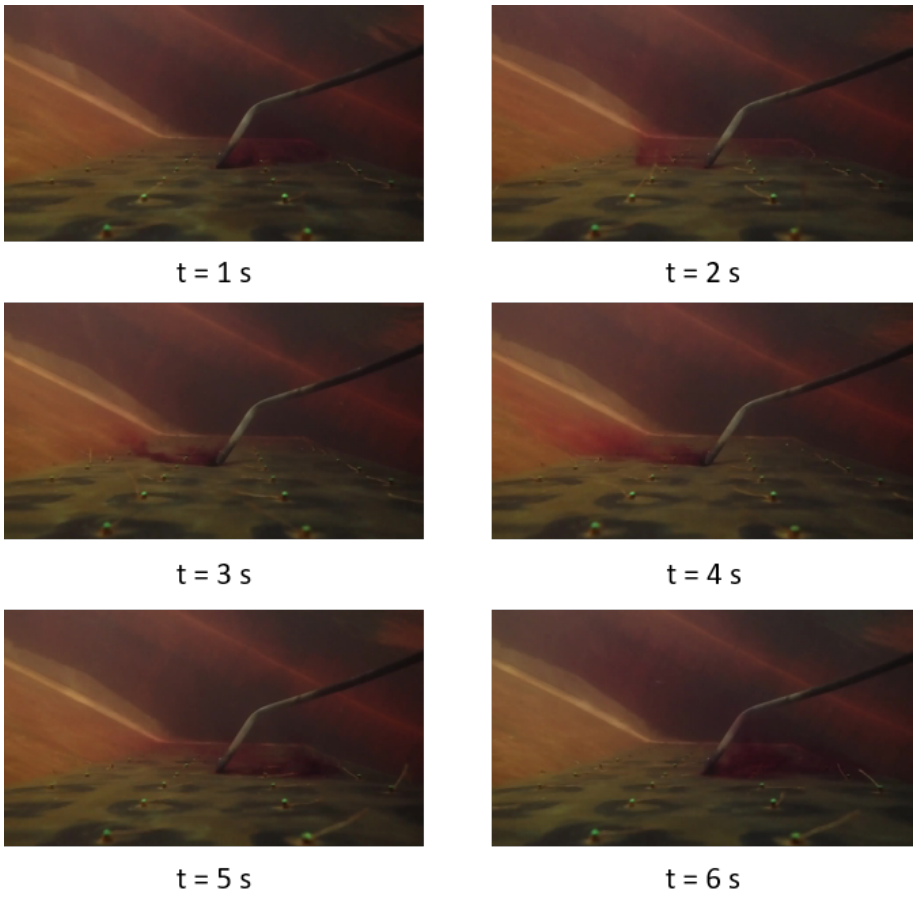

Figure 6.19: Snapshot of the near-bed flow pattern at Test 2.2. Dye was injected at x' = 0.112 m, y'= 0.48 m. The camera filmed parallel to the downward slope.

Near-bed dye injections at the slope were carried out to obtain qualitative insights in the near-bed flow behaviour and the vertical flow state. The injected dye illustrated an alternating vertical flow pattern. Upward and downward flow succeeded each other in a period of several seconds. Simultaneously, constant horizontal contraction towards the centre of the jet was visible. Figure 6.19 shows a six-second snapshot that illustrates these observations. The same conclusion can be drawn from plotting

the ADV-measured u' against time (Figure 6.20).

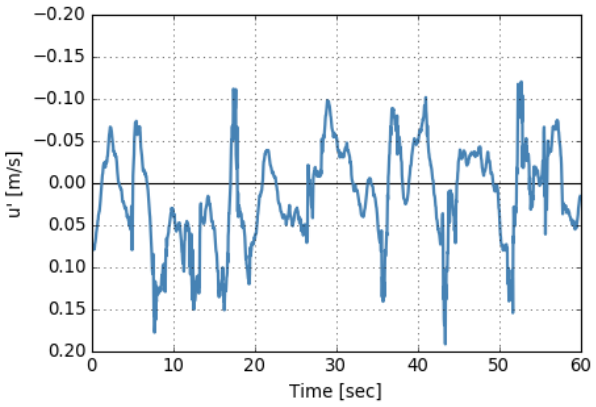

Figure 6.20: Development of the u' (velocity in x' direction) in time in the centre of the mixing layer (Test 2.2, x' = 0.112 m, y' = 0.625 m)

Spectral analysis was conducted on u' in the centre of the mixing layer to further analyse the vertical flow state. Figure 6.21 compares the time-averaged flow directions and the frequency spectrum during Test 1.2, Test 2.2 and Test 3.2. The compared configurations only differ in terms of bed protection length L_b. Clear energy peaks can be distinguished. The frequencies that correspond to the energy peaks roughly match the visually observed alternating frequencies. Interesting to note is the linear relation between bed protection length and high-energy frequency. Peaks at approximately 0.14 Hz, 0.25 Hz, and 0.43 Hz correspond to bed protection of 1.5 m, 1.0 m and 0.5 m respectively. Dominant frequencies were also determined for Test 1.1 and 2.1.B. The dominant frequency of Test 1.1 matches the dominant frequency of Test 1.2 (both L_b = 0.5 m) and Test 2.1.B matches Test 2.2 (both L_b = 1.0 m). This reinforces the belief that a linear relation is present between bed protection length L_b and the alternating frequency. Note that dominant frequencies can only be determined by approximation as a result of limited sample size.

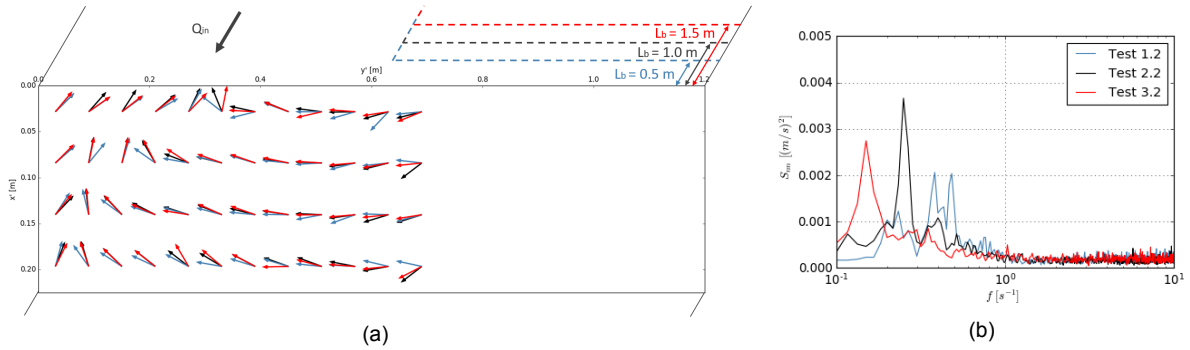

(a) (b)

Figure 6.21: Comparison of Test 1.2, 2.2 and 3.2 by (a) time-averaged near-bed flow direction and (b) frequency spectra of u' in the centre of the mixing layer (x' = 0.112 m, y' = 0.625 m).

The observed linear relationship is in line with the Strouhal equation introduced in Section 2.4.1 (Equation 2.1). The bed protection length is proportional to the turbulence length scale (mixing layer width) and the velocity scale is constant across the tests. Hence, $f * L_b$ is constant across the testes, which is shown in Figure 6.22. The same high-energy frequencies are visible in the v-spectrum at the slope's crest. This indicates a physical relation between 2DCS and the vertically alternating flow state.

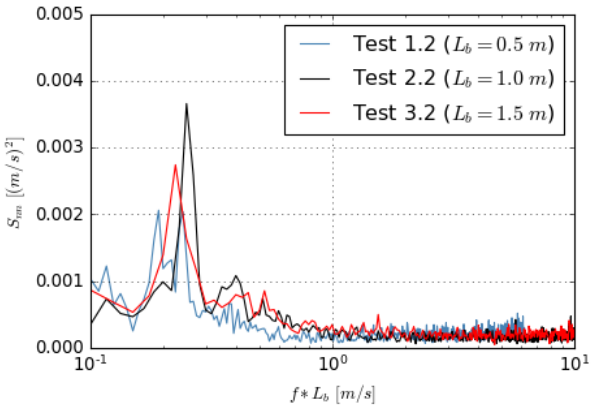

Figure 6.22: Comparison of Test 1.2, 2.2 and 3.2 by frequency spectra of u' in the centre of the mixing layer (x' = 0.112 m, y' = 0.625 m). In addition to Figure 6.21 (b), the horizontal axis is multiplied by the corresponding bed protection length.

Accidentally, an interesting observation was made regarding particle movement at the downward slope. The presence of small dirt in the flume provided a first impression on particle movement in flow state 1. Figure 6.23 sketches the visually observed particle movement. Dirt enters the system upstream. A particle that reaches the downward slope in zone two is transported towards the centre of the jet. Once there, the particle gets caught in a rotational movement. Particle movement occurs in gusts. A particle can be stationary for a while before being picked up and moved some distance. Sometimes a particle is picked up in such a way that it escapes the rotational system, and continues downstream.

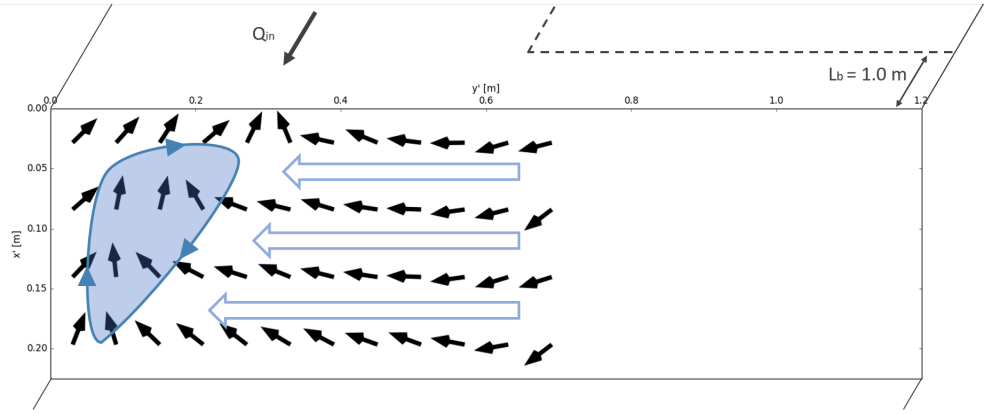

Figure 6.23: The blue arrows roughly indicate the movement of occasionally present dirt particles in the flume at the downward slope. The shaded area illustrates the equilibrium location of the particles and its rotational movement. Black arrows show time-averaged flow directions near bed (Test 2.2).

Flow state 2: horizontal divergence

Flow state 2 is associated with very different near-bed flow behaviour. Figure 6.24 shows the time-averaged near-bed flow. The slope is subdivided into two zones. The vertically separating area indicated by zone one spans the entire width of the inflow channel. Although some horizontal effects are visible in this zone, the flow direction is primarily opposite to the main flow direction. Figure 6.25 demonstrates that upward flow is consistently present. This upward near-bed flow is associated with constant vertical flow separation.

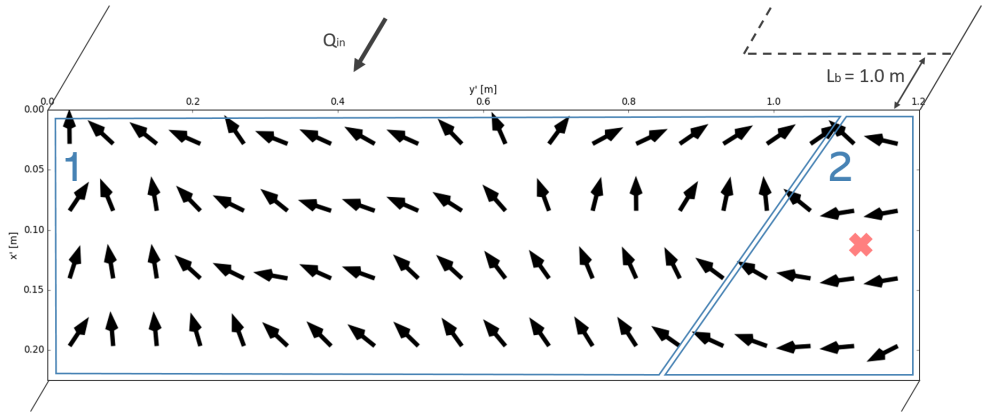

Figure 6.24: Time-averaged near-bed flow directions at Test 2.1. The slope is subdivided into two zones. The red cross at x' = 0.112 m, y' = 1.125 m (centre mixing layer) shows the location of additional ADV measurements.

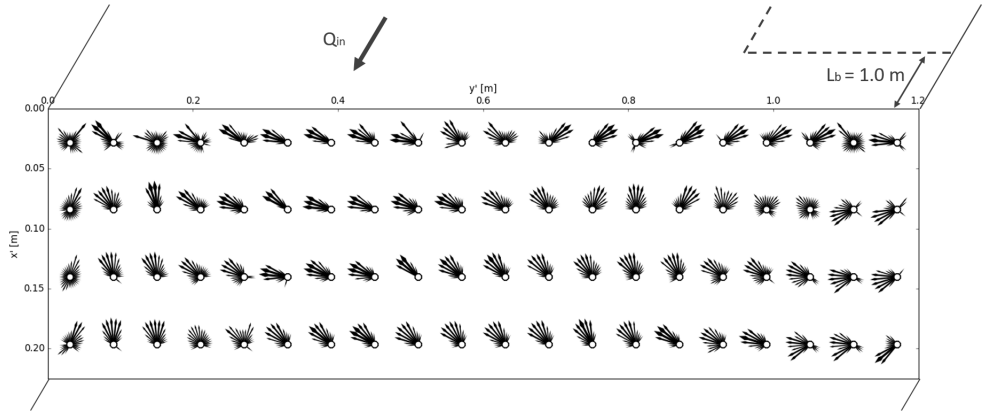

Figure 6.25: Distribution of the near-bed flow directions during Test 2.1. Arrow size relates to the prevalence of the corresponding flow direction occurs.

The conclusion that constant vertical separation is present is confirmed by near-bed dye injection, captured in Figure 6.26. It indicates the relation between a near-bed flow in upward direction and vertical flow separation.

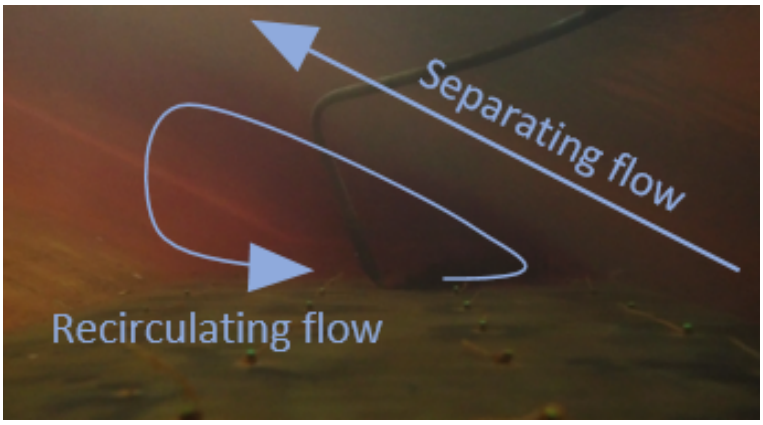

Figure 6.26: Snapshot of the vertical flow pattern at Test 2.1. Dye was injected at x' = 0.112 m, y'= 0.60 m. The camera filmed parallel to the downward slope.

The second zone is located behind the horizontal expansion. It matches the location of the deflected

mixing layer at the crest of the slope. A vastly different flow pattern was observed. Constant contraction towards the jet was present. In addition, neither vertical separation nor vertical attachment is present. Further ADV measurements are conducted to obtain more detailed insight into the near-bed flow behaviour.

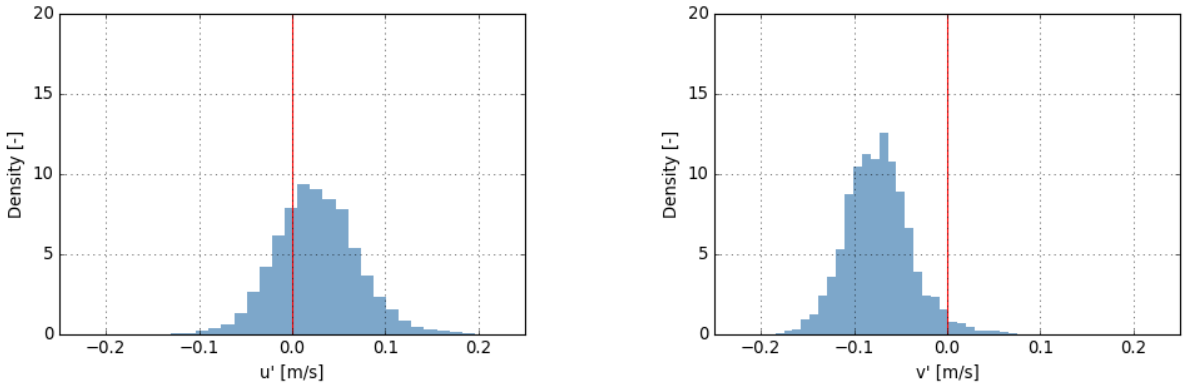

Figure 6.27: Histogram of (a) u' and (b) v' near the bed of the downward slope. The measurements were carried out using ADV at the location highlighted in 6.24 (Test 2.1, x' = 0.112 m, y' = 1.125 m)

The histograms of Figure 6.27 show the distribution of u' and v' in the centre of the mixing layer. From u' can be concluded that vertically attached flow prevailed over vertically separated flow. Figure 6.28 confirms this observation. It can be concluded that vertical separation is consistently suppressed in this case.

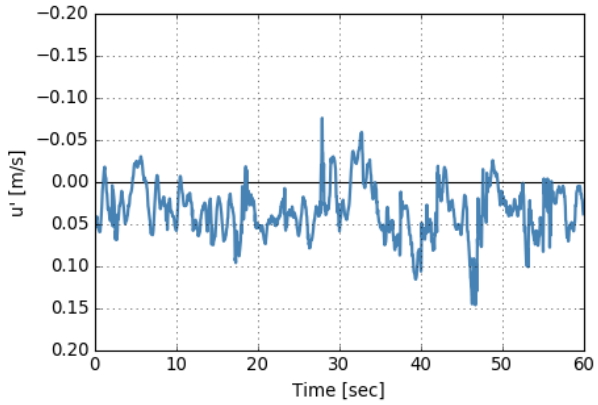

Figure 6.28: Development of u' in time in the centre of the mixing layer (Test 2.1, x' = 0.112 m, y' = 1.125 m)

On the other hand are the observed values of u' rather small. This is different from Test 2.2, in which significant near-bed velocities were observed, both in upward and downward direction. Figure 6.29 compares the spectra of flow state 1 (Test 2.2 and 3.2) with the spectra of flow state 2 (Test 2.1 and 3.1.B). For 2.2 and 2.1 on the one hand and 3.2 and 3.1.B on the other hand, the bed protection length L_b is constant. No convincing energy peaks are present in the spectra of flow state 2 in contrast to the spectra of flow state 1, which show pronounced energy peaks. This observation corresponds with the lack of an alternating pattern in Figure 6.28.

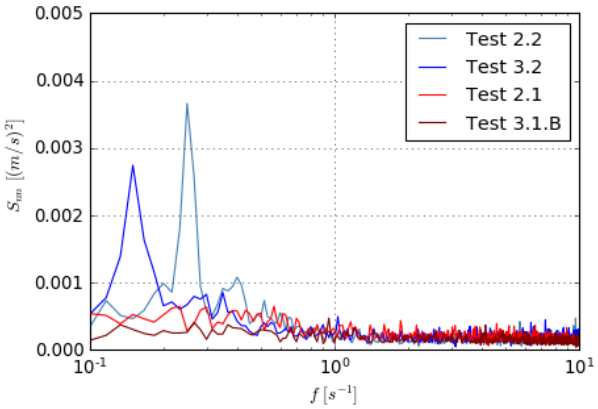

Figure 6.29: Comparison of the frequency spectra of flow state 1 (Tests 2.2 and 3.2) and flow state 2 (Tests 2.1 and 3.1.B).

7

Discussion

7.1 Nonuniformity-induced flow attachment

A novel vertical flow state was identified in this study, namely a dynamic flow state in which vertical attachment and vertical separation alternate. The alternating vertical flow was accompanied by horizontal contraction of the main flow and unidirectional transverse flow near the bed. The combination of horizontal contraction and vertical alternation can be added to the two flow states identified in previous studies: horizontal contraction in combination with vertical attachment and horizontal divergence in combination with vertical separation. The horizontally diverging flow state was also observed in some configurations tested for this study.

The discovery of the alternating vertical flow state provides valuable insights that can be used to further develop the understanding behind nonuniformity-induced flow attachment. The mechanisms that drive this phenomenon are still not fully understood. This section explains how the findings of this study shed new light on these mechanisms.

7.1.1 Flow state 1: horizontally contracting + vertically alternating flow

First, the horizontally contracting flow state is addressed. Across the bed protection, flow behaviour is in line with the traditional understanding of mixing layers (Talstra, 2011), as well as with Broekema et al. (2019) and Van der Zande (2018). The mixing layer initially develops straight ahead and penetrates the stagnant area with an angle of approximately 1:6, which matches traditional understanding on shallow mixing layer development (Rajaratnam, 1976). A large recirculation zone develops leeward of the lateral expansion. At the moment that the mixing layer reaches the downward slope, it strongly deflects towards the centre of the jet, contracting the main flow.

Observations start to deviate from previous understanding at the slope's bed. Visual observations, tuft measurements as well as ADV measurements demonstrate a near-bed flow regime in which upward and downward flow occurs in an alternating manner. The alternating frequency seems to depend on the mixing layer width at the slope's crest. A linear relation between both quantities was observed. The same relation that defines the dominant frequency of 2-D coherent turbulence structures (2DCS) in a mixing layer (Equation 2.1) appears to be valid for the alternating frequency of the upward and downward flow. This observation points out the possible existence of a mechanism in which coherent turbulence structures in a mixing layer induce alternating vertical flow. The physical background of this mechanism can be explained by conservation of potential vorticity, as defined in Appendix A.

Note that the linear relation for 2DCS was initially formulated for shallow mixing layers ($\mathcal{L} >> H$). As the experimental setup does not completely fulfil this requirement, the formula might not entirely hold for this case. Nevertheless, as visual observations of developing 2DCS during this study's experiments closely resemble 2DCS defined for shallow mixing layers, the underlying logic is expected to be valid.

Besides, Broekema et al. (2019) and Van der Zande (2018) showed that contraction of the main flow and the subsequent acceleration and positive pressure gradient, most likely play an important role in the suppression of flow separation. It is hypothesised that horizontal contraction and coherent turbulence structures independently contribute to the positive pressure gradient that suppresses vertical flow separation. Following this reasoning, horizontal contraction provides a constant positive pressure gradient, whereas the contribution of coherent turbulence structures constantly changes depending on the current state of the turbulence structure.

Differences in shallowness across the laboratory setups used in previous studies provide additional insights into the mechanisms that drive vertical attachment. Experiments of Broekema et al. (2019) were conducted in a deep setup, whereas Van der Zande (2018) performed experiments in a rather shallow setup. The shallowness of the setup used for this study is somewhere in between. The most convincing flow suppression was observed in the configuration of Broekema et al. (2019), the deepest of the three. No alternating flow pattern was present here. Hence, the positive pressure gradient from horizontal contraction is expected to be sufficient to suppress flow separation in a deep configuration. The next paragraph provides the reasoning that supports this assumption.

A deep configuration is associated with a relatively narrow inflow channel, and consequently with a relatively narrow jet. Deflection of the mixing layer at the downward slope causes the jet to contract. The extent of the mixing layer deflection at the slope is expected to be independent of the inflow channel width. Hence, contraction of the streamlines in the jet is more severe in case of a narrow jet. Streamline contraction is associated with a positive acceleration, and subsequently with a positive pressure gradient. The positive pressure gradient from contraction is therefore greater in case of deep configurations.

Following this reasoning, an alternating flow pattern would be expected for the shallow configurations tested by Van der Zande (2018). No mention was made though of an alternating flow pattern by Van der Zande. Nevertheless, there is reason to believe that an alternating flow regime was present. Van der Zande used dye injection and sinking particles to visually determine the vertical flow state. The residence time of dye and tracer particles was in the order of 1 to 2 seconds. Conversely, this study found a much longer period of vertical alternation. One can therefore conclude that dye injection and sinking particles were not the optimal measuring techniques to accurately recognise an alternating flow pattern. Moreover, time-averaged near-bed ADV measurements show lateral rather than a downward near-bed flow (Figure 2.6). The similarities with the time-averaged flow directions that belong to the alternating flow state are notable. The combination of these two reasons makes it likely that an alternating vertical flow pattern was present, but went unnoticed.

To conclude, two vertical flow regimes that involve nonuniformity-triggered vertical flow attachment can be distinguished: 1) a regime with constantly attached flow and 2) a regime in which attachment and separation alternate. In deep configurations, the positive pressure gradient from contraction contributes enough to fully suppress separation, which results in the former flow regime. In shallow setups, the effects of coherent turbulence structures in the mixing layer are more prevalent, triggering an alternating regime.

This theory also supports observations regarding the spatial extent to which flow attachment is present. In deep cases, flow attachment occurs along the entire width of the jet, whereas in shallow cases, flow attachment is a local phenomenon that is limited to the direct proximity of the mixing layer. This can be explained as follows: the contraction component that prevails in deep configurations affects the entire jet, whereas the effects of coherent turbulence structures are by definition limited to the direct surroundings of the mixing layer.

7.1.2 Flow state 2: horizontally diverging + vertically separating flow

In addition to the horizontally contracting and vertically alternating flow, also configurations with horizontally diverging flow were present. In contrast to the diverging flow state observed by Broekema et al. (2019), the mixing layer starts deflecting well before the downward slope is reached. The recirculation zone is cut off before reaching the slope. The mixing layer appears to 'catch' the flume wall when it gets sufficiently close, triggering complete and persistent deflection of the mixing layer. However, in case the mixing layer does not make it to the confining wall before the downward slope, no divergence is observed at all and the horizontally contracting flow state is present. A complete explanation for the sudden leeward deflection of the mixing layer halfway the bed protection cannot be provided. However, since the deflection is related to a small horizontal expansion width and a long bed protection, which together forms the space the recirculation has to develop, the mechanism that triggers the leeward deflection is expected to be related to the recirculation zone. In line with previous research, horizontal divergence was accompanied by vertical separation of the main flow.

7.1.3 Limitations

A few remarks should be made regarding the validity of the findings of this study. First of all, the experiments were ideally conducted in a larger flume. To make optimal use of the space available, a non-symmetrical setup was used. This implies a wall being present in the centre of the jet that is being replicated. A wall induces additional friction in the jet's centre. In addition, non-confined jets tend to prefer one side (Talstra, 2011, Van der Zande, 2018). A wall in the centre of the jet blocks such macroinstabilities from occurring.

Also, the flume length is a constraining factor. A trade-off was made between inflow channel length and development space for recirculation zones. Ideally, to ensure full development of the logarithmic velocity profile, the inflow channel length is a few dozen times the water depth. In the least favourable configuration that was tested, the inflow channel length was only 10 times the water depth. On the other hand, a gyre development length of 7.2 m is required for configurations with a horizontal expansion of 0.9 m (Broekema, 2020). Only 5 m was available in one of the configurations tested.

Additional uncertainties are related to the ADV measurements conducted near the slope's bed for flow velocity visualisation and frequency spectral analysis. ADV measurements could not be conducted closer than a centimetre to the bed, which corresponds to a distance to the bed of about 7 per cent of the local flow depth. Particularly with flat vertical reticulation zones, this can cause significant discrepancies between the ADV-measured and the actual bed flow velocities.

7.2 Scour development under the vertically alternating flow state

Broekema et al. (2019) showed that consistent flow attachment has the ability to maintain scour potential while a scour hole deepens, and therefore cause deeper scour holes than vertically separated flow. Added scouring potential is driven by a consistent unidirectional near-bed flow in downward direction.

The vertically alternating flow state identified in this study is also associated with a unidirectional near-bed flow. But instead of unidirectional flow in downward direction, a unidirectional flow in lateral direction from the mixing layer to the centre of the jet is present. This consistent unidirectional flow is expected to increases scour in the mixing layer and transport sediment to the centre of the jet. Here, due to the upward near-bed flow associated with vertical flow separation, the sediment is retained. A large scour hole develops in and around the mixing layer, whereas in the centre of the jet, scour depths are much smaller. The observed movement of dirt particles across the downward slope (6.23) is in line with this reasoning.

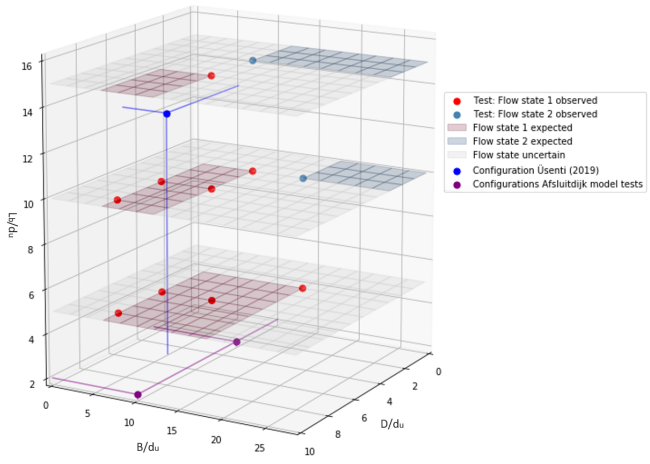

Figure 7.1: Adapted version of Figure 6.12 for prediction of the flow state based on this study's experimental results. Geometry parameters of Üsenti (2019) and the Afsluitdijk model (Levvel, 2018) tests are added. Using interpolation and extrapolation shows that the vertically alternating flow state (flow state 1) was most likely present in both configurations. Note that this figure only compares geometry parameters. The effect of other setup dissimilarities is not considered.

7.2.1 The vertically alternating flow state in relation to the experimental findings of Üsenti (2019)

Üsenti (2019) conducted experiments in a setup very similar to the setup used for this study. Üsenti however used a naturally erodible bed instead of a fixed bed and observed a deviant scour pattern that might be linked to the presence of alternating vertical flow. To confirm this premise, it should first be assessed whether the vertically alternating flow state was present during Üsenti's experiments. Unfortunately, no near-bed flow characteristics were measured by Üsenti. Hence, the assessment is based on other characteristics.

Üsenti observed horizontal contraction of the main jet, which matches the horizontal flow behaviour of the vertically alternating flow state. In addition, the configurations of both experiments are compared. Table 7.1 demonstrates the close similarities between the setup used for this study and the setup used by Üsenti. Figure 7.1 illustrates that the vertically alternating flow state is most likely present in the geometric configuration of Üsenti. Based on these observations, one can conclude that the vertically alternating flow state was most likely present during the formation of the 3-D scour hole of Üsenti.

The time-averaged near-bed flow directions of Test 2.2.B are projected on the scour hole of Üsenti in Figure 7.2. Bed topography matches the predicted scour behaviour based on near-bed flow behaviour in a fixed bed setup, as scour is much more significant in the mixing layer than in the centre of the jet. A slight discrepancy is present at the transition from lateral to upward near-bed flow. One would expect a wider area with upward flow. The discrepancy can probably be attributed either to the difference in bed topography or to the general differences between both setups.

Parameter name	Units	Test 2.2.B	Üsenti (2019) (Test B = 0.4 m)
Bed protection length	L_b/d_u	10	12.8
Inflow width	B/d_u	6	5.1
Horizontal expansion	D/d_u	6	5.1
Bed slope	i_b	1:2	1:2 (Mixing layer) 1:5 (Jet centre)
Depth increase	d_d/d_u	2	2.4 (Mixing layer) 1.8 (Jet centre)
Bed roughness	k_r/d_u	$O(10^{-5})$	0.18
Froude number	$U/\sqrt{gd_u} = Fr$	0.42	0.5
Reynolds number	$\rho UL/\mu = Re$	> 4000	> 4000

Table 7.1: Experimental parameters of Test 2.2.B compared to the parameter values of the experiments of Üsenti (2019). The configuration of Test 2.2.B is closest to the configuration used by Üsenti, and is therefore used for this comparison. In the symmetrical setup of Üsenti (2019), two mixing layers are present. The side of the mixing layer that corresponds to the deepest scour depth is considered in this table.

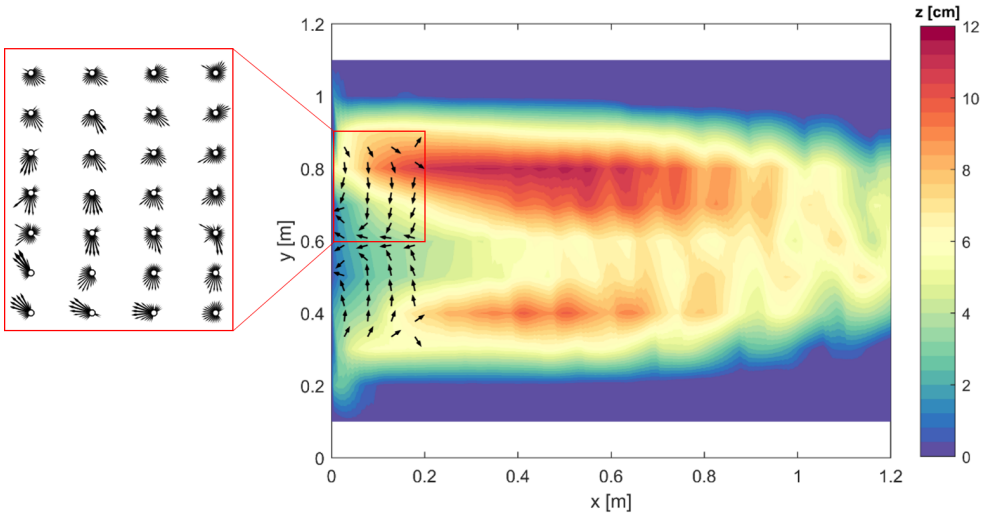

Figure 7.2: Near-bed flow directions of Test 2.2.B compared to the scour hole of Üsenti. Black arrows show the time-averaged flow directions in Test 2.2.B. At the left, the flow direction distribution that corresponds to these time-averaged flow directions is shown. The mixing layers are triggered 1 m upstream of the crest, at y = 0.4 and y = 0.8 m. Table 7.1 provides the details of both experiments. An important caveat to this comparison is that the naturally eroded 3-D scour hole differs from the fixed bed used in this study, potentially severely affecting flow behaviour.

7.2.2 The vertically alternating flow state in relation to the Afsluitdijk model tests

The next step is to evaluate whether the alternating flow state also causes the 3-D scour pattern that was observed at the Afsluitdijk model tests (Levvel, 2018). Again, near-bed flow directions were not measured. Horizontal contraction of the jet was observed though. Evaluation of the geometry parameters in Figure 7.1 points out that the vertically alternating flow state could have been present. However, the setups differ too much to deduce the flow state from a comparison of geometry parameters (Table 7.2). Supercritical instead of subcritical flow, a far shorter bed protection, and a large vertical step behind the bed protection are examples of the discrepancies between both setups that prevent such an inference.

As previously discussed, the vertically separating flow state was most likely present during the formation of the scour holes of Üsenti. The Afsluitdijk model tests in Figure 7.3 show a very similar scour pattern. It also compares near-bed flow directions to the scour hole at the Afsluitdijk model tests. Flow directions again fit well with the Afsluitdijk bed topography.

Parameter name	Units	Test 1.3 / Test 1.2.B	Afsluitdijk tests B/d_u = 10	Afsluitdijk tests B/d_u = 3
Bed protection length	L_b/d_u	5 / 5	2	2
Inflow width	B/d_u	6 / 6	10	10
Horizontal expansion	D/d_u	9 / 6	10	3
Bed slope	i_b	1:2	1:2 (Mixing layer) 1:5 (Jet centre)	1:2 (Mixing layer) 1:5 (Jet centre)
Depth increase	d_d/d_u	2	5 (Mixing layer) 2.5 (Jet centre)	4 (Mixing layer) 2.5 (Jet centre)
Bed roughness	k_r/d_u	$O(10^{-5})$	$O(10^{-4})$	$O(10^{-4})$
Froude number	$U/\sqrt{gd_u} = Fr$	0.42	> 1	> 1
Reynolds number	$\rho UL/\mu = Re$	> 4000	> 4000	> 4000

Table 7.2: Comparison of the experimental parameters of Test 1.3 and Test 1.2.B, and the estimated parameter values of the Afsluitdijk model tests. Geometry parameters were visually determined from Figure 7.3. Both sides of the scour hole are separately considered in this table as they are each characterised by a different horizontal expansion width.

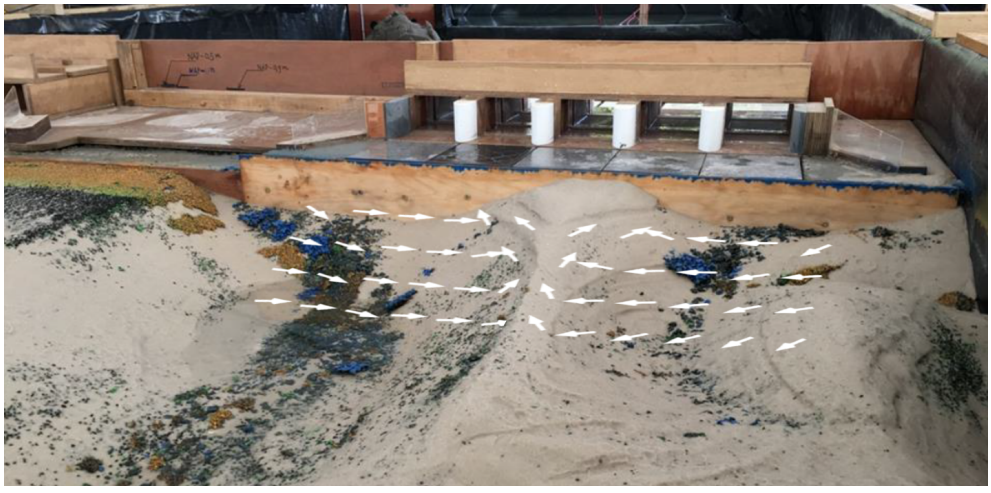

Figure 7.3: Near-bed flow directions of Test 1.3 (left) and Test 1.2.B (right) in comparison to the scour hole at the Afsluitdijk model tests. The white arrows show the time-averaged flow directions. Table 7.2 provides the specifics of the tests that are compared. Please note that the flow directions were measured in configurations that differ from the Afsluitdijk configuration. Subsequently, this figure is not just a first indication of the near-bed flow directions during the Afsluitdijk tests.

The combination of 1) matching horizontal flow behaviour, 2) matching geometry parameters, and 3) very similar scour profiles makes it likely that the vertically alternating flow state was present at the Afsluitdijk model tests. Further analysis of near-bed flow behaviour is required to solidify this presumption.

7.3 Scour under vertically alternating flow in the light of Breusers' scour prediction method

The elaboration on Breusers' scour prediction method in Section 2.5 revealed that Breusers' method in its current form is not able to accurately predict scour dimensions under laterally non-uniform flow conditions. The current study's findings provide additional insights into the observed discrepancies between scour predictions by Breusers' method and scour dimensions measured in the laboratory by Üsenti (2019). As discussed in the previous section, the vertically alternating flow state was most likely the trigger of excessive scour in Üsenti's experiments. This indicates that Breusers' method in its current form is not able to accurately capture the effects of the alternating flow state.

This might be surprising since Breusers' method contains the 'dustbin-factor' α, which is supposed to deal with configuration-specific variables, while the occurrence of the vertically alternating flow state is a configuration-specific variable. However, when decomposing Breusers' method, a plausible cause for the misrepresentation of the vertically alternating flow state in the α factor is identified.

α was originally defined by de Graauw and Pilarczyk (1981) as a function of the local geometry of a hydraulic structure. A drawback of this approach is that α could only be determined for a very specific range of geometries. To make the function generally applicable, Jorissen and Vrijling (1989) defined α as a turbulence factor.

Jorissen and Vrijling developed an α prediction relation based on experiments conducted for the Delta project. A setup was used that included a sill across the entire width of the flume, vertically confined the flow depth. Vertical flow separation occurred at the downstream end of the sill, generating extensive turbulence across the entire channel width. 3-D effects were included by raising the height of the sill only in a part of the channel, generating additional turbulence at the transition in sill height. In Breusers' method, this added turbulence leads to an increased scour.

This approach, however, does not entail the scour-driving mechanism that is associated with the vertically alternating flow state. In the alternating flow state, it is not the turbulence generated at the horizontal expansion that triggers increased scour. Instead, the horizontal expansion triggers a lateral unidirectional near-bed flow in the mixing layer that greatly increases scour potential. Predicting scour dimensions using a turbulence-based α is consequently an ill-considered approach.

Note that besides the discrepancies regarded to α, Breusers' method seems to be generally valid in the vertically alternating flow state. Üsenti (2019) observed scour development that was very much in line with Breusers' predictions, as long as an experimentally determined α was used instead of a calculated one. In case an α prediction method for vertically alternating flow conditions would be available, Breusers' method could still be used. For such a case, α would not be a turbulence parameter but a unidirectional near-bed flow parameter. So far, however, this idea is still conceptual. It is expected that several additional studies are required before it can be applied in the field.

8

Conclusion and recommendations

This chapter concludes the most important findings and implications of this study. In addition, it provides recommendations for future research, namely what are the next steps to further develop the understanding of nonuniformity-induced flow attachment to take a step towards its application in practice.

8.1 Conclusion

Visualisation of near-bed flow directions across an entire flow field

A measurement technique based on tufts, tiny threads attached to a surface that follow the local flow direction, is used to visualise near-bed flow patterns. A processing technique was developed to automatically capture tuft orientations during an experiment in an accessible data set on flow directions. It works like this: tufts are recorded by camera. A self-developed algorithm converts the resulting video footage to numerical data on local flow directions per tuft per frame. The soundness of the tuft measurement technique was successfully validated using ADV. Measuring an entire flow field requires approximately one hour, making it highly suitable to efficiently test large numbers of configurations.

Flow states that occur under laterally non-uniform flow conditions

The tested configurations replicate depth-to-width ratios that are common in the field. Two distinct flow states can be clearly distinguished within the limits of the tested parameter ranges: 1) a horizontally contracting flow state, and 2) a horizontally diverging flow state. In contrast to the large differences in flow behaviour between both flow states, differences across different configurations within the same flow state are negligible. The transition between both flow states is very sudden. A slight change in geometry can be sufficient to pass the boundary between both flow states and completely change flow behaviour.

Mixing layer behaviour plays an important role in the characterisation of the flow states. The mixing layer in the first flow state develops straight ahead until it encounters the downward slope. There, it strongly contracts, squeezing the streamlines of the main flow. The second flow state is characterised by strong deflection of the mixing layer in leeward direction. Deflection starts well before the mixing layer reaches the downward slope. The reattachment point is located upstream of the downward slope, such that the time-averaged streamwise flow velocity $\bar{u}$ at the slope's crest is positive along the entire flume width. Deflection of the mixing layer is accompanied with horizontal divergence of the main flow.

Divergence continues across the downward slope. Each flow state is associated with distinct near-bed flow patterns at the downward slope, which are addressed later in this chapter

Geometry effects on the flow state

It was found that the three tested parameters, bed protection length, lateral expansion width and inflow channel width, all affect the flow state. The horizontally contracting flow state tends to be present in case of short bed protections, large horizontal expansions and narrow inflow channels, whereas the horizontally diverging flow state is triggered by long bed protections, limited horizontal expansions and wide inflow channels.

The flow state can be predicted for other situations with similar setups using the insights gathered on 1) the effect of each geometry parameter on the flow state and 2) the flow states that correspond to the tested configurations. Figure 6.12 shows a plot of the observed flow state against their corresponding geometry parameters. One could for example infer from this figure that for a configuration with a bed protection length of ten times the water depth (L_b/d_u = 10), the contracting flow state is present whenever:

- Inflow channel width divided by water depth is smaller than twelve (B/d_u < 12); and
- Expansion width divided by the water depth is larger than three (D/d_u > 3).

Alternatively, the diverging flow state is present in case:

- Inflow channel width divided by the water depth is larger than eighteen (B/d_u > 18); and
- Expansion width divided by the water depth is smaller than three (D/d_u < 3).

The numbers do not link up perfectly due to the limited number of configurations that were tested. The transition point between both flow states was never approached. Hence, for certain configurations, the flow state cannot be predicted with certainty. Note that predicting the flow state based on the experimental results of this study is only legitimate for setups that closely match this study's laboratory setup. In other words, Froude numbers, bed roughness as well as other parameters, also need to correspond.

Near-bed flow behaviour in the scour hole

The horizontally contracting flow state is associated with not previously observed vertical flow behaviour at the end of the bed protection. The slope can be divided into two regions with clearly distinct vertical flow states. Constant vertical flow separation occurs in the centre of the jet. In and around the mixing layer, however, an alternating vertical flow state is present. In the alternating flow state, vertical flow attachment and vertical flow separation succeed each other in a period of several seconds. It is the first time that an alternating vertical flow state is observed in this context.

The frequency of alternation matches the dominant frequency of coherent 2-D turbulence structures in the horizontal mixing layer triggered upstream by the lateral expansion. This observation raises the idea of a physical mechanism in which mixing layer instabilities suppress vertical flow separation. The existence of a such a mechanism would be a valuable addition to the current understanding of the phenomena that trigger nonuniformity-induced flow attachment.

The diverging flow state on the other hand shows vertically separating flow across the entire width of the jet. Limited scour potential is expected. In addition, no signs of an alternating vertical flow state are observed.

Implications of the vertically alternating flow state for scour

Together with the alternating vertical flow state, a constant unidirectional near-bed flow in lateral direc-

tion from the mixing layer towards the centre of the jet is present. This unidirectional flow most likely enhances scour development at the sides of the jet that leaves the hydraulic structure. Conversely, separating flow in the centre of the jet triggers a constant upward near-bed return current, which is associated with considerably less scour potential. Thus, the vertically alternating flow state is likely to trigger a strongly 3-D scour hole, formed by increased scour in and around the mixing layers and limited scour in the centre of the jet. This scouring pattern perfectly matches the unforeseen scour hole observed by BAM Infra at the Afsluitdijk model tests. Hence, the vertically alternating flow state most likely explains the origin of these previously inexplicable scour patterns.

Implications of the vertically alternating flow state for hydraulic structure design

The increased scour related to the vertically alternating flow state is undesirable and potentially dangerous. In case during the design of a hydraulic structure becomes apparent that vertically alternating flow state is likely to occur, three types of measures can be considered. Firstly, geometry parameters can be adapted to prevent the vertically alternating flow state from happening. This could be achieved by extending the bed protection, by narrowing the horizontal expansion width and by widening the inflow channel. Applying guide walls to narrow the horizontal expansion width might be an economical solution. Secondly, the transverse near-bed flow that drives increased scour can be blocked. A measure to further explore could be the use of longitudinal sheet piling behind the bed protection. Thirdly, the bed protection design could be modified to deal with increased hydraulic loading. An option could be to reinforce the area behind the bed projection that is subjected to increased scour, for example by using block mats.

To conclude, this study underlines the importance of understanding 3-D flow characteristics to accurately predict scour. Current empirical prediction methods on scour often do not adequately include 3-D effects, as demonstrated in this thesis. Hydraulic engineers should consequently be extremely cautious when basing a (final) design on empirical scour predictions, especially when 3-D flow patterns can be expected.

8.2 Recommendations for future research

This section provides four suggestions for follow-up research to further refine the insights developed by this study.

Recommendation 1: Further development of the tuft measuring technique

Although this thesis demonstrates the potential of tuft measuring for near-bed flow, both the tufts and the processing algorithm are not fully optimised yet. Currently, the method only works under specific conditions and therefore lacks general robustness. Much effort is currently required to get the method operational in a new setup. A study dedicated to the measurement technique would be a great step forward to further optimise the tufts and the processing algorithm and explore the potential of tuft measuring. Various aspects of the processing algorithm like tuft identification and data filtering could be improved. Moreover, software with an easy-to-use interface that allows for easy deployment of the technique could be created. Furthermore, the effect of the nails on bed roughness is assumed to be negligible for the current study. Confirmation of this hypothesis would increase the validity of its results.

Recommendation 2: Further study the interaction between near-bed flow and scour in laterally-nonuniform flow

Every study dedicated to the effect of lateral flow nonuniformities on scour is a step forward towards the application of this knowledge in practice. Broekema et al. (2018) hypothesised a new scouring mechanism existed, Broekema et al. (2019) demonstrated and described the mechanism in a conceptual setup, and the present study illustrates how the mechanism manifests itself in a simplified version

of a geometry that is common in the field. These studies all focused on flow behaviour that drives scour instead of scour itself. The next study should take this step and focus on the implications of the identified flow patterns on scour. A laboratory setup with a naturally erodible bed can be used to find the corresponding scour patterns. Additionally, it shows to what extend the previously tested fixed-bed setups replicate the complex geometry of a real-life scour hole.

It is not easy to study the dynamic interaction between flow and scour. During the scouring process, flow behaviour constantly changes due to a changing bed topography. Therefore, one needs to measure both flow behaviour and scour development at a specific moment in time to study the interaction between both. Based on these measurements, the cause of a change in bed topography can be identified. Bed topography can be easily measured, but determining flow characteristics near a naturally eroded bed is more challenging. Tufts are not applicable due to the sand-coloured background, whereas an ADV device cannot conduct flow velocity measurements nearby to the eroding bed. The next paragraph proposes an approach that circumvents these issues.

Firstly, one should let a scour hole fully develop and regularly measure its topography. In the meanwhile, near-bed dye injections provide first insights into near-bed flow patterns in the different stages of the scouring process. The combination of these two allows for a first impression of scour behaviour. The researcher then selects a few topographies that correspond to key stages in the scour development process. Subsequently, these 3-D bed topographies are simplified, replicated in wood or concrete, and installed in the flume. Tufts at the fixed scour hole then provide an accurate picture of the near-bed flow behaviour corresponding to various stages of the scouring process. Based on this information, the researcher can draw solid conclusions on the scouring patterns that drive the scour hole development.

In case multiple configurations are tested, it is recommended to design the configurations in such a way that both a horizontally diverging and a horizontally contracting flow state are present. For experiments with a naturally erodible bed, a fully symmetrical setup should be used. The wall in the centreline of the jet in an asymmetrical setup is expected to severely affect scour development.

Recommendation 3: Further study the effect of bed roughness on the vertical flow state in laterally non-uniform flow

Another interesting topic for further research is the effect of parameters on the flow state that have not been studied yet. Especially the effect of bed roughness on the flow state is still a black box. Traditional research on scour development – e.g. research by Breusers (1967) – argues that bed roughness contributes to a 20-30 percent reduction in scour dimensions (Schiereck and Verhagen, 2012). A rough bed generates a smoother velocity profile, decreasing near-bed flow velocities. Since near-bed flow velocity is the main driver of scour, added roughness is understood to reduce scour dimensions. This understanding is widely supported by (2-D) experimental research.

In spite of this mechanism, there is reason to suspect that bed roughness can increase instead of decrease scour in certain 3-D situations. In the context of nonuniformity-induced flow attachment, roughness is believed to increase the tendency to vertically attach, which comes with an increased scouring potential. This mechanism works as follows: bed protection roughness increases local turbulence, which boosts the exchange of momentum between the boundary layer and the main flow across the bed protection. The exchange of momentum impedes boundary layer development (Van Prooijen, 2004). Disturbed boundary layers are generally more likely to bend along sharp-edged corners than well-developed boundary layers. Consequently, additional bed roughness has the potential to trigger vertical flow attachment, which can lead to increased scour. It would be interesting to study whether this mechanism can trigger vertical attachment under certain conditions and whether the increase in scouring potential due to flow attachment could be bigger than the decrease in scour potential due to reduced flow velocities.

Recommendation 4: Develop a method to predict the α value of Breusers' method for vertically alternating flow

In addition to research focused on understanding flow and scour behaviour under the vertically alternating flow state, the development of a more accurate scour prediction method is another engaging area of interest. Currently, developing an alternative way to predict α of Breusers' method seems to be the most promising approach. Especially since Breusers' method is suitable to predict scour in vertically alternating flow, as long as the α parameter is accurately determined, as was discussed earlier in this thesis (Section 7.3).

References

Balachandar, R., Kells, J. A. and Thiessen, R. J. (2000). The effect of tailwater depth on the dynamics of local scour, *Canadian Journal of Civil Engineering* 27(1): 138–150.

Breusers, H. N. C. (1966). Conformity and time scale in two-dimensional local scour, *Hydraulic Research Laboratory, Poona, India* .

Breusers, H. N. C. (1967). Time Scale of Two Dimensional Local Scour, 3: 275–282.

Broekema, Y. B. (2020). *Horizontal shear flows over a streamwise varying bathymetry*, PhD thesis, TU Delft.

Broekema, Y. B., Labeur, R. J. and Uijttewaal, W. S. J. (2018). Observations and Analysis of the Horizontal Structure of a Tidal Jet at Deep Scour Holes, *Journal of Geophysical Research: Earth Surface* 123(12): 3162–3189.

Broekema, Y. B., Labeur, R. J. and Uijttewaal, W. S. J. (2019). Suppression of vertical flow separation over steep slopes in open channels by horizontal flow contraction, *Journal of Fluid Mechanics* 885(A8).

Cherrye, E. M., Elkins, C. J. and Eaton, J. K. (2008). Geometric sensitivity of three-dimensional separated flows, *International Journal of Heat and Fluid Flow* 29(3): 803–811.

Dietz, W. J. (1969). Kolksicherung durch Befestigungsstrecken für das Eidersiel, *Mitteilungsblatt der Bundesanstalt für Wasserbau* (29).

Gao, F., Wei, M., Zambonini, G., Boudet, J., Ottavy, X., Lu, L. and Shao, L. (2015). Large-eddy simulations of 3-D corner separation in a linear compressor cascade, *Physics of Fluids* 27(8): 085105.

Gerthart, P. M. and Bober, L. J. (1974). Comparison of Several Methods for Predicting Separation in a Compressible Turbulent Boundary Layer, *Technical report*, NASA.

Graauw, de, A. F. F. and Pilarczyk, K. W. (1981). Model-Prototype Conformity of Local Scour in Non-Cohesive Sediments Beneath Overflow-Dam., *Proceedings, Congress - International Association For Hydraulic Research* (January 1981): 7–15.

Hak, Gad-el, M. and Bushnell, D. M. (1991). Separation control: Review, *Journal of Fluids Engineering, Transactions of the ASME* 113(1): 5–30.

Hoffmans, G. J. C. M. (2009). Closure problem to jet scour, *Journal of Hydraulic Research* 47(1): 100–109.

Hoffmans, G. J. C. M. and Booij, R. (1993). The Influence of Upstream Turbulence on Local-Scour Holes, *Congress IAHR, Tokyo*.

Hoffmans, G. J. C. M. and Verheij, H. J. (2020a). Case: Scour development in front of culvert (Rammegors), *Scour Manual*.

Hoffmans, G. J. C. M. and Verheij, H. J. (2020b). Jets, *Scour Manual*.

Hughes, S. A. (1993). *Advanced Series on Ocean Engineering 7. Physical Models and Laboratory Techniques in Coastal Engineering*, World Scientific, London.

Jorissen, R. E. and Vrijling, J. K. (1989). Local scour downstream hydraulic constructions, *Congress IAHR, Ottawa*.

Kantoush, S. A. and Schleiss, A. J. (2009). Large-scale piv surface flow measurements in shallow basins with different geometries, *Journal of Visualization* 12(4): 361–373.

Levvel (2018). Presentation Results Physical Model Tests Afsluitdijk.

Melville, B. W. and Lim, S. Y. (2014). Scour caused by 2D horizontal jets, *Journal of Hydraulic Engineering* 140(2): 149–155.

Meulen, van der, T. and Vinjé, J. (1975). Three dimensional local scour in non-cohesive sediments, *Congress IAHR, Sao Paolo*.

Munson, B. R., Young, D. F., Okiishi, T. H. and Huebsch, W. W. (2009). *Fundamentals of Fluid Mechanics*, sixth edit edn, J. Wiley & Sons, Hoboken, NJ.

NASA (1979). KC-135A in flight - closeup of winglet with attached tufts, *DFRC Photo Collection* .

Nieuwstadt, F. T. M., Boersma, B. J. and Westerweel, J. (2015). *Turbulence: Introduction to Theory and Applications of Turbulent Flows*, Springer.

Pearson, R. K. (1999). Data cleaning for dynamic modeling and control, *European Control Conference (ECC)*, IEEE, Karlsruhe, pp. 2584–2589.

Poulin, F. J. and Flierl, G. R. (2005). The influence of topography on the stability of jets, *Journal of Physical Oceanography* 35(5): 811–825.

Prooijen, van, B. C. (2004). *Shallow mixing layers*, PhD thesis, TU Delft.

Prooijen, van, B. C. and Uijttewaal, W. S. J. (2002). A linear approach for the evolution of coherent structures in shallow mixing layers, *Physics of Fluids* 14(12): 4105–4114.

Rajaratnam, N. (1976). *Turbulent Jets*, Elsevier, Amsterdam.

Schiereck, G. J. and Verhagen, H. J. (2012). *Introduction to Bed, bank and shore protection*, VSSD, Delft.

Simpson, R. L. (1996). Aspects of turbulent boundary-layer separation, *Progress in Aerospace Sciences* 32(5): 457–521.

Stewart, R. H. (2008). *An Introduction to Physical Oceanography*, University, Texas A & M.

Talstra, H. (2011). *Large-scale turbulence structures in shallow separating flows*, PhD thesis, TU Delft.

Uijttewaal, W. S. and Tukker, J. (1998). Development of quasi two-dimensional structures in a shallow free-surface mixing layer, *Experiments in Fluids* 24(3): 192–200.

Üsenti, B. (2019). *Scour hole formation for lateral non-uniform flow in non-cohesive sediments*, PhD thesis, TU Delft.

Watson, G. (1983). *Statistics On Spheres*, John Wiley & Sons.

Welch, P. D. (1967). The Use of Fast Fourier Transform for the Estimation of Power Spectra: A Method Based on Time Averaging Over Short, Modified Periodograms, *IEEE Transactions on Audio and Electroacoustics* 15(2): 70–73.

White, F. (1999). *Fluid mechanics*, 7th editio edn.

Yates, L. A. and Chapman, G. T. (1992). Streamlines, Vorticity Lines, and Vortices Around Three-Dimensional Bodies, *AIAA Journal* 30(7): 1819–1829.

Zande, van der, B. J. (2018). *Jet behaviour in longitudinal deepening shallow flows*, PhD thesis, TU Delft.

Zanke, U. C. E. (1978). Zusammenhänge zwischen Strömung und Sedimenttransport, Teil 2: Berechnung des Sedimenttransportes hinter befestigten Sohlenstrecken -Sonderfall zweidimensionaler Kolk, *Mitteilungen des Franzius Instituts, Hannover, Germany* (Heft 48).

A

Conservation of potential vorticity

Broekema et al. (2018) and Broekema et al. (2019) argue that conservation of potential vorticity most likely plays a role in vertical flow attachment at a downward slope.

Vorticity is essentially the rate of rotation in a fluid. It can be defined as:

$$\bar{\omega}_z = \frac{\partial \bar{u}_x}{\partial y} - \frac{\partial \bar{u}_y}{\partial x}, \tag{A.1}$$

in which $\bar{\omega}_z$ is the depth-averaged vertical vorticity, $\bar{u}_x$ is the depth-averaged longitudinal velocity component and $\bar{u}_y$ the depth-averaged lateral velocity component (Stewart, 2008). In a situation in which lateral velocities are small, lateral velocity gradients are believed to be the main driver for vorticity (Broekema et al., 2019).

Vorticity is conserved as the flow travels streamwise. When the flow encounters a downwards slope, the vertical water column stretches out, causing the flow to contract (Poulin and Flierl, 2005). As the width of the water column decreases, individual flow particles accelerate to conserve angular momentum. Stewart (2008) (p. 203) explains the phenomenon as follows: 'The concept is analogous with the way figure skaters decreases their spin by extending their arms and legs. The action increases their moment of inertia and decreases their rate of spin'. Figure A.1 visualises this concept.

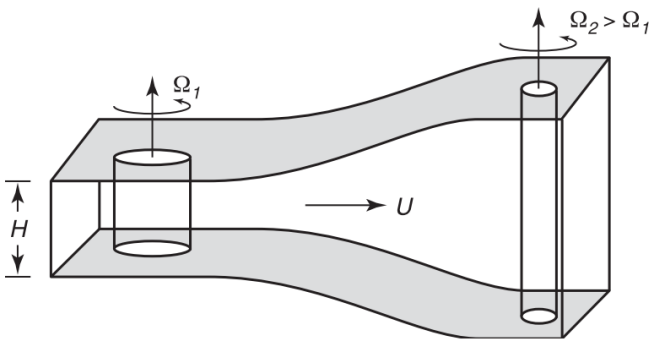

Figure A.1: Schematisation of the development of angular velocity (ω) when potential voriticity is conserved. Vertical stretching of the water column causes the vertical fluid column to spin faster (Stewart, 2008).

The acceleration that follows from this mechanism comes with a positive pressure gradient that counteracts the adverse pressure gradient.

B

Results tuft measurements

This appendix systematically presents the results of the tuft-measurement flow directs of each experimental run. Table B.1) provides an overview of the experimental runs that were carried out. Figure B.1 to B.24 present the time-averaged flow directions as well as the flow direction distributions near the slope's bed.

Test No.	L_b/d_u	D/d_u	$0.5B/d_u$	Flow state
0		No horizontal expansion		Flow state 0
1.1	5	3	9	Flow state 1
1.2	5	6	6	Flow state 1
1.2.B	5	6	3	Flow state 1
1.3	5	9	3	Flow state 1
2.1	10	3	9	Flow state 2
2.1.B	10	3	6	Flow state 1
2.2	10	6	6	Flow state 1
2.2.B	10	6	3	Flow state 1
2.3	10	9	3	Flow state 1
3.1.B	15	3	6	Flow state 2
3.2	15	6	6	Flow state 1

Table B.1: Overview of tested configurations and the flow state that was observed.

Test 0

Test No.	L_b/d_u	D/d_u	$0.5B/d_u$	Flow state
0		No horizontal expansion		Flow state 0

Table B.2: Test characteristics.

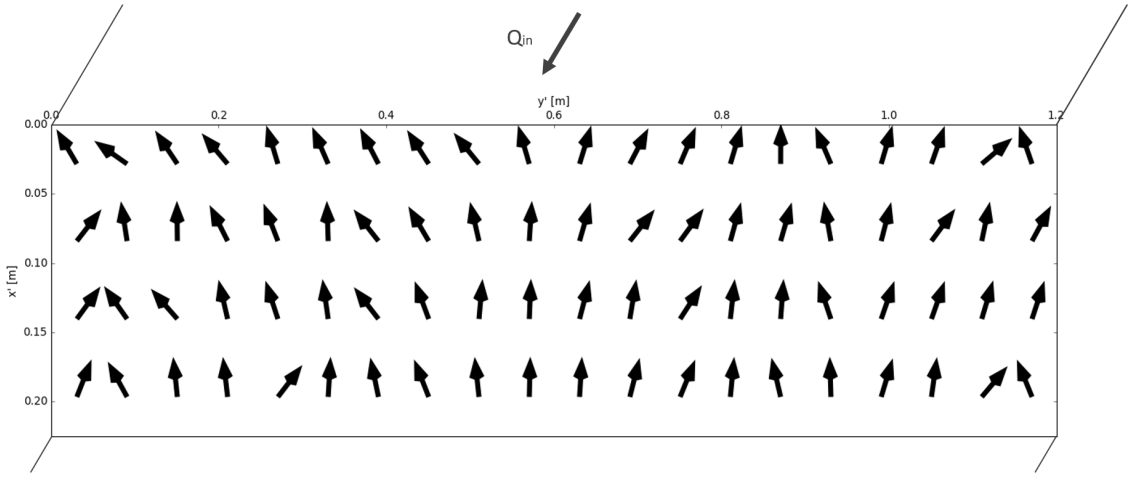

Figure B.1: Time-averaged near-bed flow directions during Test 0.

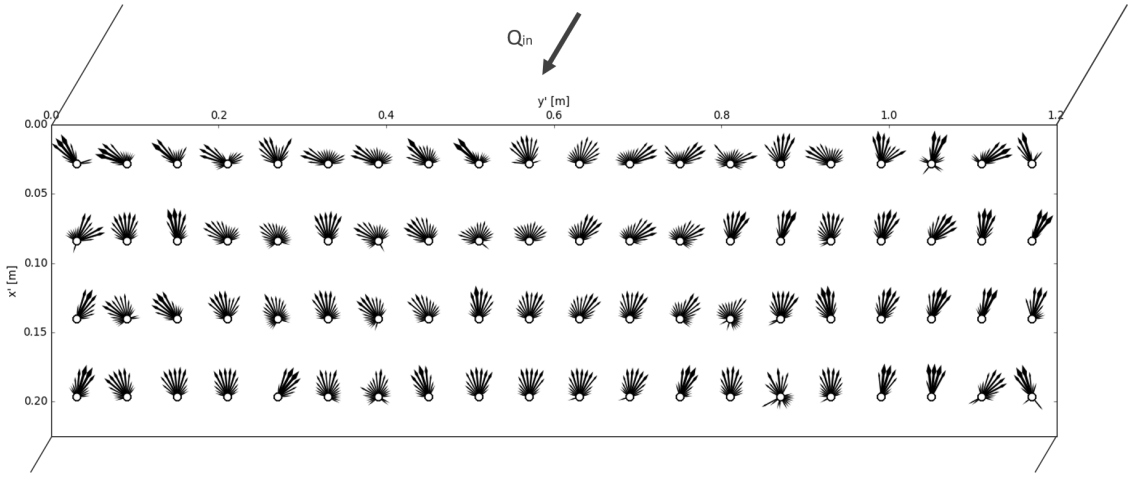

Figure B.2: Distribution of the each near-bed flow direction during Test 0. Arrow size relates to the prevalence of the corresponding flow direction occurs.

Test 1.1

Test No.	L_b/d_u	D/d_u	$0.5B/d_u$	Flow state
1.1	5	3	9	Flow state 1

Table B.3: Test characteristics.

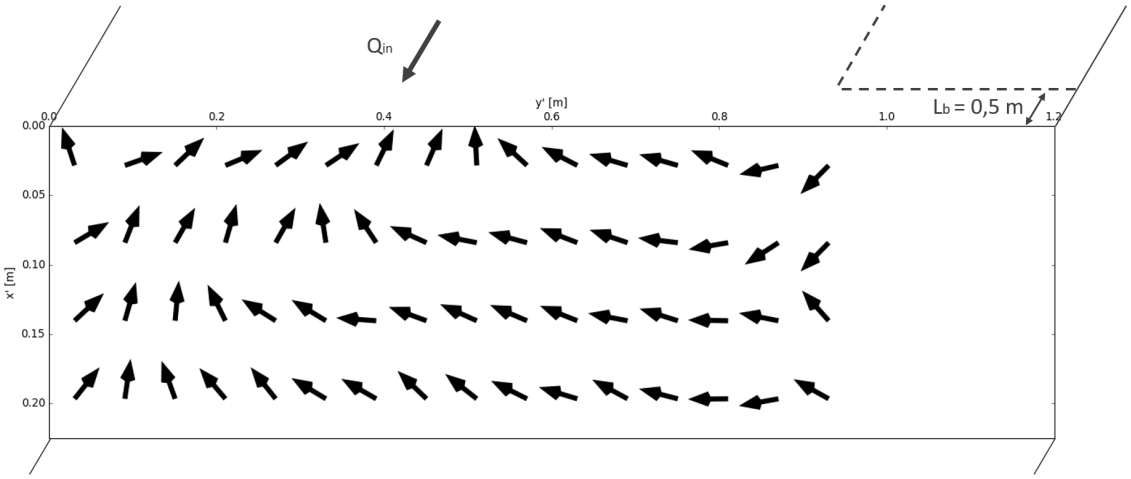

Figure B.3: Time-averaged near-bed flow directions during Test 1.1.

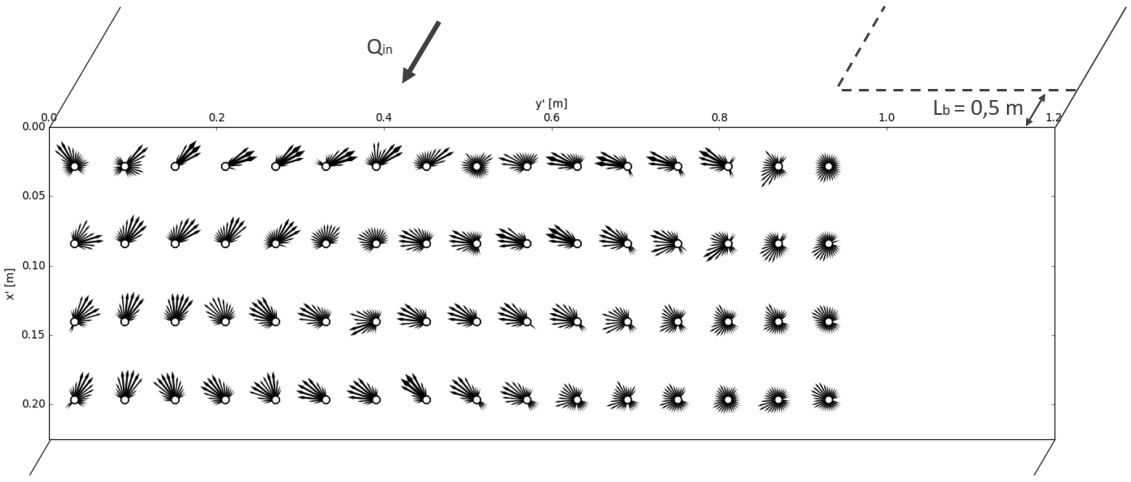

Figure B.4: Distribution of the each near-bed flow direction during Test 1.1. Arrow size relates to the prevalence of the corresponding flow direction occurs.

Test 1.2

Test No.	L_b/d_u	D/d_u	$0.5B/d_u$	Flow state
1.2	5	6	6	Flow state 1

Table B.4: Test characteristics.

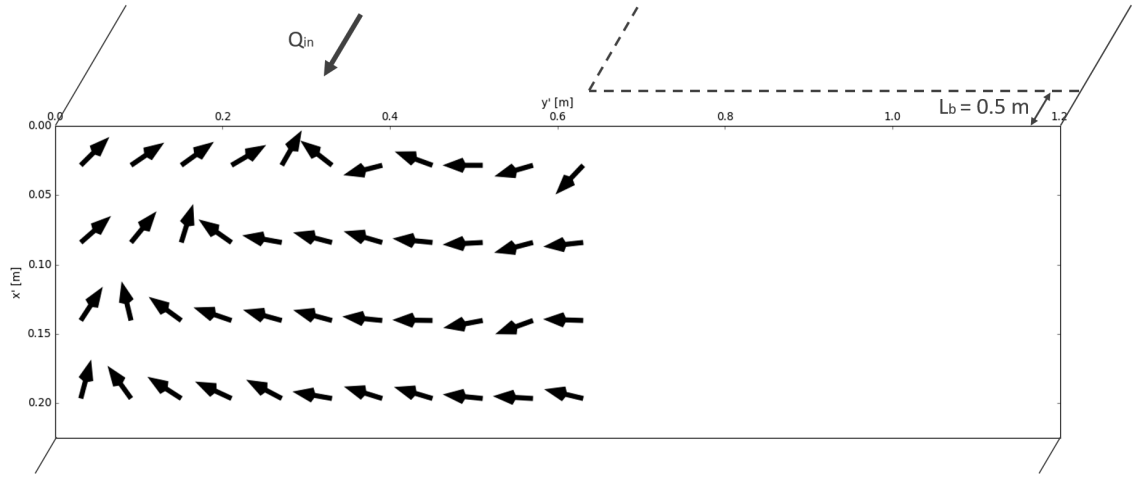

Figure B.5: Time-averaged near-bed flow directions during Test 1.2.

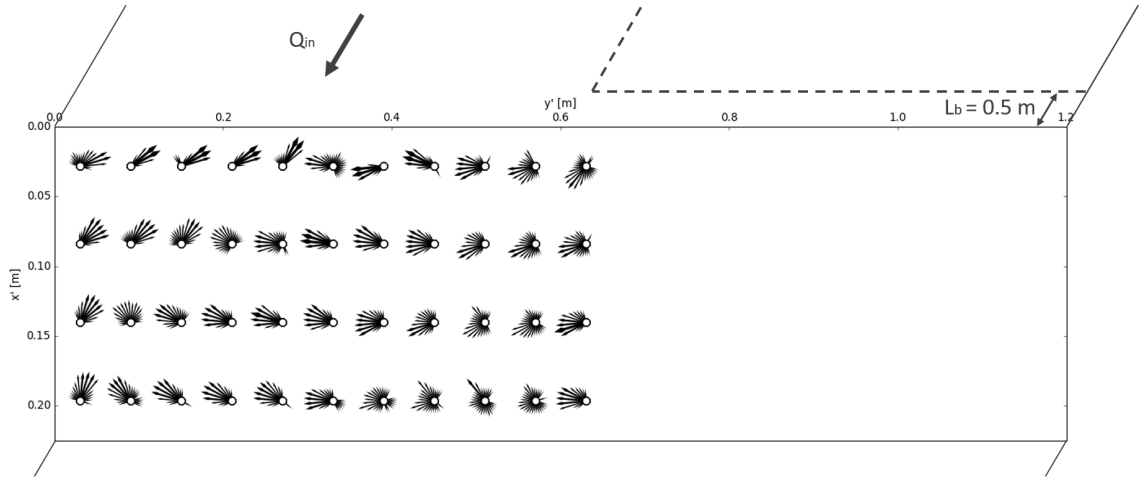

Figure B.6: Distribution of the each near-bed flow direction during Test 1.2. Arrow size relates to the prevalence of the corresponding flow direction occurs.

Test 1.2.B

Test No.	L_b/d_u	D/d_u	$0.5B/d_u$	Flow state
1.2.B	5	6	3	Flow state 1

Table B.5: Test characteristics.

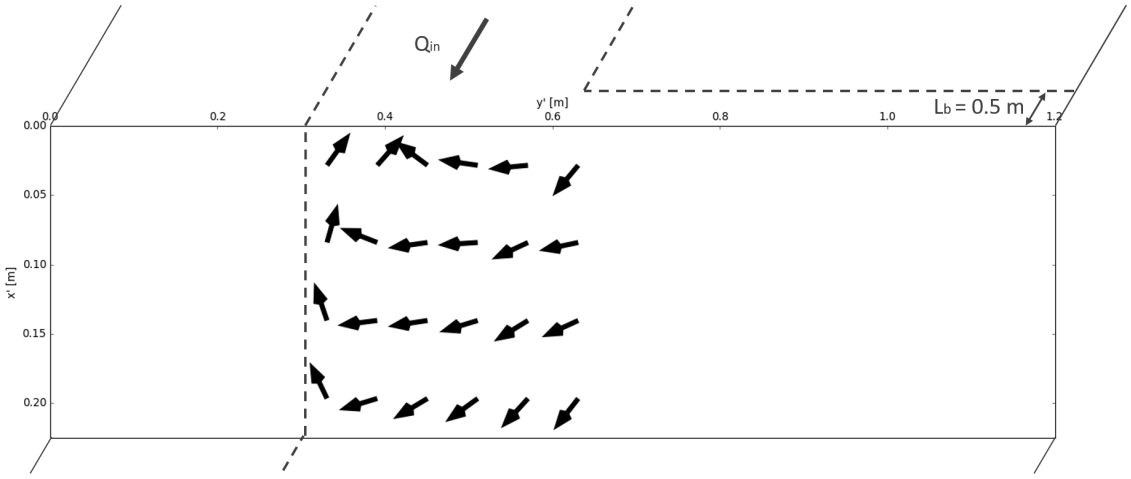

Figure B.7: Time-averaged near-bed flow directions during Test 1.2.B.

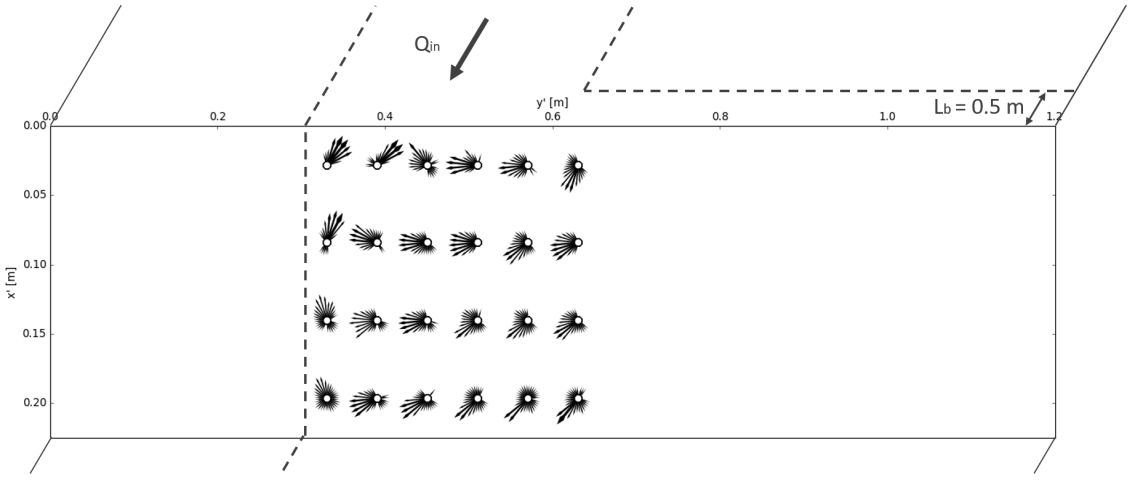

Figure B.8: Distribution of the each near-bed flow direction during Test 1.2.B. Arrow size relates to the prevalence of the corresponding flow direction occurs.

Test 1.3

Test No.	L_b/d_u	D/d_u	$0.5B/d_u$	Flow state
1.3	5	9	3	Flow state 1

Table B.6: Test characteristics.

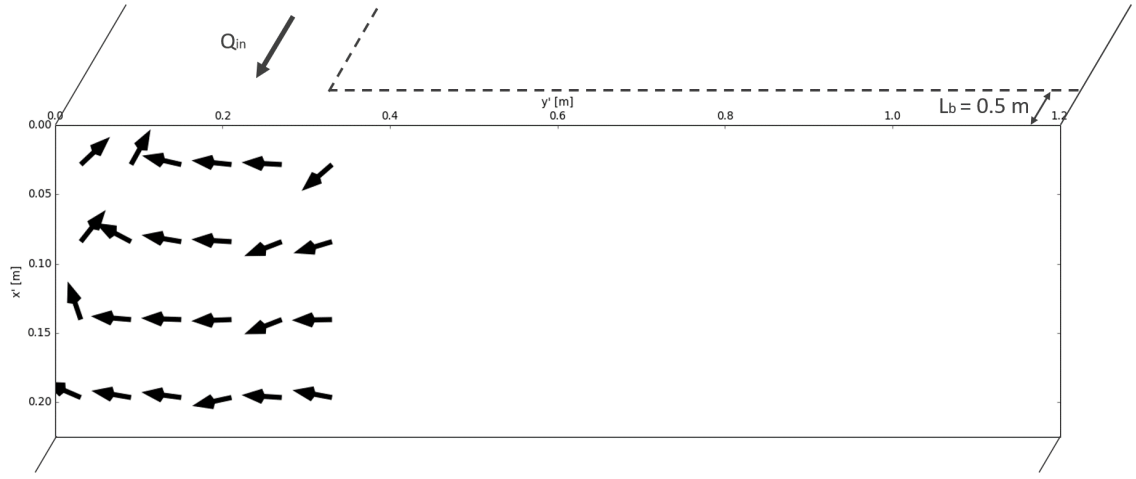

Figure B.9: Time-averaged near-bed flow directions during Test 1.3.

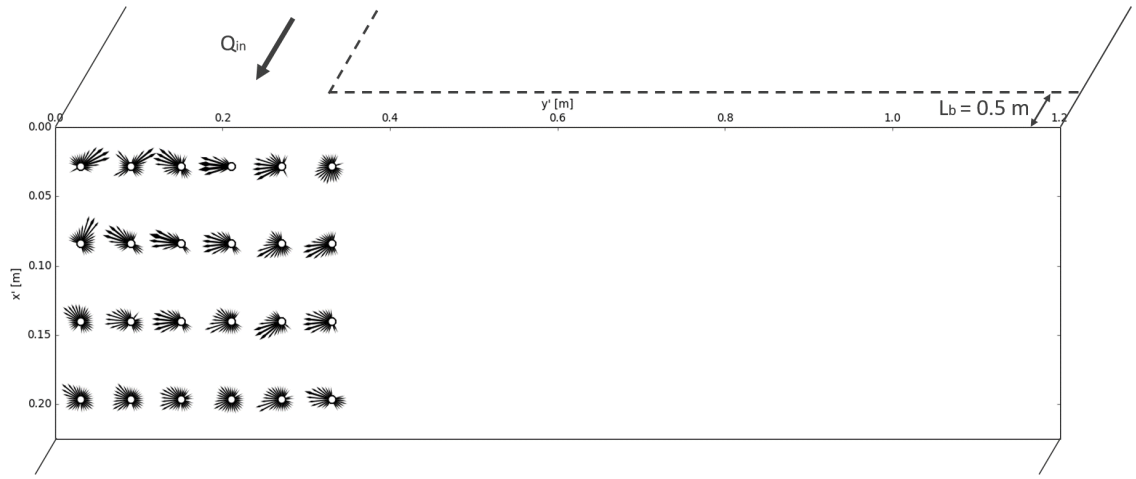

Figure B.10: Distribution of the each near-bed flow direction during Test 1.3. Arrow size relates to the prevalence of the corresponding flow direction occurs.

Test 2.1

Test No.	L_b/d_u	D/d_u	$0.5B/d_u$	Flow state
2.1	10	3	9	Flow state 2

Table B.7: Test characteristics.

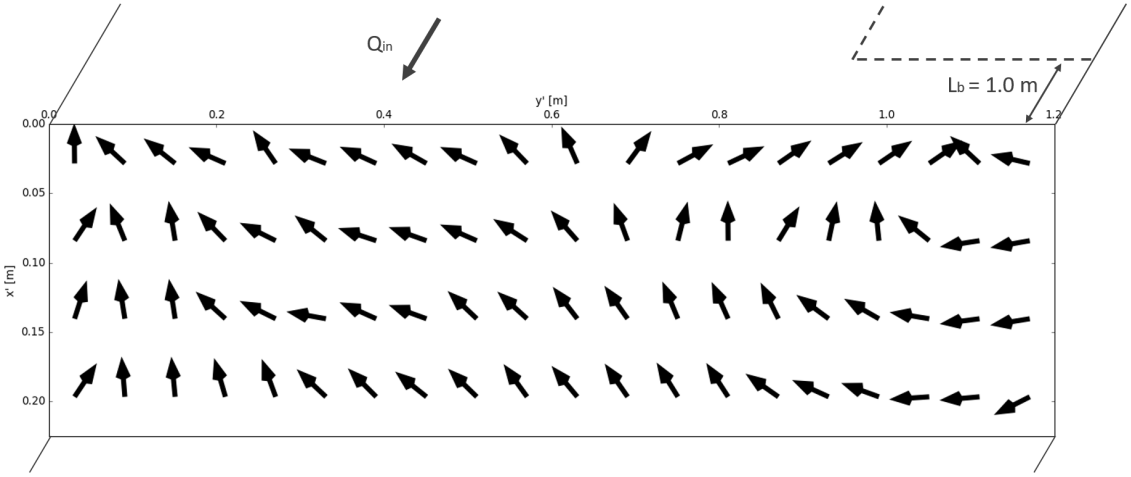

Figure B.11: Time-averaged near-bed flow directions during Test 2.1.

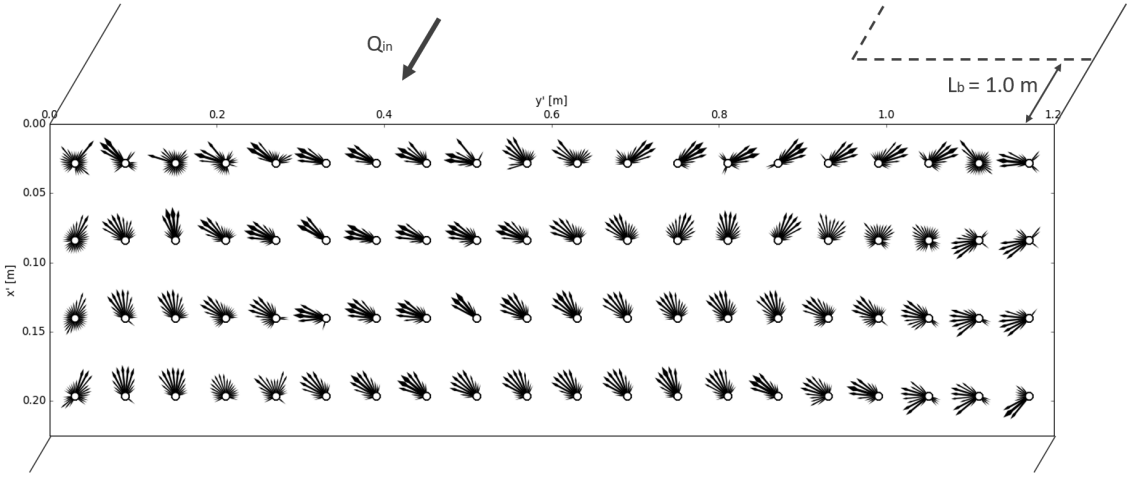

Figure B.12: Distribution of the each near-bed flow direction during Test 2.1. Arrow size relates to the prevalence of the corresponding flow direction occurs.

Test 2.1.B

Test No.	L_b/d_u	D/d_u	$0.5B/d_u$	Flow state
2.1.B	10	3	6	Flow state 1

Table B.8: Test characteristics.

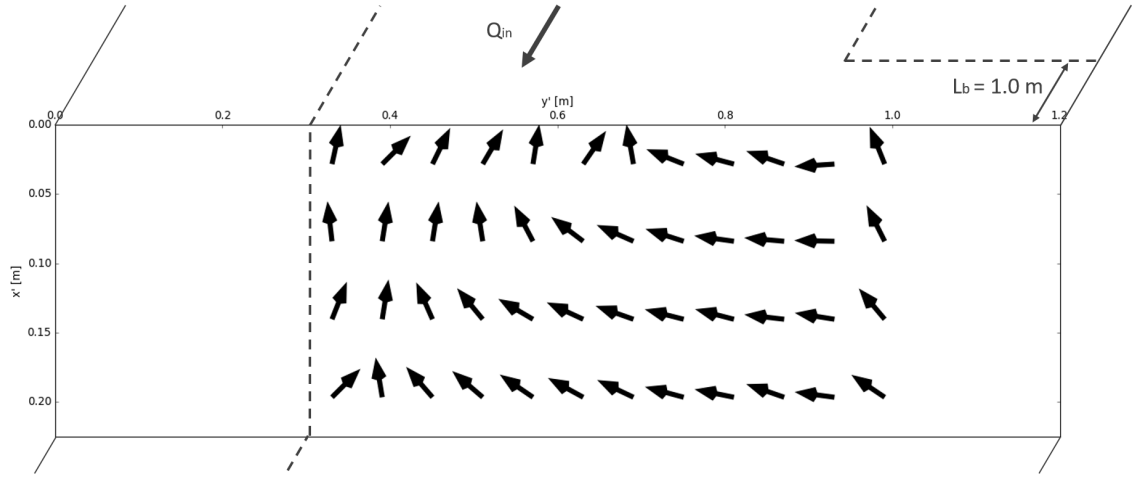

Figure B.13: Time-averaged near-bed flow directions during Test 2.1.B.

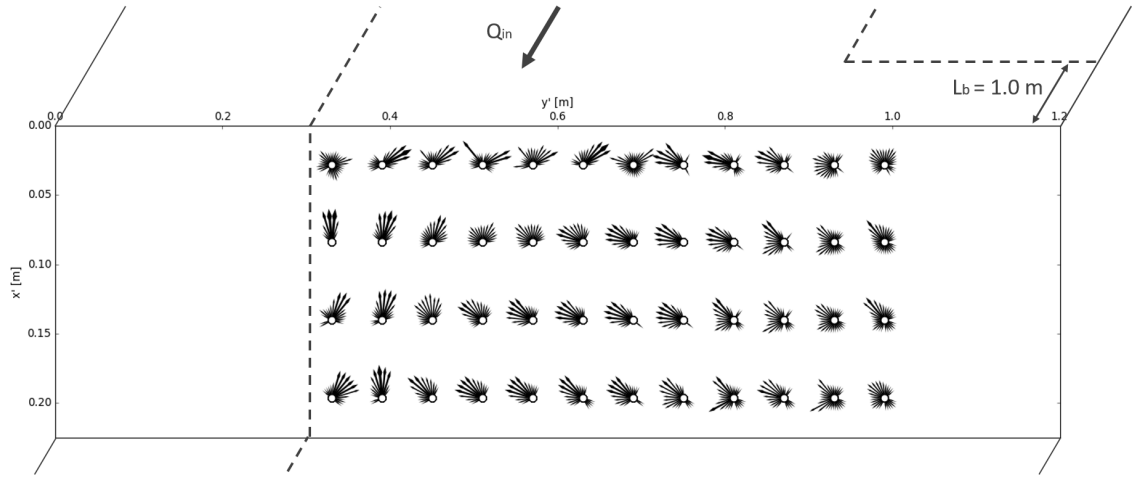

Figure B.14: Distribution of the each near-bed flow direction during Test 2.1.B. Arrow size relates to the prevalence of the corresponding flow direction occurs.

Test 2.2

Test No.	L_b/d_u	D/d_u	$0.5B/d_u$	Flow state
2.2	10	6	6	Flow state 1

Table B.9: Test characteristics.

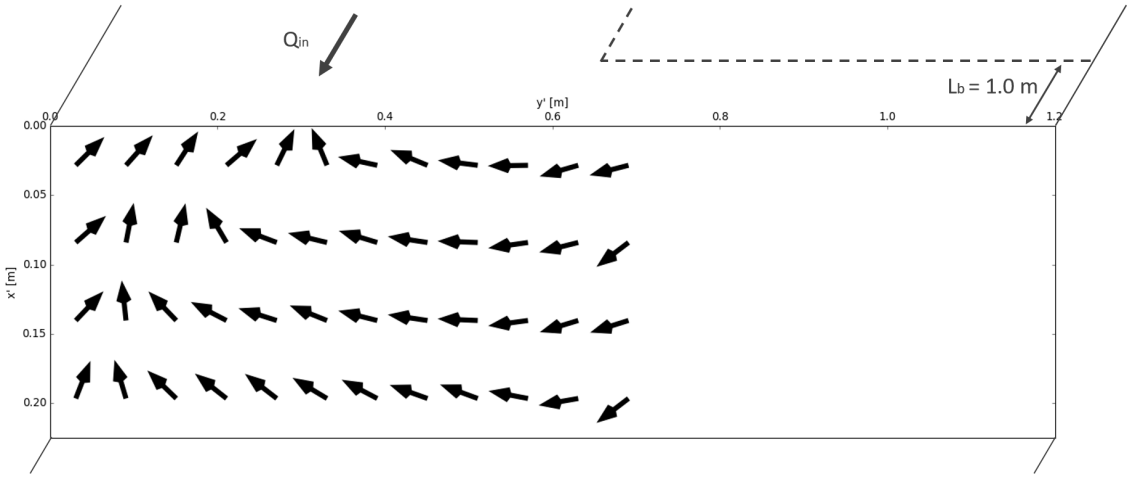

Figure B.15: Time-averaged near-bed flow directions during Test 2.2.

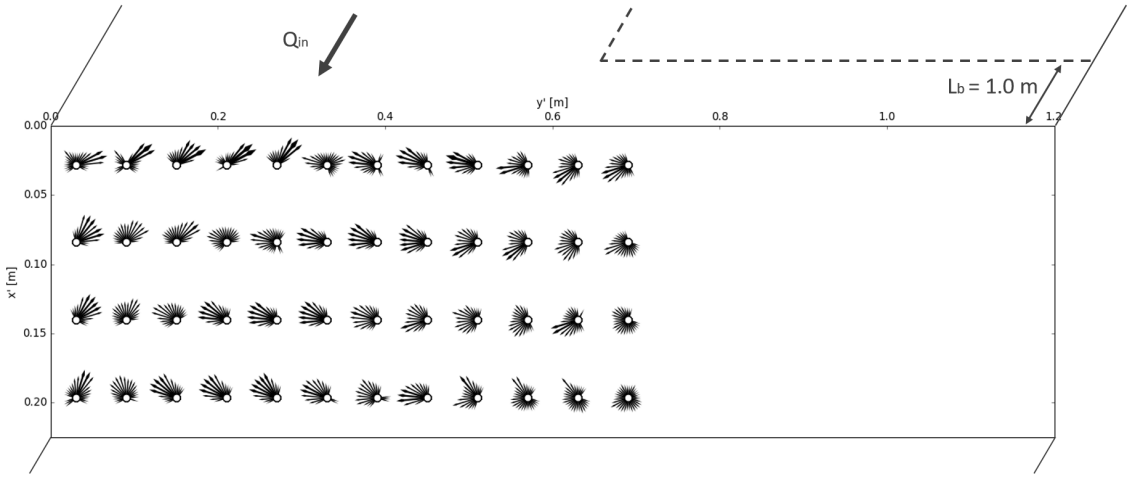

Figure B.16: Distribution of the each near-bed flow direction during Test 2.2. Arrow size relates to the prevalence of the corresponding flow direction occurs.

Test 2.2.B

Test No.	L_b/d_u	D/d_u	$0.5B/d_u$	Flow state
2.2.B	10	6	3	Flow state 1

Table B.10: Test characteristics.

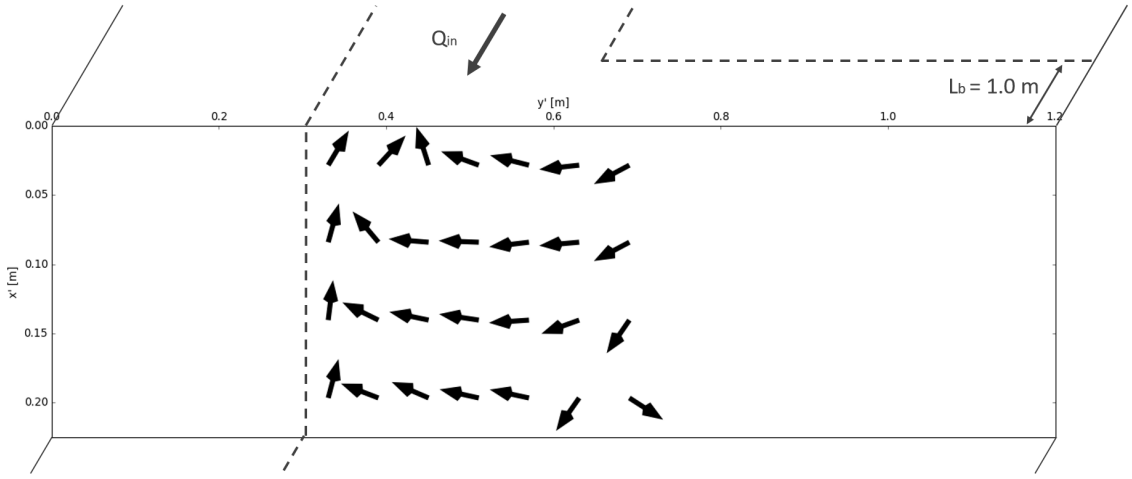

Figure B.17: Time-averaged near-bed flow directions during Test 2.2.B.

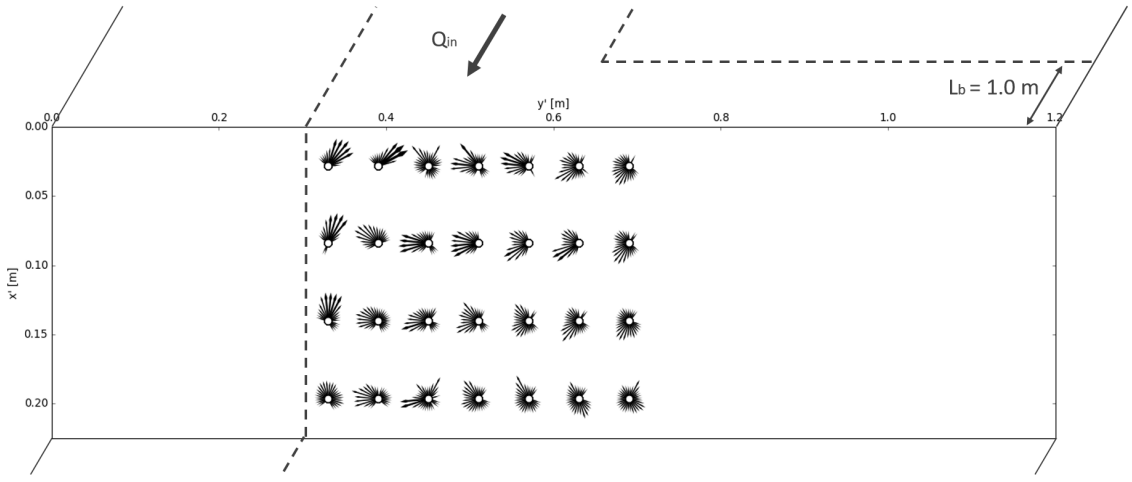

Figure B.18: Distribution of the each near-bed flow direction during Test 2.2.B. Arrow size relates to the prevalence of the corresponding flow direction occurs.

Test 2.3

Test No.	L_b/d_u	D/d_u	$0.5B/d_u$	Flow state
2.3	10	9	3	Flow state 1

Table B.11: Test characteristics.

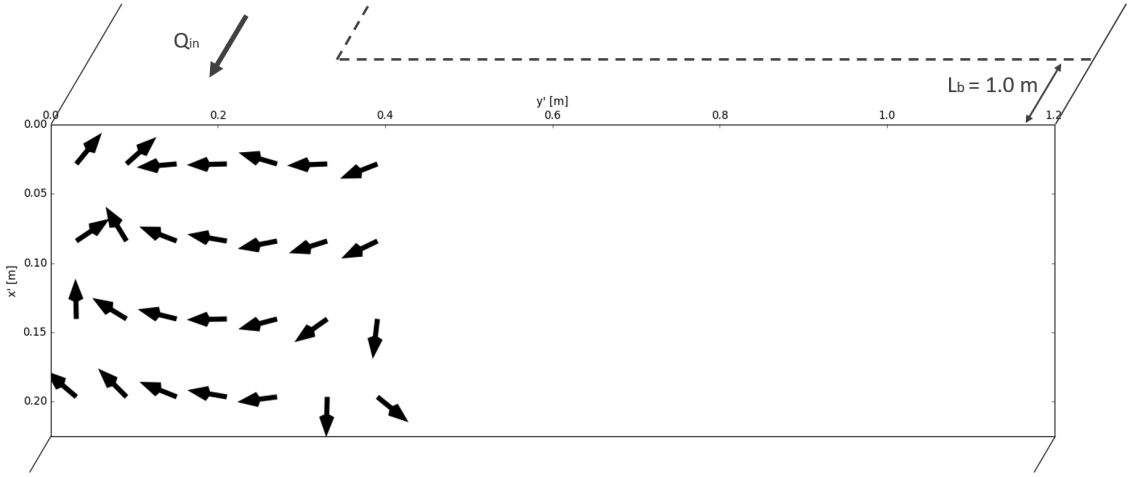

Figure B.19: Time-averaged near-bed flow directions during Test 2.3.

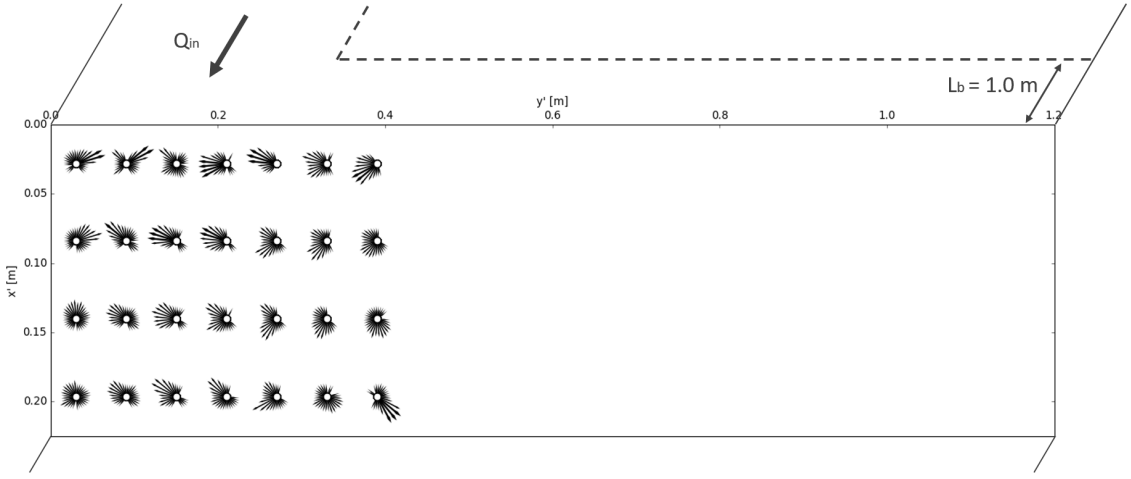

Figure B.20: Distribution of the each near-bed flow direction during Test 2.3. Arrow size relates to the prevalence of the corresponding flow direction occurs.

Test 3.1.B

Test No.	L_b/d_u	D/d_u	$0.5B/d_u$	Flow state
3.1.B	15	3	6	Flow state 2

Table B.12: Test characteristics.

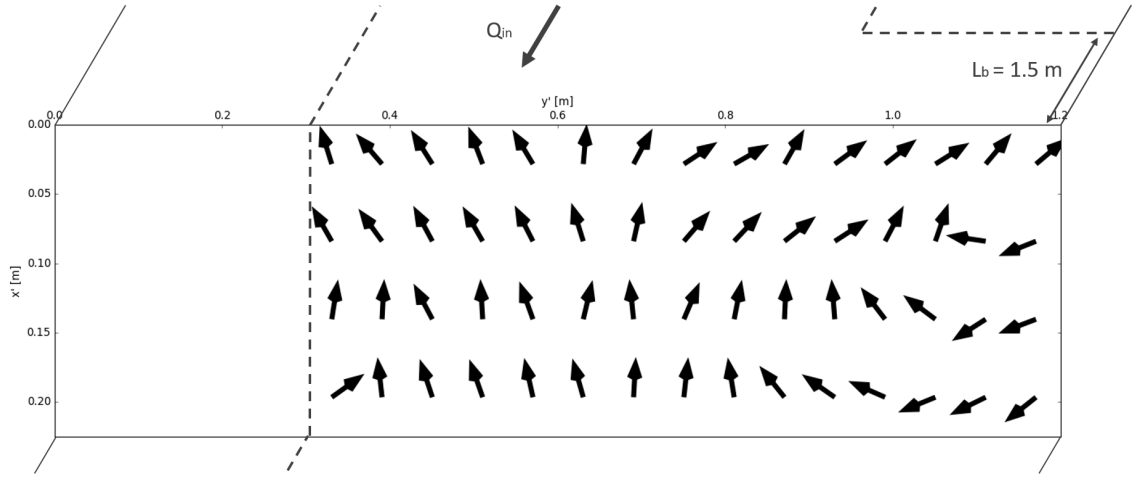

Figure B.21: Time-averaged near-bed flow directions during Test 3.1.B.

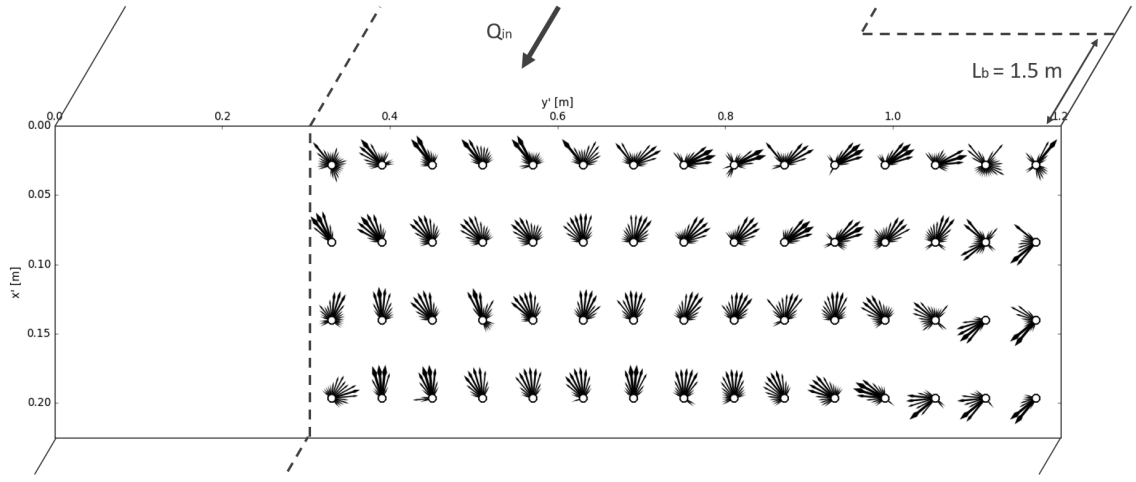

Figure B.22: Distribution of the each near-bed flow direction during Test 3.1.B. Arrow size relates to the prevalence of the corresponding flow direction occurs.

Test 3.2

Test No.	L_b/d_u	D/d_u	$0.5B/d_u$	Flow state
3.2	15	6	6	Flow state 1

Table B.13: Test characteristics.

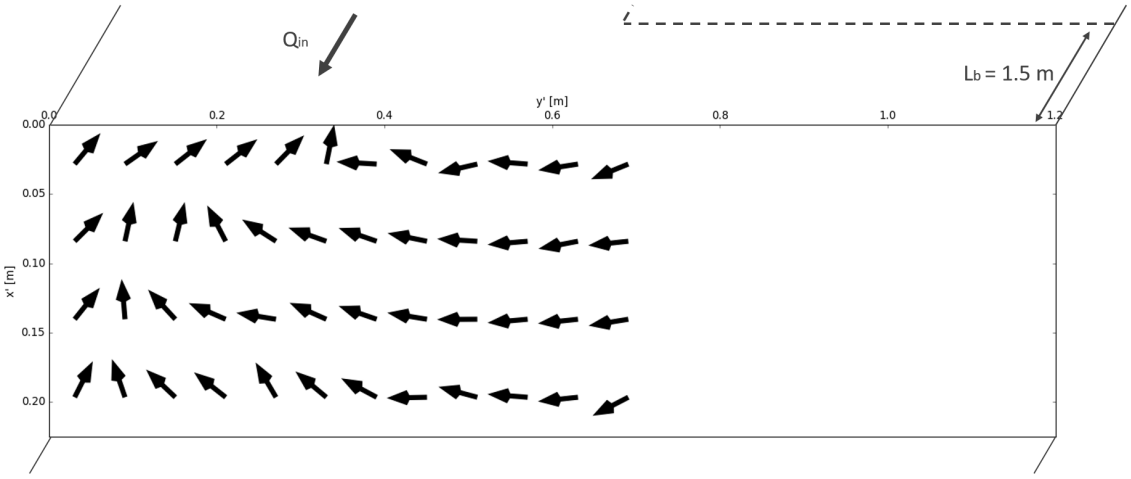

Figure B.23: Time-averaged near-bed flow directions during Test 3.2.

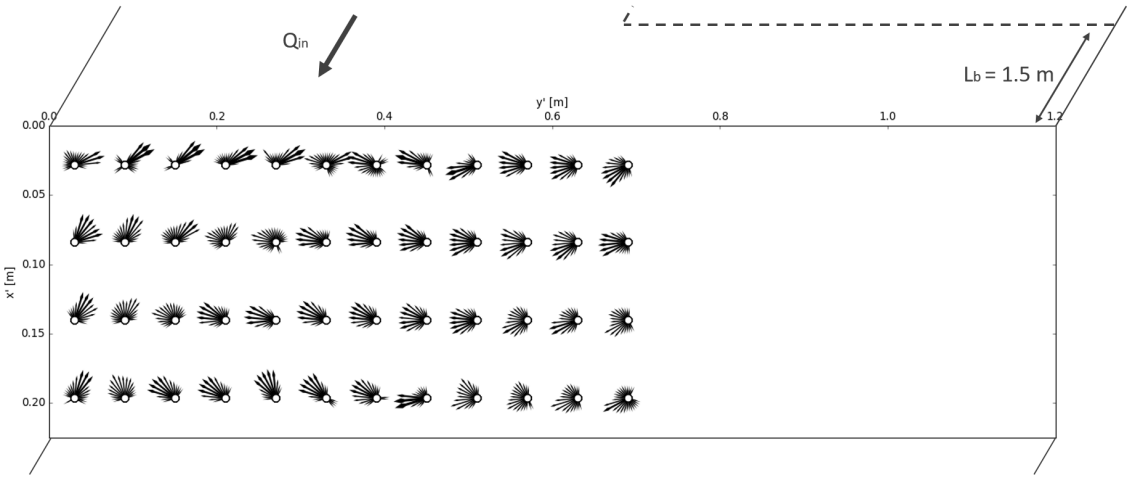

Figure B.24: Distribution of the each near-bed flow direction during Test 3.2. Arrow size relates to the prevalence of the corresponding flow direction occurs.